Model systems for the investigation of metal-support interactions in cobalt based Fischer-Tropsch.

Nontsikelelo Dyasi

BSc (Chem, Eng) UCT

This thesis was submitted to the University of Cape Town in partial fulfilment of the requirements for the degree of Master of Science in Chemical Engineering

Catalysis Research Unit

Department of Chemical Engineering

Acknowledgement

I would first want to acknowledge the power, presence and sustenance of God in the completion of my master's degree. The verse in Jeremiah 29:11, "For I know the plans that I have for you, declares the Lord, plans to prosper you and not to harm you, to give you a future and a hope", really summaries how God has worked in me to produce this dissertation. All praise and honour to Him as the source of all wisdom.

Ndi khou tama u livhuwa na u dzhiela n̓nṱha Dakalo Nemauluma kha ṱhuṱhuwedzo na ngeletshedzo ye a ntsumbedza yone misi ya u kuvhangana maṅwalo a ngudo dzanga dza masiṱasi. O vha muthu we a tenda kha n̓ne, nahone a d̓i n̓ea na tshifhinga tshau nthusa u vhekanya mihumbulo yanga lwa khwine. Lufuno na u ṱhogomela hanu ndo zwi vhona.

Mandibabulele abazali bam nabantakwetu ngukundixhasa xa bedifundela esisidanga. Ukusukele ebusaneni nihambe nam kuluhambo lwenfunda. Lencwadi sisiqamo sayo yonke leminyaka.

I would like to especially thank my supervisor Eric van Steen for his support and guidance during my masters. I can't forget to mention Gerard Lebebe and Lebohang Macheli who were of great assistance to me in the lab work. I also want to thank those who were a formidable support to me in the department, Nobuhle Mpofu, Avela Kunene and Robert Nohamba. Lastly, I want to appreciate the support of the administrative and technical staff.

Declaration

I, Nontsikelelo Dyasi certify that this submission is my own, unaided work, except for the information obtained from literature sources and my supervisors. All sources of information have been adequately acknowledged and referenced. I have not received assistance from any other sources in completing this submission.

Signature: …..Signed by candidate. Date: …….

Synopsis

The Fischer-Tropsch synthesis is a catalytic reaction which can be been used for the production of synthetic fuels. The Fischer-Tropsch catalyst contains a catalytically-active phase which is supported predominantly on refractory oxides and may be promoted to improve activity and/or selectivity. Silica is a widely used support, whose surface chemistry enables high reducibility of cobalt precursors to the metallic state (Munirathinam *et al.*,2018). The understanding of the role of the support on the activity and selectivity of the catalyst in the Fischer-Tropsch synthesis has evolved over time. Inverse catalysts isolate the effect of metal-support interactions from other support effects, and are therefore suitable for investigating metal-support effects. Investigations on the effect of metal-support interactions with silica supported cobalt catalyst have been reported previously (Morales *et al.*, 2005; Johnson *et al.*, 2015; Macheli *et al.*, 2018; Petersen *et al.*, 2018). This work sought to further investigate the nature of the metal-support interactions when silica support precursors are adsorbed on cobalt nanoparticles, with cobalt in different oxidation states, as it applies to the Fischer-Tropsch process.

Model cobalt nanoparticles, with cobalt in different oxidation states, were modified with tetraethoxysilane or triphenylethoxysilane and used to gain insight into the interaction between cobalt and silica support. The model catalyst was prepared by the thermal decomposition of a cobalt complex in the presence of trioctylamine and oleylamine as surfactants to yield cobalt nanoparticles. Their surface was modified with triphenylethoxysilane or tetraethoxysilane. Energy dispersive X-ray (EDX) was used to verify the presence of silica on the surface of the modified cobalt nanoparticles and FTIR confirmed that Co-O-Si bonds had been formed on the modified cobalt nanoparticles. XRD analysis of the modified cobalt nanoparticles showed that there was no evidence of the formation of a crystalline silica phase, as its characteristic diffraction lines were absent. The TPR profiles showed a shift to higher reduction temperatures with increasing silica loading, suggesting that the surface modification results in retardation of reduction of the cobalt nanoparticles. CO-TPD studies of the model catalyst indicated that the total number of active sites available for CO adsorption and bond cleavage decreases upon surface modification, but it leads to a more facile CO bond cleavage as evidenced by decrease in energy of dissociation.

The activity of these materials in the Fischer-Tropsch synthesis decreased with increasing silicon content for the oxidized cobalt nanoparticles. This was attributed to the decline in the total number of active site available for CO bond cleavage with increasing silicon content. The methane selectivity passes a minimum with increasing silicon content. This may be related to the carbon coverage on the surface of the nanoparticles affecting the chain growth. It is recommended that Fischer-Tropsch synthesis studies be conducted on the modified as-synthesized cobalt nanoparticles to compare the performance of the two catalysts.

Table of content

Table of Figures

List of Tables

Chapter 1 Introduction

Catalysts make reactions possible that would otherwise not occur or would take place at much lower rates. Although catalyst do not experience significant changes during reaction, they facilitate the breaking and formation of chemical bonds during the catalytic process. The industrialization of the world has been influenced significantly by the development of heterogeneous catalysis (George, 1995). The emergence of the automobile industry led to an increasing demand for gasoline. This demand fuelled the development and advancement of catalytic cracking processes of crude oil to fuels and other petrochemical products (George, 1995). Germany, having poor crude oil resources, developed a Fischer-Tropsch process to convert coal to hydrocarbon products which were further processed to synthetic fuels (Arsalanfar *et al.,* 2014; Khodakov *et al.,* 2007; Jahangiri *et al.*, 2014).

The Fischer-Tropsch (FT) synthesis is a catalytic reaction that has been used for decades as a method of producing synthetic fuels. Various raw materials can be used as a feedstock for the overall Fischer-Tropsch process these mainly are natural gas, coal and biomass. Waste with a high carbon content can also be used as feedstock (Jahangiri *et al.*, 2014). These raw materials are transformed through gasification or reforming into synthesis gas, a mixture of hydrogen and carbon monoxide. The synthesis gas is fed into the Fischer-Tropsch reactor where it is converted into (preferably) long chain hydrocarbons. The Fischer-Tropsch synthesis is catalyst-driven with the industrial catalyst based on either iron or cobalt as the catalytically-active material (Adesina, 1996; Arsalanfar *et al.,* 2014). Nowadays, cobalt seems to be the favoured catalytically-active material for the Fischer-Tropsch synthesis using hydrogen rich synthesis gas due to its high activity, resistance towards oxidation under reaction conditions and the low propensity to transform some of the carbon monoxide into CO_2 (Arsalanfar *et al.,* 2014; Khodakov *et al.,* 2007). Cobalt as the catalytically-active metal is predominantly supported on refractory oxides although other materials have been used as supports as well (Jahangiri *et al.,* 2014). The active metal may be promoted to improve its activity and/or selectivity.

The support is thought to aid in the dispersion of the catalytically-active material by maintaining the obtained dispersion under reaction conditions (Jahangiri *et al., 2014)*. It is thought to have no further effect on the performance of the catalyst in the Fischer-

Tropsch synthesis. Tauster and Fung (1978) first proposed that the support could interact strongly with active metal affecting the performance of the Fischer-Tropsch synthesis. This phenomenon was termed ‘strong metal-support interaction’. It was further shown that the metal-support interaction in reducible oxide supports behaved differently from those of irreducible oxide supports (Ahmadi *et. al.*, 2016; Pan *et al.* 2017). With reducible supports, it was observed that the hydrogen uptake diminishes, which was ascribed to the encapsulation of the active metal by the support or by the formation of irreducible mixed-metal oxides (Pan *et al.* 2017). The effect of irreducible supports on the Fischer-Tropsch activity has been suggested to be a result of electronic effects that could enhance the activity or result in deactivation (Ahmadi *et al.*, 2016; Pan *et al.* 2017).

The isolation of the effect metal-support interactions from other support parameters was realized by the preparation of inverse catalysts (Mogorosi *et al.*, 2012). The preparation of inverse catalyst involves the bonding of a support-like ligand to the active metal precursor. The bonding of the ligand is thought to occur through the hydroxyl groups on the surface of the active metal precursor. Recent studies have suggested that the adsorption of typical support precursors, such as tri sec-butoxide aluminium and tetraethoxysilane on the active metal results in the formation of support (oxide) islands (Macheli *et al*., 2018; Petersen *et al*., 2018). These islands on the active metal precursor may be a good model to mimic metal-support interactions.

Investigations of the effect of metal-support-interactions with silica supported cobalt catalysts have been reported previously (Johnson *et al.*, 2015; Macheli *et al.*, 2018). However, the effect of the oxidation state of the active metal precursor on the formation of metal-support interactions has not yet been tested. This work sought to elucidate formation of metal-support interactions in cobalt (II, III) oxide and cobalt (II) oxide and its effect on the activity and selectivity of the Fischer-Tropsch synthesis.

Chapter 2 Literature Review

The development of more efficient catalysts has been stimulated by increasing environmental and economic concerns (George, 1995). An efficient catalyst could facilitate the conversion of the reactants to the desired product(s) more selectively at lower reaction temperatures/pressures, while having an infinite lifespan. Since catalysts were developed empirically, a thorough understanding on the detailed functioning of catalysts is still lacking. This work focuses on the understanding of Fischer-Tropsch catalysts, which are used to convert synthesis gas (a mixture of hydrogen and carbon monoxide obtained from e.g. natural gas, coal, biomass or carbon containing waste) into long chain hydrocarbons, which can be converted into high quality diesel (Jahangiri *et al.*, 2014).

2.1. Fischer-Tropsch catalysts

The Fischer-Tropsch (FT) catalyst contains three components: the active phase, chemical and structural promoters (van Steen and Claeys, 2008; Arsalanfar *et al.*, 2014). Each of these components has an effect on the selectivity and activity of the Fischer-Tropsch synthesis although the promotors and the support are thought to be catalytically inactive on their own. The requirements of a good Fischer-Tropsch catalyst are high activity, high selectivity towards the desired products, easily accessible active sites of the catalysts to the reactants, suitable shape, strength and low cost involved in using the specific catalyst (Mogorosi, 2012).

Since the discovery of the formation of hydrocarbons from synthesis gas by Fischer and Tropsch, iron-based catalyst and cobalt-based catalyst are the only catalysts, which have been used in industrial application. However, nickel and ruthenium are known to also be catalytically-active for the Fischer-Tropsch synthesis (Arsalanfar *et al.,* 2014). With increasing reaction temperature, the selectivity changes to mainly methane with nickel (Schulz, 1999a). It should be noted that at low reaction temperatures, the rate of reaction is low, which may be countered by operating at high pressures. However, at elevated pressures nickel tends to form nickel carbonyl resulting in a continuous loss of the catalytically-active metal from the reactor (Steynberg and Dry, 2004). Although ruthenium catalysts are more active, it comes at a high cost (de Beer *et al.*, 2014) and its use is therefore not economically viable.

2.1.1. Iron-based Fischer-Tropsch catalysts

Iron is readily available and the cheapest catalytically-active metal for the Fisher-Tropsch synthesis. The catalytically-active phases of iron are metallic iron and iron carbides because of their ability to dissociate and hydrogenate carbon monoxide (Gracia *et al*., 2009).

There are two main directions that have been pursued with the iron catalyst. The first direction focuses on the production of low molecular weight olefins in an entrained phase or fluidised bed (Schulz, 1999a). This is done at relatively high temperatures (ca. 300-380°C). Due to the high reaction temperature and the low average molecular weight of the products, no liquid phase is formed under these reaction conditions. The other direction of iron catalyst development is aimed at producing wax at a low reaction temperature (ca. 245-285°C), where most hydrocarbons products are in the liquid phase (wax) (Li *et al.*, 2017). High quality diesel fuel can be produced by selectively hydrocracking the obtained wax from the Fischer-Tropsch process.

The low temperature Fischer-Tropsch process is hampered by low rates of reaction, experienced because of the rather low reaction temperature, which are necessary to obtain the high selectivity towards liquid hydrocarbons (C_{5+}). To offset the low rate of reaction, a high surface area of the catalytically-active phase is required. However, a high surface area leads to a weaker catalyst, therefore structural promotors or binders are essential to enhance the mechanical strength of the catalyst (Steynberg and Dry, 2004). The amount of the catalytically-active iron can be improved by improving the reducibility of iron catalysts, e.g. by the addition of copper as a promoter (Chonco *et al., 2013)*. Potassium is generally used as a chemical promoter for iron-based Fischer-Tropsch catalysts. It has been shown that potassium improves the activity and the selectivity to higher carbon numbers (Schulz and Claeys, 1999).

2.1.2. Cobalt as a Fischer-Tropsch catalyst

Cobalt-based Fischer-Tropsch catalysts operate in a narrow range of temperatures and give high yield of hydrocarbons, long life time and produce mainly linear alkanes in the middle distillate region and high molecular weight products (van der Laan and Beenackers, 1999). An increase in reaction temperature leads to a strong increase in the methane production (Khodakov *et al*., 2007). Thus, the activity and selectivity of the cobalt catalyst is highly dependent on the operating conditions.

The catalytically-active phase of the cobalt-based Fischer-Tropsch catalyst is metallic cobalt (Khodakov *et. al.*, 2007). Cobalt oxide phase has been known to be inactive in the Fischer-Tropsch synthesis (Khodakove *et al.*, 2007; Jahangiri *et al.*, 2014; Tsakoumis *et al.*, 2010). Cobalt is expensive (Jahangiri *et. al.*, 2014). Therefore, minimizing the cobalt content while obtaining a high metal surface area is important to increase the cost-efficiency of the catalyst. This is achieved by supporting cobalt on stable oxides having the required surface area and pore size distributions. Present catalyst design makes use of several preparation techniques, with the intention to produce a well-dispersed cobalt phase in a wide pore support remains the same (Schulz, 1999a; Schulz, 1999b). A common technique for catalyst synthesis is incipient wetness impregnation of the support with a cobalt salt solution in the appropriate concentration after which it is dried to remove solvent (Steynberg and Dry, 2004). The catalyst precursor is subsequently calcined to transform the cobalt salt into a less mobile precursor, e.g. cobalt oxide (Ling *et al., 2011)*. The catalyst precursor is finally reduced with hydrogen to its active metallic cobalt form (Garces *et al*., 2015).

The metal surface area increases with decreasing cobalt particle size (see Figure 2-1) as more active sites per catalyst mass will be available on the surface. Bezemer *et al*. (2006) showed that the turnover frequency (TOF) in the Fischer-Tropsch synthesis over cobalt impregnated on an inert support (carbon nanofiber to avoid metal-support interactions) decreased steeply for cobalt crystallite sizes smaller than 6 nm when the reactor is operated at 1 bar and at approximately 8 nm when the reactor is operated at 35 bar. This trend was confirmed by Borg *et. al.* (2008), Martinez and Prieto (2007), and Fischer *et al.* (2013). They all analysed cobalt particles ranging from 3 to 18 nm and observed that the activity and selectivity improved with increasing particle size remaining rather constant for particle sizes larger than 8 nm. A consequence of the increase in the turnover frequency with increasing crystallite size is a mass specific activity of the cobalt catalyst which passes a maximum upon changing the cobalt metal particle size (see Figure 2-1).

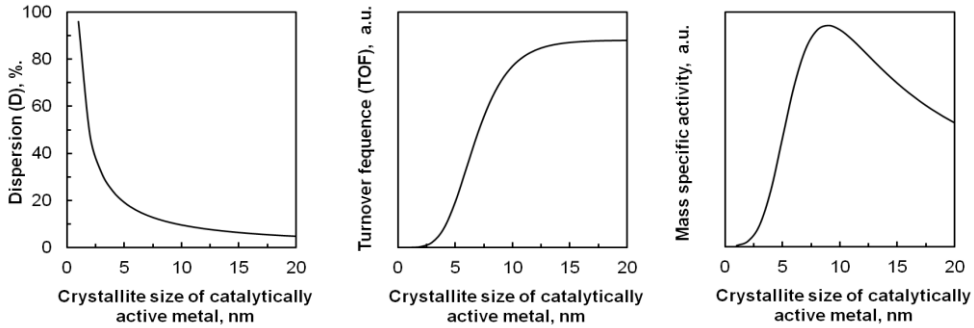

Figure 2-1: Schematic dependence of the dispersion, i.e. the number of surface atoms relative to the total number of atoms in a metallic cobalt crystallite (left), observed catalytic activity per surface atom in cobalt-based Fischer-Tropsch synthesis (Bezemer *et al.*, 2006; Fischer *et al.*, 2013) (centre), and the corresponding activity per unit cobalt mass (right) as a function of the cobalt metal crystallite size (re-created from de Beer *et al.*, 2014)

Supported cobalt catalyst are essential in the Fischer-Tropsch synthesis to produce long chain paraffin's which can be hydrocracked yielding diesel (Jacobs *et al*., 2002; Storsæter *et al*., 2005). They enable for a high conversion per pass to be attained with longer catalyst life time (Kababji *et al.*, 2009). High surface area supports such as metal oxides (SiO_2, TiO_2 and Al_2O_2) and carbon have been used for cobalt based Fischer-Tropsch synthesis. The role of the support has been to hold the active metal crystallites in place minimizing the extent of sintering. The support holds the active metal in place through the interaction that occur between the metal particles and the support at the interface. This interaction allows for the number of active sites to remain constant for longer durations maintaining a high metal surface area. The choice of support not only determines the number of active sites available but also affects the fraction of cobalt oxide species that can be reduced. The reducibility of cobalt oxide particles on a support have been shown to follow the order SiO_2 >TiO_2 >Al_2O_3 with cobalt on SiO_2 being the most reducible (Jacobs *et al*., 2002).The interaction that occurs between the support and the active metal not only reduces the possibility of sintering but also affect activity and selectivity of the catalyst.

2.2. Fischer-Tropsch synthesis

The Fischer-Tropsch synthesis is the catalytic hydrogenation of carbon monoxide over metal/metal carbide catalyst yielding long chain hydrocarbons.

2.2.1. Reaction stoichiometry

The Fischer-Tropsch synthesis is a complex set of reactions, with multiple pathways along which a wide range of organic products are formed. The main Fischer-Tropsch products are α-olefins and n-paraffins. Although the elementary chemical steps for the Fischer-Tropsch reaction are well-established, the overall reaction for the formation of olefins can be represented as:

$$CO + 2H_2 \rightarrow \frac{1}{n} C_n H_{2n} + H_2O \quad \Delta H_{R,\,270°C} = -154 \text{ kJ/mol CO}$$

Equation 2-1

The reaction conditions determine the hydrocarbon chain length and the branching that occurs (Khodakov *et al.*, 2007). There are two Fischer-Tropsch modes of operation that have been applied industrially: high temperature Fischer-Tropsch (HTFT) and low temperature Fischer-Tropsch (LTFT).

The high temperature Fischer-Tropsch is mainly used for the production of short chain chemicals and liquid fuels in the petrol range. Valuable chemicals like α-olefins can be extracted from the crude synthetic oil. The temperature range for the high temperature Fischer-Tropsch synthesis is 300 - 350 °C using an iron based catalyst and the reactor operated at 20 to 40 bar (Dry, 2002; Mogorosi, 2012).

The low temperature Fischer-Tropsch process (LTFT) operates within 200-240 °C temperatures and reactor pressure of 20-45 bar (Khodakov *et al.*, 2007; Jahangiri *et al.*, 2014). It is used for the synthesis of linear long-chain hydrocarbon waxes and paraffins. High quality sulphur-free diesel can be produced from these hydrocarbons via hydro-cracking (Khodakov *et al.*, 2007).

The water gas shift (WGS) is a well-known side reaction which may occur in parallel to the Fischer-Tropsch reaction resulting in the conversion of carbon monoxide into carbon dioxide.

$$H_2O + CO \rightarrow CO_2 + H_2 \quad \Delta H_{R,\,270°C} = -39.3 \text{ kJ/mol}$$

Equation 2-2

This side reaction is important for iron-based Fischer-Tropsch synthesis. The water gas shift reaction produces hydrogen, the high activity for the water gas shift makes

the iron-based Fischer-Tropsch catalysts flexible allowing the conversion of synthesis gas with a low H_2:CO feed ratio. A feed composition with low H_2:CO ratio can be adjusted in the reactor via the reaction of CO and H_2O, produced during the Fischer-Tropsch reaction, to form additional H_2 (Mabaso, 2005). However, the presence of this side reaction leads to lower carbon efficiency, in particular for a hydrogen-rich feed containing H_2/CO >2. Cobalt-based catalyst has almost no activity for the water gas shift under typical Fischer-Tropsch conditions (Tsakoumis *et. al., 2010)*.

At high temperature the Boudouard reaction results in the deposition of elemental free carbon in the catalyst particles. The activity of the catalyst may therefore decline as active sites for reaction are not available, if carbon is deposited on the surface (Steynberg & Dry, 2004; Mogorosi, 2012).

$$2CO \rightarrow CO_2 + C \quad \Delta H_{R,\,270^{\circ}C} = -172 \text{ kJ/mol}$$

Equation 2-3

2.2.2. Product distribution

The Fischer-Tropsch process produces predominantly alkenes, alkanes and a variety of minor components including a range of oxygenate compounds (Davis, 2001). Oxygen containing organic product compounds or oxygenates including 1-alcohols, aldehydes, ketones and carboxylic acids are minor product compounds (Rabiu *et al.*, 2012). A number of mathematical models have been developed to describe the product distribution in the Fischer-Tropsch synthesis. A complete predictive model for the Fischer-Tropsch product distribution is not available. Current models give guidelines as to how some reaction parameters can be expected to impact the kinetic steps involved and therefore on the final composition and product distribution (Schulz and Claeys, 1999b).

The high degree of order in the product distribution with repeating selectivity patterns on different carbon numbers fractions suggests a strict kinetic basis of this surface polymerization reaction with stepwise addition of a C_1 monomer species which is well suited for selectivity modelling (Schulz and Claeys, 1999b). The most basic model which assumes ideal chain growth with a C_1 monomer yielding one type of product, i.e. negating the formation of oxygenates and branched hydrocarbons, was developed by Anderson in 1984 based on the polymerization kinetics developed by Schulz and Flory (Steynberg and Dry, 2004; Mabaso, 2005). A basic growth scheme of the

polymerization taking place during the Fischer-Tropsch synthesis occurring at the surface of the catalyst is depicted in Figure 2-2.

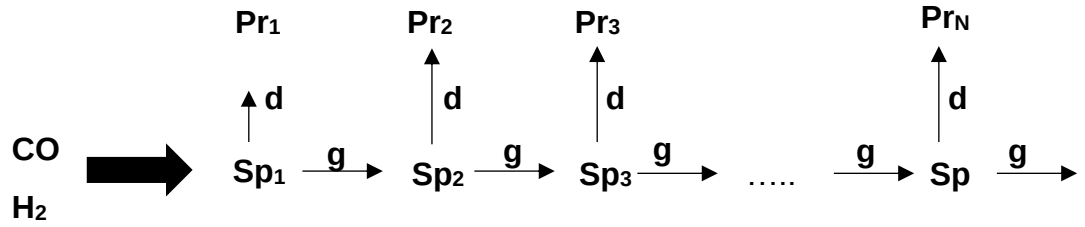

Figure 2-2**:** Schematic for chain growth and product formation assuming formation of one kind of product (Pr_N) (Schulz and Claeys, 1999b).

A single parameter, chain growth probability (α), is used to characterise the whole product distribution as a function of carbon number. The chain growth probability is defined as:

$$\alpha = \frac{r_g}{r_g + r_d}$$

Equation 2-4

where r_g and r_d are the rates of chain growth and desorption respectively (Schulz and Claeys, 1999b). When a steady state mass balance is conducted over all surface species, Sp_N, it results in the theoretical Anderson-Schulz-Flory (ASF) distribution (Tavakoli *et al.*, 2008; Schulz and Claeys, 1999a; Dry, 1996).

$$\log(x_N) = (N-1) * \log(\alpha) + \log(1\text{-}\alpha)$$

Equation 2-5

where x_N is the mole fraction of a product consisting of N carbon atoms in the fraction of organic products compounds. A semi-logarithmic plot of mole fraction of the product with N atoms in the organic product as a function of carbon number, should yield straight line where the slope represents the chain growth probability, if the Anderson-Schulz-Flory (ASF) distribution is being followed.

The Anderson-Schulz-Flory (ASF) model implies that a single reaction product can be only obtained in the Fischer-Tropsch synthesis when the chain growth probability is zero or one (see Figure 2-3). With high values of the chain growth probability, higher molecular weight products with a range of carbon numbers are anticipated. The

product range is divided into the following possible products: C_1 (methane), C_2-C_4 (gaseous hydrocarbons), C_5-C_{11} (hydrocarbons in the gasoline), C_{12}-C_{18} (hydrocarbons in the middle distillate/diesel range) and C_{19+} (wax) (Mabaso, 2005). The maximum selectivity that can be achieved according to the ideal Anderson-Schulz-Flory model is for methane 100 wt. % (α=0), C_2-C_4: 56.7 wt. % (α=0.464), C_5-C_{11}: 47.6 wt. % (α=0.764) and C_{12}-C_{15}: 24.3 wt. % (α=0.873). In order to maximize the diesel yield in XTL-process (taking any carbon containing feed and transforming into using the Fischer-Tropsch process to liquid hydrocarbons), the Fischer-Tropsch synthesis is optimised for the synthesis of waxes (α>0.9) which are subsequently cracked into diesel range.

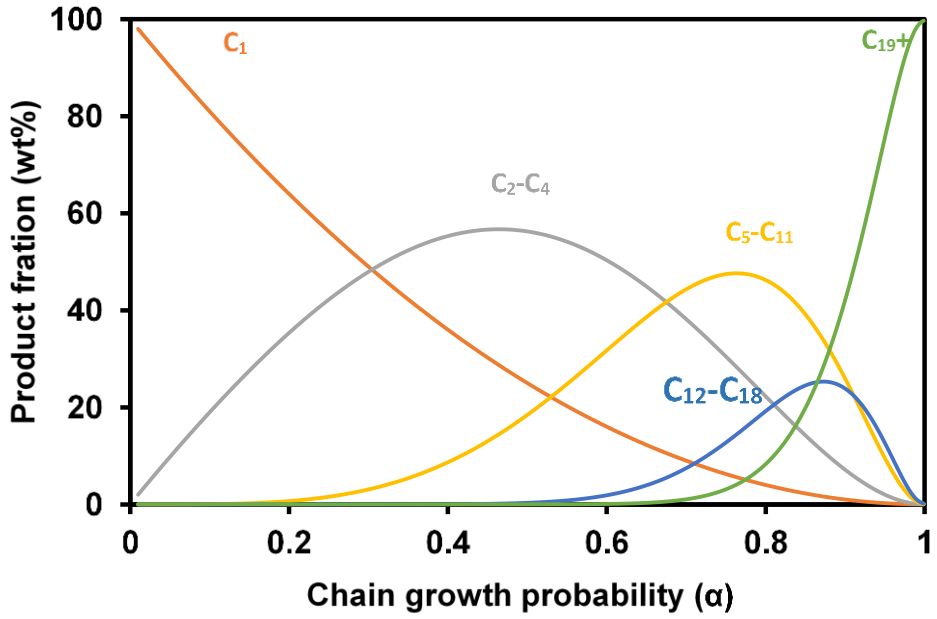

Figure 2-3: Product composition (wt. %) as a function of chain growth probability according to the ideal Anderson-Schulz-Flory (ASF) model

Three major deviations of the ideal Anderson-Schulz-Flory (ASF) model are typically observed in the experimental product spectrum of the Fischer-Tropsch synthesis (Kruit *et al.*, 2013; Tavakoli *et al.*, 2008). These deviations are (i) a higher than predicted methane selectivity, (ii) a lower C_2 selectivity than anticipated at all chain growth probabilities and (iii) a higher middle distillate/wax selectivity in low temperature Fischer-Tropsch. Since, especially at low temperature, the ideal ASF distributions are not obtained in the Fischer-Tropsch synthesis and the ASF model has been extended/modified to take into account the different products are present in the total product (Tavakoli *et al.*, 2008). For instance, Novak *et al*. (1982) incorporated

additional chain growth and desorption steps (via a combination of growing chains or additional cracking and chain growth via C_1 and C_2 monomers).

2.3. Metal-support interactions

The activity and selectivity of catalysts for the Fischer-Tropsch synthesis can be optimised through the improvement of the catalyst i.e. the active metal, the support material and the choice and level of promotors. The reactivity of the active metal nanoparticles is known to be affected by the shape, size, surface composition and oxidation state (Iglesia, 1997; Bezemer *et al.*, 2006; Cuenya, 2010; Liu *et al.*, 2017). As an illustration, the change in the particle size of the cobalt catalyst in the Fischer-Tropsch process has been shown have a critical size of 6 nm (at 1 bar) and 8 nm (at 35 bar) below which the turnover frequency (TOF) and the C_{5+} selectivity decreases (Bezemer *et al.*, 2006). The effect of particle size on catalytic performance has been attributed to size dependent change in the electronic structure and changes in surface structure at smaller particle sizes were different site are exposed (Bezemer *et al.*, 2006; Ahmadi *et al.*, 2016). The deconvolution of the parameter affecting the activity and selectivity of the Fischer-Tropsch synthesis is paramount in the understanding of their singular and collective impact. This can be achieved by the development of model catalyst systems that are studied under realistic reaction environments (Ahmadi *et al*., 2016).

The interaction between the support and the active metal is another parameter that affects the reactivity of nanoparticles. The basic function of the support is to anchor the active metal to prevent sintering which may lead to a loss of surface area on which the reaction occurs. The degree to which the active metal nanoparticles interact with the support depends on the type, structure and composition of the support *(*Olthof *et al.*, 2000; Jacobs *et al.*, 2002; Li *et al*., 2003; Bellido and Assaf, 2009). The interaction between the support and the catalytically-active metal may influence the catalytic activity by affecting the mechanical stability of the nanoparticles, modifying the morphology of the nanoparticles, inducing strain on the nanoparticles due to lattice mismatch, changing the electronic structure via charge transfer process and/or enabling spill-over of reactants/reaction intermediates from support to the nanoparticles (Ahmadi *et al*., 2016). The role of the support in the catalytic activity

must be understood in each reactive system in order be able to optimize the catalytic performance. In this work, particular interest is given to support induced changes to the catalytic properties of the active metal nanoparticles in the Fischer-Tropsch process.

Support induced changes to the catalytic properties occur when the catalytic performance is altered as a result of the support changing the chemical properties of the nanoparticles. The chemical properties of the nanoparticles can be changed through an electron exchange between partially reduced support and the metallic nanoparticle or with a bond between the (oxidic) support and the metallic nanoparticle which modify the adsorption/reaction properties of a metal (Riva *et al.*, 2000; Cargnello *et al*., 2012; Ahmadi *et al*., 2016). When an electronic exchange between the reduced support and the metallic nanoparticle occurs, the nanoparticle is encapsulated or forms irreducible metal-support complexes. Due to the decoration/encapsulation of the active sites with support atoms, the Fischer-Tropsch synthesis activity decreases. When a bond is formed between the (oxidic) support and the metallic nanoparticle a change in the nanoparticle structure is expected due to charge transfer from the support to the nanoparticle. These two mechanisms have been termed contact effect and ligand effect, respectively.

2.3.1. Contact effect

Partially reducible supports are generally known to experience the contact effect. The contact effect occurs at the interface where the active metal is in contact with the support (Mogorosi, 2012). Depending on the reduction conditions mixed-metal oxides can be formed or the support can creep on to the active metal and/or metal-support compounds can be formed (Ahmadi *et al.*, 2016; Bartholomew, 2001; Pan *et al.*, 2017). Creep of the support may be enhanced when oxygen vacancies on the partially reduced support are created during reduction, since this increases the surface energy. The support then creeps on the surface of the active metal to reduce the surface energy of the overall system (Pan *et al.*, 2017). Support creep on to the metal particle may result in a catalytically-active metal and/or precursor becoming encapsulated by the support, blocking access to the active metal and thereby prevent its reduction and the accessibility of the reactants to the catalytically-active site. Hence, the catalytic activity decreases as active sites are blocked by the support.

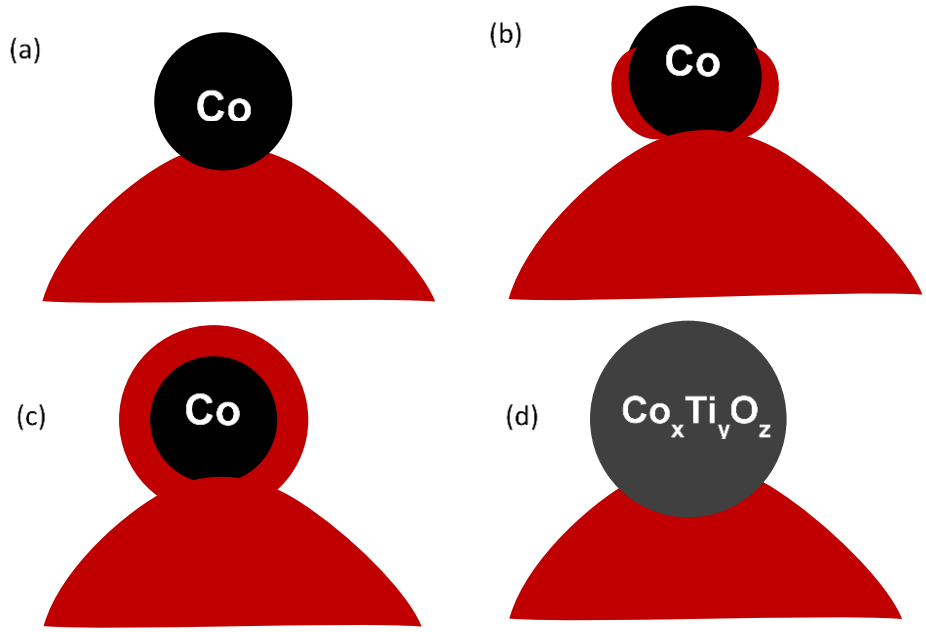

Figure 2-4: (a) metal particle on support, (b) creeping of support over metal surface, (c) fully encapsulated metal particle, (d) formation of metal-support compound

Reduction at high temperatures results in an increase in the degree of encapsulation of the active metal which lead to the formation of mixed-metal oxides (Bernal *et al.*, 1999). The mixed-metal oxides that are formed in the Fischer-Tropsch catalyst can cause permanent loss of activity because these compounds are hard to reduce (Tsakoumis *et al., 2010)*. This may be countered by an decrease in the temperature during the reduction, since it decreases the degree of incorporation (Bernal *et al.*, 1999).

2.3.2. Ligand effect

When an active metal is chemically bonded to the support it may induce the so-called ligand effect. The active metal may be anchored to the support material via a chemical bond. The anchoring of the active metal to the support is believed to be occurring at the interface where there is direct contact to the support. As the size of the active metal crystallites decreases, more active metal atoms will be exposed to the interface and may show a greater degree of metal-support interaction.

The formation of the bond between the active metal and the support may occur during catalyst preparation (Che, 1993; van Steen *et al.*, 1996). High calcination temperatures, reducing environment and activation of the support before metal loading are preparation steps that improve the degree of metal-support interactions (Dlamini

et al., 2002; Puska *et al.*, 2006). Calcination of the active metal and the support before they are mixed decreases the extent of interaction between the active metal and the support (Duvenhage and Coville, 2002; Puskas *et al.*, 2006; Puskas *et al.*, 2007). This is because it is believed that the interaction between the active metal and the support material is dependent on the concentration of surface hydroxyl groups.

The ligand bond formed between the support and the active metal is said to alter the electronic distribution of the surface metal atoms in the vicinity of the bond. An electronic donation or withdrawal occurs leading to a change in product selectivity. Improvement in catalytic performance is due to changing the adsorption/desorption properties. Ligand effect can also result in a change in the rate of deactivation by altering adsorption or desorption properties of the reagents/reaction products (Morales and Weckhuysen, 2006).

The ligand effect may be studied by synthesizing model systems, e.g. inverse catalysts (Mogorosi *et al.*, 2012). The preparation of inverse catalyst involves the bonding of a support-like ligand to the active metal precursor. The bonding of the ligand is thought to occur through the hydroxyl groups on the surface of the active metal precursor.

The bonding of manganese, alumina and silica support-like ligands on cobalt-based Fischer-Tropsch catalysts has been investigated previously (Morales *et al*., 2005; Johnson *et al*., 2015; Macheli *et al.*, 2018; Petersen *et al.*, 2018). It was shown through annular dark field imaging on TEM that during modification with manganese and alumina, the manganese oxide and aluminium oxide were distributed in small islands on the cobalt catalyst (Morales *et al*., 2005; Petersen *et al*., 2018). The bonding of silica on cobalt oxide has been reported to result in the formation of neso-silicates on the surface of the cobalt oxide nanoparticles (Macheli *et al*., 2018). These neso-silicates have a lower degree of polymerization than that of quartz and α-SiO_2, suggesting the formation of small silica islands on cobalt.

The presence of the small support-like clusters on the cobalt catalyst has been reported to decrease the reducibility of Co_3O_4 (Morales *et al*., 2005; Petersen *et al.*, 2018). A decrease in the reducibility of Co_3O_4 may result in low availability of metallic cobalt during the Fischer-Tropsch synthesis. Despite the lower reducibility of the modified catalyst compared to unmodified catalyst, an improved activity and an improved selectivity to higher carbon numbers was reported. Further investigations

where conducted to understand the mechanism of the promotional effect of the small manganese (Mn) clusters on the cobalt catalyst (Johnson *et al*., 2015). Cobalt catalyst modified with varying amounts of Mn was characterized using TPD and in-situ IR spectra. It was reported that the amount of strongly adsorbed CO species increased upon the addition on Mn and that with increasing Mn presence resulted in more adsorbed CO with weakened C-O bonds (Johnson *et al*., 2015). It was postulated that the MnO cluster/islands act as Lewis acids which results in a facile C-O bond cleavage due to the weakened C-O bond of adsorbed CO.

Through the use of inverse model catalysts (Macheli *et al*., 2018; Petersen *et al*., 2018) it was observed that supports may have a promotional effect on the active metal. They improve the activity and selectivity by decreasing the strength of adsorption of CO and dissociation energy of CO on the catalyst (Macheli *et al*., 2018). This promotional effect has been observed to plateau as the coverage of the active sites by the support increases (Macheli *et al*., 2018).

The formation of these small clusters/islands has been investigated only on Co_3O_4. In this work cobalt(II,III)oxide and cobalt(II)oxide will be modified to observe how metal-support interactions are formed and how they affect activity and selectivity of these catalysts in the Fischer-Tropsch synthesis.

2.4. Surface coordination chemistry

Heterogeneous catalysis is intimately associated with detailed surface structure of catalysts as it is a surface controlled process (Liu *et al*., 2017). Solid metal and metal oxides surface has different facets each of these facets have different coordination environments which result in different activation capabilities to reactants. The surface coordination environment for the two cobalt oxides that are known to be stable in ambient conditions are affected by the lattice structure. Cobalt monoxide (CoO) has rocksalt structure as depicted in Figure 2-5 with a lattice constant of 4.260 Å. It can be viewed as two interpenetrating FCC sublattices of Co^{2+} and O^{2-}, respectively. The thermodynamically stable cobalt oxide in air at room temperature is the normal spinel structure Co_3O_4 with lattice constant of 8.080 Å. This form has two types of Co ions, namely tetrahedrally coordinated Co^{2+} (II) and octahedrally coordinated Co^{3+} (III).

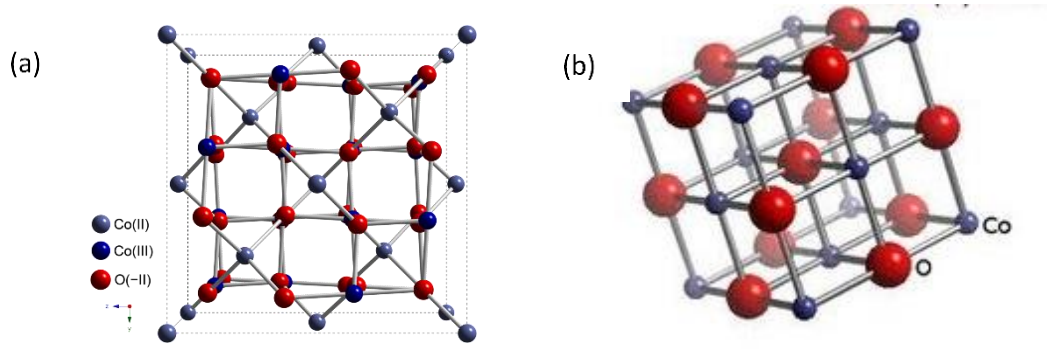

Figure 2-5**:** Lattice structure of (a) cobalt (II, III) oxide and (b) cobalt (II) oxide

The manner, in which the Co ions and/or O ions are arranged in the crystal structure, allow for different reaction sites to be available on the surface. Therefore, these materials can have different adsorption and catalytic properties.

Knowledge of the surface chemistry is necessary to gain an understanding of the adsorption processes (Blyholder and Wyatt, 1966). The surface chemistry of a cobalt surface is affected by its oxidation state. Reaction sites available on the surface differ with each oxidation state. This affects the manner, in which reactants interact with the catalyst surface. The characterization of surface interface between cobalt and the support can be conducted using electron-based spectroscopy such as X-ray photo-electron spectroscopy (XPS), ultraviolet photoelectron spectroscopy (UPS), auger electron spectroscopy (AES) and electron energy-loss spectroscopy (EELS) (Fu and Wagner, 2007). An understanding of the mechanism in which the alkoxysilane adsorbs on oxidized and metallic cobalt surfaces may yield insight on how metal-support interactions (MSI) are formed during catalyst synthesis.

The reaction of adsorbed ethanol on oxidized and metallic cobalt surfaces was investigated by Hyman *et al*. (2011). An analysis of the TPD-spectra indicated a different reaction path for the removal of adsorbed ethanol on the Co^0 and cobalt oxide surfaces. No desorption of molecular ethanol was observed from Co-foil. This suggests that ethanol adsorbs strongly on the Co^0 surface as an ethoxide species. Ethanol was observed desorbing from Co_3O_4 surface implying it is not strongly adsorbed on this oxide. However, the adsorbed ethoxide species seems to be more thermally stable on Co_3O_4 than on Co(II)O since the acetaldehyde is observed as a desorption product from Co_3O_4 at a higher temperature (by ca. 100K) than from Co(II)O.

The cleavage of the C-C bond in the ethoxide species was concluded to be facilitated more readily on Co^0 than on oxidized cobalt surfaces, since the desorption as CO and H_2 with increasing O_2 exposure shifted towards at a low temperatures in comparison to desorption from the oxide.

The adsorption of an alkoxide species occurs more readily on a metallic cobalt surface than a cobalt oxide surface. According to the Bronsted-Polanyi relationship the activation energy of reaction is directly proportional to the adsorption energy of the reactants. This makes the bond formed on an oxide surface much stronger. TEOS is a bulk alkoxide which would follow a similar adsorption mechanism as ethanol. Due to its bulk nature its adsorption on cobalt oxide would be significantly reduced in comparison to a metallic surface.

Chapter 3 Experimental

In this study, cobalt nanoparticles were synthesized and subsequently modified with silanes to understand the formation of metal-support interactions and their effect on catalytic performance of these materials in the Fischer-Tropsch synthesis. The model catalysts were characterized using X-ray diffraction, FTIR, TPR, CO-TPD and electron microscopy to determine morphology of the catalyst, elemental composition, the formation of a Co-O-Si bond and the effect of modification on reducibility.

3.1. Catalyst synthesis

3.1.1. Synthesis of cobalt nanoparticles

Cobalt nanoparticles were synthesized by the thermal decomposition of cobalt carbonyl ($Co_2(CO)_8$), (0.5 g; Sigma-Aldrich, moistened with hexane (1-10%) was mixed with 30ml benzyl ether (Sigma-Aldrich, 98%) in a round bottom flask. Trioctylamine (Sigma-Aldrich, 98%) (20 ml) was added to the solution. The solution was sonicated for 20 minutes to ensure complete dissolution of cobalt carbonyl. After sonication, 20 ml of oleylamine (Sigma-Aldrich, 70%) was added to the solution. This solution was placed in a heating mantle set at 220 °C and was swirled periodically by hand to ensure homogeneity of the mixture. Carbon monoxide gas was emitted at the onset of the thermal decomposition and light brown translucent colour appeared upon complete decomposition, which takes approximately 15 minutes. The round bottom flask was removed from the heating mantle immediately after complete reduction was observed in order to prevent further growth of the nanoparticles (NPs).

After cooling down to room temperature, the suspension was transferred to reagent bottles where the surfactants (trioctylamine and oleylamine) were washed off the cobalt nanoparticles using 300 ml of absolute methanol (Kimix, ≥99.8%). The particles dispersed in the methanol were allowed to settle at the bottom, after which the clear supernatant liquid was decanted. The washing process was repeated 6 times to ensure that most surfactants had been removed. After completion of the washing process the obtained particles were transferred into a 5 ml vial to be air dried in the fume hood for 4 hours.

The effect of annealing time and binary surfactants on the size and morphology of the cobalt nanoparticles was investigated. The above described synthesis method for cobalt nanoparticles was followed and the reaction contents were sampled at 20, 40 and 60 min during synthesis. The surfactant combination was changed to trioctylamine with octylamine and oleylamine with octylamine (Sigma-Aldrich, 99%).

3.1.2. Synthesis of Co_3O_4

The synthesized cobalt nanoparticles in a 5 ml vial were placed in an aerated fume hood for 48 hours in order to oxidize them. This transformed the material into Co_3O_4 as will be shown in Chapter 4

3.2. Modification of cobalt nanoparticles

The modification of the catalyst surface was achieved by using possible precursors of the SiO_2 support, i.e. tetraethoxysilane (TEOS) or triphenylethoxysilane (TPEOS). The self–condensation of the silica precursors during the modification of catalyst surface was controlled by diluting the silica precursor in a solvent. Using n-hexane as a solvent resulted in the formation of cobalt nanoparticles clusters. Hence, the solvent was changed to chloroform. The change in the solvent necessitated a change in the silane used and triphenylethoxysilane, which is soluble in chloroform was used.

3.2.1. Modification of cobalt nanoparticles *ex* cobalt carbonyl

Cobalt nanoparticles *ex* cobalt carbonyl were modified with triphenylethoxysilane (Sigma-Aldrich) (TPEOS) which was diluted in chloroform (Kimix, Analytical Reagent (AR)) (TPEOS was highly soluble in chloroform). Furthermore, nanoparticles can disperse well into chloroform possibly resulting in a more homogeneous adsorption on all nanoparticles. The concentration of TPEOS in the solution was varied from 0.2 to 1.5 mmol/l in 0.4 mmol/l increments to study the effect of the initial concentration on the silylation process.

The cobalt nanoparticles were dispersed in 50 ml of chloroform in a Schott bottle of 250 ml. A defined amount of TPEOS was weighed in and dissolved in 150 ml of chloroform. The TPEOS solution was then added to the nanoparticles in the Schott bottle. The suspension was sonicated for 3 hours to enhance contact between the modifying agent and the nanoparticles after which the nanoparticles were allowed to settle before the aliquot was decanted. The nanoparticles were washed twice with 300

ml of methanol in order to remove any residual TPEOS, which was physisorbed on to the nanoparticles. Methanol allows for different settling rates between the cobalt nanoparticles and the residual TPEOS.

3.2.2. Modification of oxidized cobalt nanoparticles

Oxidized cobalt nanoparticles were modified using TEOS diluted in n-hexane (Kimix, > 99%). The oxidized cobalt nanoparticles were synthesized from 0.5 g of $Co_2(CO)_8$ and it was assumed that all the cobalt carbonyl was converted to cobalt nanoparticles. After synthesis they were oxidized in the fume hood and thereafter dispersed in 200 ml of n-hexane. To the dispersed cobalt nanoparticles was added 50 ml of TEOS in solution of varied initial concentration (0.9 -7.2 mmol/l) to study its effect on the silylation process. The total volume of the dilute solution was 250 ml. The solution was stirred using a magnetic stirrer at 500 rpm for 24 hours. TEOS may react with hydroxyl groups on the cobalt oxide surface yielding Co-O-Si ligands (Honda *et al. 2001*; Mogorosi *et al.*, 2012; Macheli, 2014) as depicted in Figure 3-1. Thereafter the catalyst was allowed to settle at the bottom of the beaker and the supernatant liquid was decanted. The modified catalyst was washed 3 times with 200 ml of n-hexane to remove all unreacted TEOS from the surface of the particles. Thereafter the catalyst was transfers to a 5 ml vial then air dried in a fume hood.

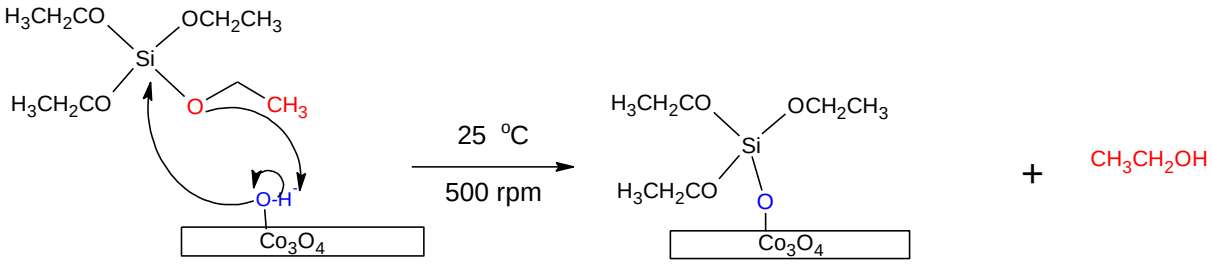

Figure 3-1: Adsorption of TEOS on cobalt oxide surface (Mogorosi *et al.*, 2012)

The rate of uptake of TEOS on the surface of the oxidized cobalt nanoparticles was determined by withdrawing 10 ml aliquot from the suspensions at regular intervals. The TEOS content in the aliquot was analysed using gas chromatograph (GC) HP6890 equipped with an FID. The procedure used for the GC-analysis of the residual TEOS in the solution is described in Appendix A1.

3.3. Catalyst support

The cobalt nanoparticles were supported on carbon black (Vulcan XC 72R, Fuel Cell Store; BET surface area: 240.2 m^2/g; BJH average pore size of 93 Å). A 10 wt.% catalyst was synthesized by weighing 0.1 g of cobalt nanoparticles in a 10 ml vial. Five millilitres of chloroform were added to the vial. The cobalt nanoparticles were sonicated for 10 min in order to disperse them in the chloroform. After which 0.9 g of carbon black was added into the vial and the vial was filled with chloroform. The vial was sonicated for 20 min before it was placed in the fume hood to evaporate chloroform.

3.4. Characterization of catalyst

3.4.1. X-ray diffraction

The phase composition and average crystallite size of the model catalysts, the reduced and the spent catalyst were measured using X-ray diffraction. XRD measurements were conducted in a Bruker D8 Advance operating at 35 kV and 40 mA using a Co sources ($\lambda_{Co\text{-}K\alpha}$= 1.79026 Å) and a LYNEYE-XE (1D mode) detector. Diffraction scans were collected in the range $20°<2\theta<120°$. All diffraction patterns were recorded in the step-scan mode with a step size of 0.05 degrees and a scan rate of 0.5 ^{o}/min. The observed diffraction lines were used to determine the crystalline phases by comparing them to known patterns from the JCPDS database using the search tool in EVA. The average particle size was calculated from themost intense diffraction line using the Debye-Scherrer equation written as:

$$\tau = \frac{K\lambda}{\beta cos\theta}$$

Equation 3-1

where

τ: mean crystallite size

K: dimensionless shape factor

β: line broadening at half the maximum intensity (FWHM)

Θ: Bragg angle

3.4.2. Fourier transform infrared spectroscopy (FTIR)

The presence of metal-support interaction (Co-O-Si) and surfactants in the modified catalyst before and after reduction was observed using FTIR spectroscopy. A wafer was prepared by first weighting 0.5 g of KBr and approximately 5 mg of unsupported cobalt nanoparticles on a mortar. A pestle was used to grind and mix the KBr and cobalt nanoparticles into a homogenous mixture. The mixture was then placed in a 7 mm diameter Pellet Die and then subjected to a 4 ton force in a press.

FTIR Nicolet 5700 spectrometer was used in transmission mode to obtain the IR spectra. The unmodified catalyst served as a baseline. The wafer was placed in the spectrometer and a total of 32 scans were taken in the range of 400 and 4000 cm^{-1} for each sample with a resolution of 4 cm^{-1}. A background scan was taken prior to every analysis. The occurrence of self-condensation of the tetraethoxysilane was monitored by observing its characteristic wavelengths at 800 cm^{-1} and 1080-1100 cm^{-1} (Huang & Chen, 2004; Yin *et al.*, 2009; Fouad *et al.*, 2011).

3.4.3. Temperature programmed reduction (TPR)

The reduction behaviour of the model catalyst was investigated using temperature programmed reduction in a quartz reactor on a Micromeritics AutoChem2920. The TPR was repeatedly calibrated using Ag_2O.

3.4.3.1 TPR calibration

Ag_2O was used as a standard for the TPR analysis because it was easily reduced. After loading 34 mg Ag_2O into the quartz reactor, the sample was degassed by passing Ar over the sample 50 ml_n/min and heat it to 120 °C using a heating rate of 10 °C/min. The reactor was then kept at 120 °C for 60 min before being cooled to 60 °C. The gas was then changed to a mixture of 5% H_2 in Ar (50 ml_n/min). The temperature was then increased to 250 °C at a heating rate of 10 °C/min. The sample being fully reduced was cooled to room temperature (see Appendix A3 for the model calculation to determine H_2 consumption).

3.4.3.2 RModel catalyst reduction behaviour

Approximately 30 mg of 10 wt.% Co catalyst (supported) was loaded and degassed with 50 ml_n/min (NTP) of He by heating it to 120 °C with a heating rate of 10 °C/min in order to remove moisture and other volatiles from the sample. The reactor was subsequently cooled to 60 °C before the gas was changed to 5% H_2/Ar (vol/vol) at a

flow rate of 50 ml_n/min (NTP). The temperature was ramped from 60 °C to 920 °C using a heating rate of 10°C/min.

3.4.4. Temperature programmed desorption of carbon monoxide

The desorption behaviour of carbon monoxide was analysed for all supported catalysts using Micrometrics AutoChem 2920. A quartz reactor was filled with 0.2 grams of supported catalysts. Hydrogen was fed into the quartz reactor at 50 ml_n/min. The temperature was increased from room temperature to 350 °C using a heating rate of 10 °C/min and kept at this temperature for 1 hour. The reactor temperature was decreased to 120 °C while feeding argon (50 ml_n/min) and was kept at 120 °C for an hour while degassing after which the temperature was decreased to 110 °C.

After the reactor was degassed, argon was kept as the carrier gas while 50 cm^3 STP/min of CO was pulsed into the reactor. A total of 15 CO pulses were completed at 5 min intervals between each other at 110 °C. The TCD signal of the CO pulse adsorption was recorded. The reactor was then degassed for an hour in argon at a rate of 50 ml_n/min to ensure all physisorbed CO was removed at 110 °C. The reactor temperature was ramped at a rate of 10 °C/min to 950 °C. During this time the TCD signal for CO desorption was recorded.

3.4.5. Transmission electron microscopy (TEM)

The cobalt nanoparticles were imaged using JEM200CX which was operated at 120 kV for the determination of their morphology and particle size. The nanoparticles were ultra-sonicated in chloroform (Kimix Analytical Reagent (AR)) for 10 min. The suspension was then added dropwise onto a carbon coated grid. A heat lamp (wattage) was used to evaporate the chloroform from the carbon grid. The nanoparticles were inserted into the microscope for viewing when they were dry. The image analysis tool (ImageJ®) was used to analyse the TEM images to determine the crystal size distribution. A minimum of 150 particles were analysed in each image in order to obtain the mean crystallite size while minimizing the error associated with the measurement.

3.4.6. Scanning electron microscopy (SEM) and Energy dispersive X-ray analysis (EDX)

The mass fraction of Si ligands on the as-synthesized and oxidized cobalt nanoparticles was determined using a scanning electron microscope (LEO S444 SEM,

La:Ka, UK) equipped with a Four Quadrant Back Scatter Detector and an energy dispersive Fission Kevex X-ray spectrometer (EDX). Sigma analysis software was used to determine the actual amount of Si on the as-synthesized and oxidized cobalt nanoparticles.

3.5. Fischer-Tropsch synthesis

A fixed bed reactor set-up was used to conduct the Fischer-Tropsch synthesis. The effect of the surface modification on the activity and selectivity of the model catalysts was monitored. The catalyst supported on carbon black (Vulcan XC 72R) (0.05 g of catalyst and 0.45 g of carbon black) was loaded onto the reactor and was reduced in-situ using hydrogen. After argon was used to pressurize the system, syngas was flown over the catalyst to start the synthesis. The reaction was carried out for 44 hours. The conversion was determined using the on-line GC equipped with a TCD and the organic compounds were analysed off-line with GC equipped with an FID to determine the product selectivity.

3.5.1 Fixed bed set-up

The Fischer-Tropsch synthesis was conducted in a fixed bed reactor set-up as shown in Figure 3-2. The gas streams (CO, H_2, N_2, and Ar) passed a filter to protect equipment downstream and then passed through mass flow controller. The mass flow controllers were used regulate the flowrate of the gasses into the reactor (calibration of mass flow controllers is given in appendix A3). Carbon monoxide and hydrogen are mixed to produce syngas with a H_2/CO ratio of 2. Argon was added in a pressure-controlled manner to the reactor and a needle valve in the exit line was used to control the reactor pressure. The reactor effluent was mixed using an in-line mixer with argon after the reactor together with the nitrogen which acts as an internal standard for the GC-TCD analysis.

The reactor feed was heated to 180 °C using an in-line heating element before entering the reactor. The temperature of the reactor was controlled using a feedback loop with a thermocouple in the centre of the catalyst bed. The reactor exit line and hot trap were maintained at 180 °C. The exit gas was sampled using gas ampoules for offline GC analysis. The wax trap further cools the exit gas before it can be split to the on-line GC for conversion analysis or discarded though the vent.

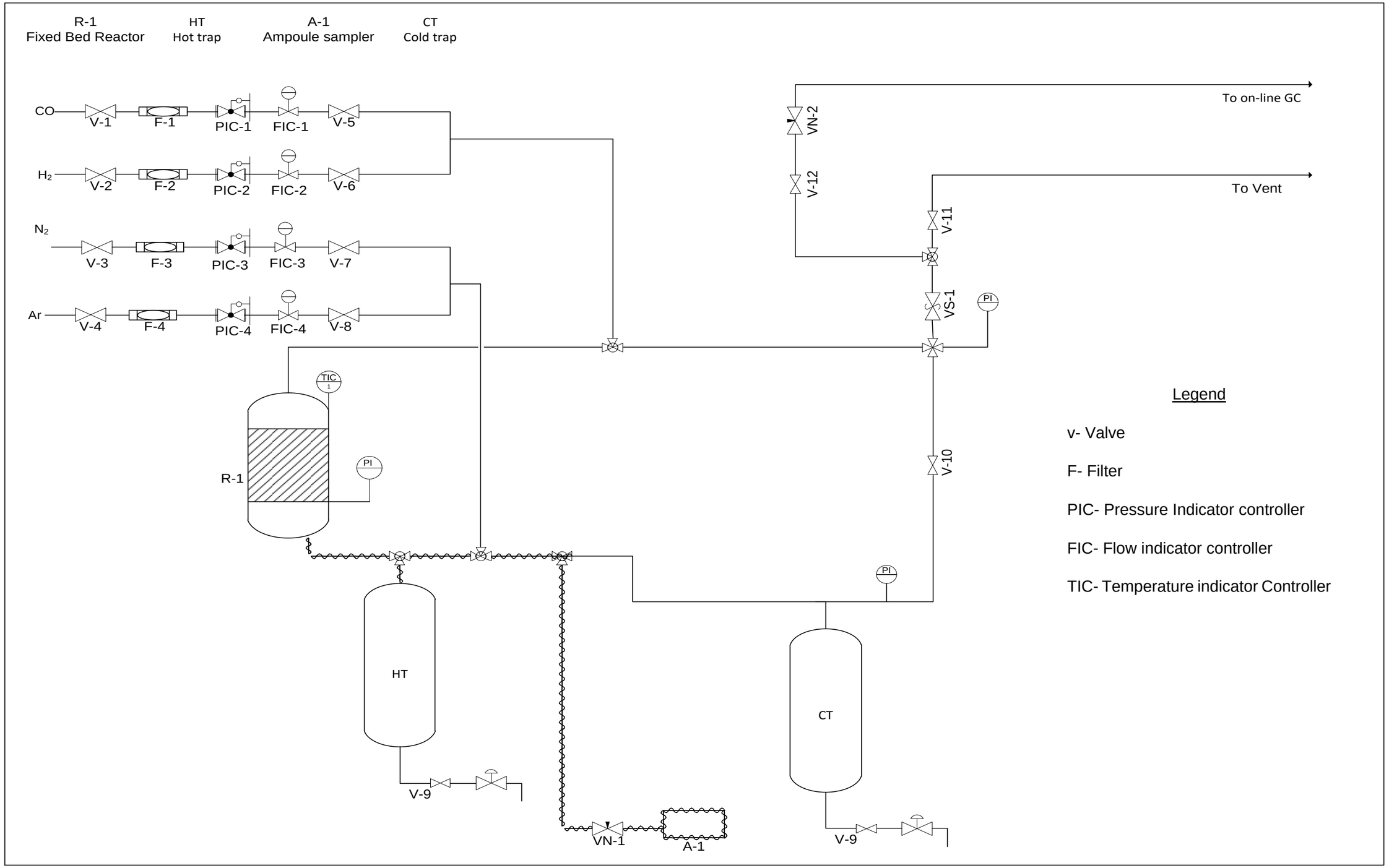

Figure 3-2: Fischer-Tropsch reactor set-up

3.5.2 Fischer-Tropsch synthesis

The reactor layout and packing are depicted in Figure 3-3. Glass wool was placed at the gas outlet and 5g of SiC was poured on the glass wool. The reactor was then loaded with 0.5 g of model catalyst (10 wt.% un/modified cobalt nanoparticles supported on carbon black Vulcan XC 72R) mixed with 5 g of SiC to improve heat transfer. SiC (5 g) was then poured on top of the model catalyst to ensure homogeneous heating on feed synthetic gasses.

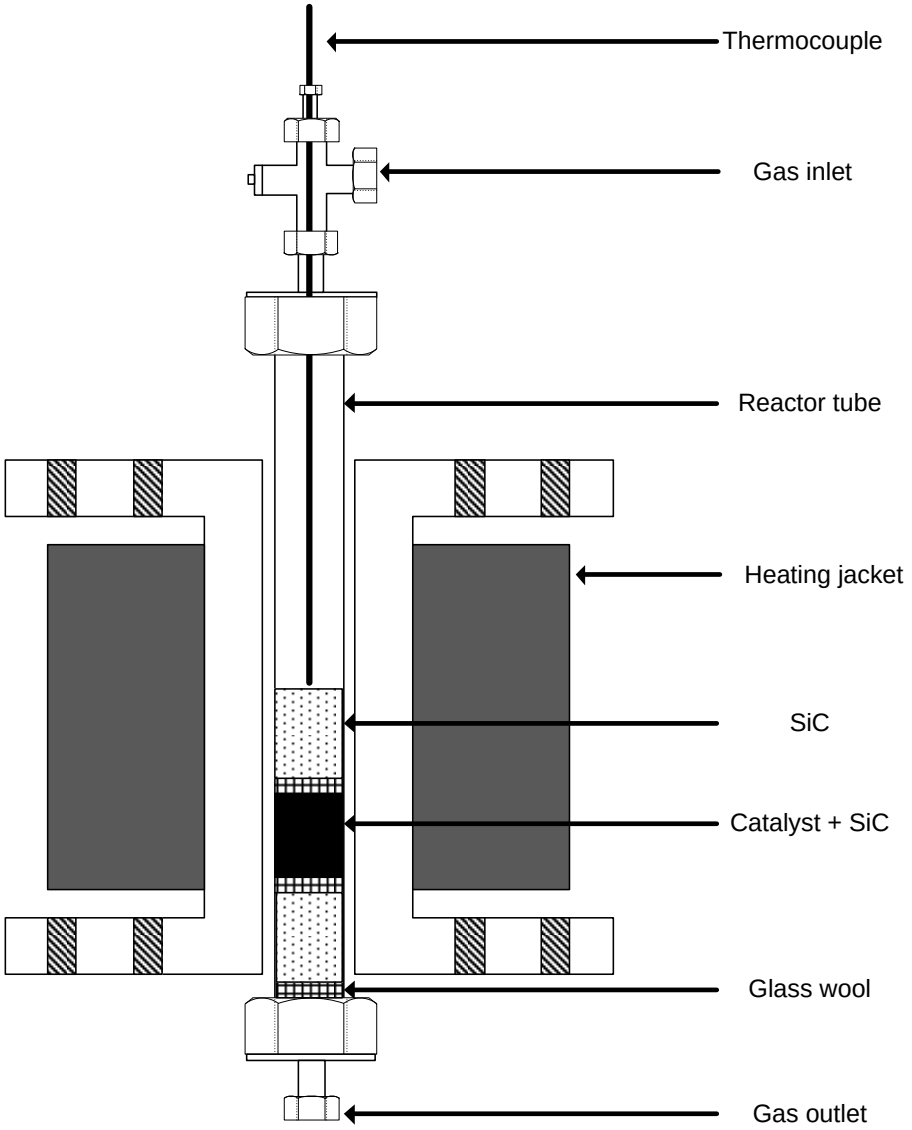

Figure 3-3: Packing of the fixed bed reactor

Prior to the reduction of the model catalyst a pressure test was conducted to ensure that there were no leaks on the rig. The connection points on the rig were tightened after which all the outlet streams in the pipeline network were closed. The pressure in

the reactor system was increased by flowing argon at the rate of 50 ml_n/min. When the reactor system had reached 20 bar, the argon flow was stopped, and inlet valves were closed. The system was left for 14 hours at high pressure to detect any leaks on the rig; the leak rate was considered to be negligible if the pressure drop was less than 1 bar over a period of 24 hours.

Metallic cobalt is known to be the active phase in the Fischer-Tropsch synthesis (Khodakov *et. al.*, 2007). Therefore, the model catalysts were reduced to the metallic state prior reaction. The reduction of the model catalysts to metallic cobalt was conducted in the reactor at 350 °C (heating rate of 10 °C /min) and 1 bar flowing hydrogen at a volumetric flowrate of 60 ml_n/min. Reduction was conducted overnight. The environment was kept under inert gas by passing argon over the catalyst when reduction had been completed.

After reduction was complete the reactor temperature was reduced to 220 °C. The temperature of the reactor feed line and hot wax trap were set to 180 °C. Mass flow controllers were used to set the flow rates for H_2 and CO at 40 ml_n/min and 20 ml_n/min, respectively. Nitrogen was used as a reference gas and its flow rate was set at 15 ml_n/min. The reactor bypass was used to analyse the composition of the feed gas into the system. The flow rates and feed ratio were confirmed by analysing 8 samples in the TCD. When the flow rates were consistent, the reaction was started by increasing the pressure of the reactor using Argon to 20 bar and switching the feed to the reactor. The online TCD and sampling ampoules were used for sampling the reactor products over a period of 44 hours. Samples of the reactor effluent collected in ampoules were then used in the FID analysis.

The reactor was switched-off after 44 hours on-line. The flow rate of N_2, H_2 and CO were turned off using mass flow controllers and inlet valves, while the argon flow rate was reduced to 5 ml_n/min. The argon flow was used to purge the system of any products that are in the pipelines. Thereafter the temperature of the reactor feed line, reactor and hot wax trap was set to 25 °C. While the temperature of the reactor decreased, the pressure of the reactor was slowly reduced to atmospheric pressure. When the reactor had completely cooled (usually overnight) the argon flow was stopped, and the spent catalyst was removed from the fixed bed reactor by shaking

the contents onto a weighing boat. Compressed air was used to blowout any catalyst particles that may have attached to the walls of the reactor.

3.5.3 Sampling

3.5.3.1 Online sampling

Inorganic gasses and methane were analysed using an on-line system. This system enables for the determination of the conversion of CO and for the methane selectivity.

A GC 7820A equipped with thermal conductivity detector (TCD) was used to analyse H_2, N_2, CO, CH_4 and CO_2 in the reactor effluent (nitrogen was used as an internal standard). It has 2 columns that are connected to one TCD: column 1 (Porapak Q) and column 2 (Molsieve 5A). In the first column CO_2 was separated from the other permanent gasses as it was cannot elute from the second column. The six way valve following the first column allows the other permanent gasses to go to the second column while the CO_2 goes directly to the TCD. The operating conditions of each column are given in Table 3-1. The TCD was calibrated using a reference gas (see Appendix A2).

Table 3-1**:** Analysis of the inorganic compounds and methane

	Column 1	**Column 2**
Compound analysed	CO_2	H_2, N_2, CH_4, CO
Column temperature (ºC)	70	70
Carrier gas	Ar	Ar
Inlet Pressure (kPa)	172.4	68.9
Injection time (ms)	10	-
Injection temperature (ºC)	200	200
Sampling time (s)	0.1	0.2
Column type	Porapak Q	Molsieve 5A

The molar flow of each component was determined based on the flow rate of the internal standard, nitrogen:

$$\dot{n}_i = f_i * \left(\frac{A_i}{A_{nitrogen}} \right) * \dot{n}_{nitrogen}$$

Equation 3-2

using the compound specific calibration factor, f_i (see Appendix A2).

The conversion of CO and the selectivity for CH_4 can then be determined as:

$$X_{CO} = 1 - \frac{\dot{n}_{CO,out}}{\dot{n}_{CO,in}}$$

Equation 3-3

$$S_{CH_4} = \frac{\dot{n}_{CH_4,out}}{\dot{n}_{CO,in} - \dot{n}_{CO,out}}$$

Equation 3-4

3.5.3.2 Offline sampling

Offline sampling was used to determine the composition of the organic product in the effluent. The product gas was sampled using heated glass ampoules. An evacuated ampoule glass with a capillary end was inserted into the product stream through a septum of the ampoule sampler. When the capillary was broken by the fork inside the ampoule sample vapour was drawn into the ampoule. The ampoule was partially withdrawn to expose the capillary and then sealed with a butane torch. This procedure is demonstrated in Figure 3-4.

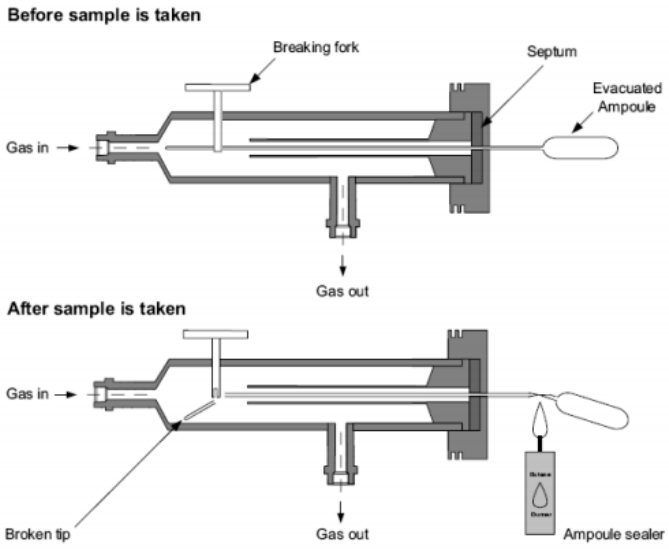

Figure 3-4**:** Ampoule sampling technique (adopted from Mogorosi, 2012)

A gas chromatograph equipped with a flame ionisation detector (FID) was used to analyse ampoule samples taken of the effluent during the Fischer-Tropsch synthesis. The gas chromatograph was operated at the conditions shown in Table 3-2.

Table 3-2: Operation conditions for GC equipped with FID for off-line analysis of reactor effluent

Detector	**Flame ionisation detector (FID), T= 200 °C**		
Column	Varian Capillary column 25m x 0.15mm		
	Stationary phase: dimethylpolysiloxane (film thickness: 2 µm)		
Carrier gas	Hydrogen		
Introduction gas	Nitrogen		
Column pressure	1.7 bar		
Injector	Split injector, T= 200 °C		
	Split ratio 1:10		
Temperature program	Rate (°C/min)	Step (°C)	Holding time (min)
	initial	-55	1.5
	10	0	1
	5	100	1
	2	120	1
	5	180	2
	5	200	3
	10	240	5
	20	310	10

The samples can be injected into the gas chromatograph through an ampoule breaker or injected directly onto the column with a GC syringe depending on the conversion of CO in the Fischer-Tropsch synthesis at the time of sampling. At high conversions the ampoule crusher was preferred because the carrier gas diluted the sample preventing over loading of the column. While at low conversions the direct injection on the column was preferred as dilution of the sample further would result in poor detection of the products. A model GC-FID trace is shown in Figure 3-5.

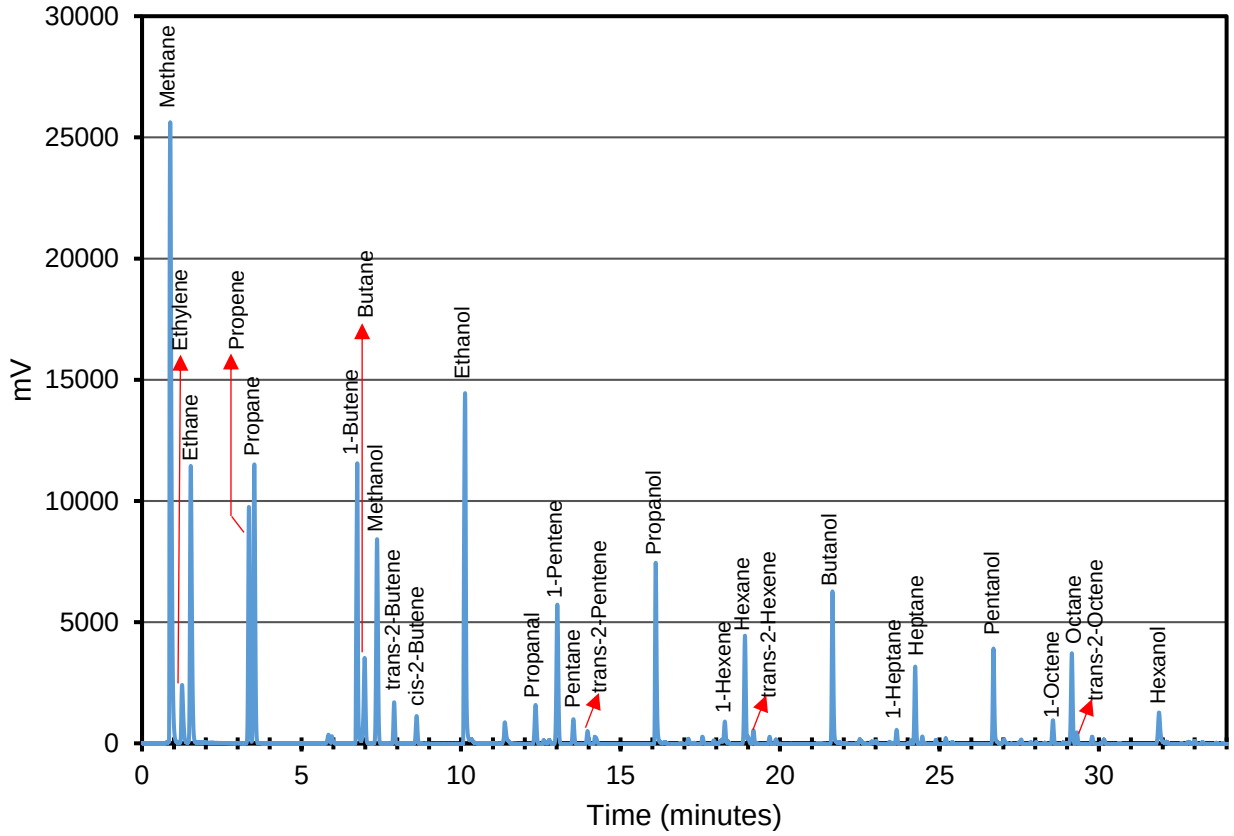

Figure 3-5: Model GC-FID trace for analysis of organic product compounds using flame ionisation detector.

A flame ionisation detector was used for the analysis of organic product compounds. The intensity of the signal obtained from the FID depends on the number of carbon atoms in the molecule and the number of carbons bonded to oxygen. A theoretical response factor was calculated using equation 3-5. An increment method was used to calculate the response factors for the different oxygenates. Increments of 1 were used for carbon atoms that have bonds with only hydrogen or other carbon atoms. Increments of 0.5 are given to carbon atoms with single bond with oxygen. While increments of 0 are given to carbons with double bond oxygen because they are not detectable by the FID.

$$f_i = \frac{N_{c,i}}{N_{C(noO)} + 0.55 * N_{c(attached\ to\ OH)} + N_{c(in\ C=O)}}$$

Equation 3-5

where

f_i: the response factor for compound i

$N_{c,i}$: total number of carbon atoms in compound i

$N_{C(noO)}$: number of carbon atoms without an oxygen bond

$N_{C(attached\ to\ OH)}$: number of carbon atoms attached to OH

$N_{C(in\ C=O)}$: number of carbon atoms in a carbonyl bond

In order to calculate the molar flow of the organic product compounds methane was used as the internal standard. Methane produced in the Fischer-Tropsch synthesis was also determined in the on-line analysis. The molar flow rate of the organic product compounds was calculated using Equation 3-6 and on a carbon basis Equation 3-7.

$$\dot{n}_i = \left(\frac{1}{N_i}\right) * \left(\frac{f_i A_i}{A_{methane}}\right) * \dot{n}_{methane}$$

Equation 3-6

$$\dot{n}_{i,C} = \left(\frac{f_i A_i}{A_{methane}}\right) * \dot{n}_{methane}$$

Equation 3-7

Where:

$\dot{n}_i$: molar flow rate of compound i

$\dot{n}_{i,C}$: molar flow rate of compound i on carbon basis

N_i: number of carbon atoms in compound i

f_i: response factor for compound i

A_i: peak area of compound i in the chromatogram

$A_{methane}$: peak area of methane in the chromatogram

$\dot{n}_{methane}$: molar flow rate in the reactor effluent as determined from the on-line GC-TCD analysis

Chapter 4 Results

4.1. Synthesis of cobalt nanoparticles

Cobalt nanoparticles can be synthesized by a variety of methods such as laser-induced vaporization condensation, thermal decomposition, gas vapour condensation and oxidation or reduction of a cobalt metal salts (Chen *et al.*, 2009). When chemical oxidation or reduction of a cobalt salt is used for the synthesis of nanoparticles, the morphological characteristics of the synthesized nanoparticles will be dependent on the solvent properties, reducing agent and the binding ligands (Staniuk *et al.*, 2014).

The synthesis of cobalt nanoparticles using reduction of a cobalt salt dissolved in an organic solvent occurs in three stages: increase in monomer concentration, nucleation and growth. The ions, atoms or molecules in the solvent are the monomers needed for nucleation. Nucleation is a process where a nucleus is formed. The nucleus is a site on which monomers can deposit on resulting in further growth (Camargo *et al.*, 2015). In order to synthesize monodispersed particles, the LaMer burst nucleation must be achieved. The LaMer burst nucleation refers to the instantaneous formation of a large number of nuclei followed by growth. No further nucleation occurs after the initial burst due to the significantly reduced concentration of monomers in solution (Thanh *et al.*, 2014; Camargo *et al.*, 2015). This allows for the separation of the nucleation and growth stages during synthesis yielding nanoparticles with a narrow size distribution. In order to attain the LaMer burst nucleation, supersaturation of the cobalt metal atoms (monomers) should be achieved through the conversion of soluble cobalt metal precursors.

Cobalt nanoparticles were synthesized using cobalt carbonyl, dissolved in an organic solvent, benzyl ether, in the presence of surfactants. The solution was heated to 220 °C using a heating mantle. The nanoparticles were separated for the reaction medium by flocculation and settling in ethanol. The effect of binary surfactants and annealing time on particle size, morphology, dispersion and oxidation state were also investigated during synthesis.

4.1.1 Effect of binary surfactants

The primary role of surfactants in a synthesis mixture is to stabilize the nanoparticles during synthesis (Jun *et al*., 2006). The binding affinity of surfactants on the surface of nanoparticles differs depending on the structure of the surfactant. Some surfactants bind strongly thus dictating the final size and morphology while some bind weakly, acting as on/off spectators and play a lesser role in the final morphological properties.

Trioctylamine and oleylamine were used as surfactants in the synthesis of cobalt nanoparticles. Trioctylamine is a bulky tertiary amine while oleylamine is a long chain primary alkylamine which acts as an electron donor at elevated temperatures (Mourdikoudis and Liz-Marzan, 2013). Figure 4-1 shows the TEM images of the as-synthesized Co nanoparticles sampled after a reaction time of 20, 40 and 60 minutes.

The Co nanoparticles were first sampled after 20 minutes of synthesis. The TEM shows a 2-dimensional image of 3 dimensional Co nanoparticles. The nanoparticles where observed to have a cubical and spherical morphology. There does not seem to be a dominant morphology in the first 20 minutes of synthesis. ImageJ® was used to determine the particle size distribution for the Co nanoparticles sampled after a reaction time of 20 minutes. The size of each nanoparticle was measured across the longest distance between its corners. A minimum of 150 nanoparticles were measured. A log-normal distribution was used to model the particle size distribution, from which the average particle size was determined to be 6.9 ± 2.5 nm.

The TEM images of the Co nanoparticles sampled after a reaction time of 40 minutes shows that there are both cubical and spherical particles. There were also a number of small particles for whom the morphology could not be determined unequivocally due to the magnification level used. The particles with a cubical morphology seem to dominate after a reaction time of 40 minutes. The particle size was measured using ImageJ® and particle size distribution modelled using a log-normal distribution. From the log-normal distribution, the average particle size after a reaction time of 40 minutes was determined to be 7.9 ± 2.8 nm. This implies that there was a slight increase in the average particle size from a reaction time of 20 minutes to a reaction time of 40 minutes. This suggests that further growth had occurred and there may have been additional nucleation occurring while other particles were growing.

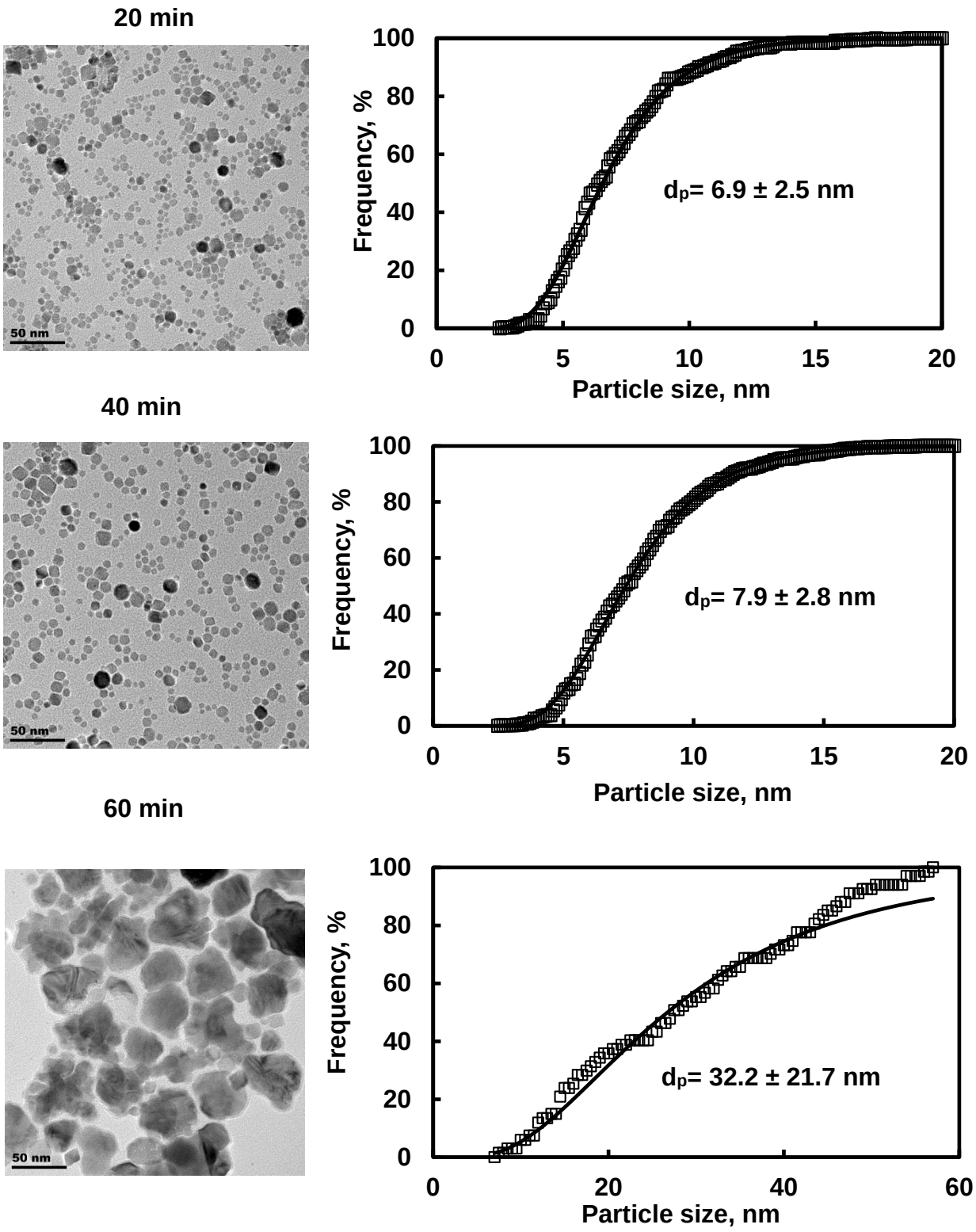

Figure 4-1**:** TEM images of Co nanoparticles synthesized with trioctylamine (TOA) and oleylamine (OA_m) mixture as surfactants and sampled after a reaction time of 20, 40 and 60 minutes

After a reaction time of 60 minutes, the TEM images show amorphous and cubic nanoparticles. The amorphous nanoparticles are thought to be formed through the

coalescence of smaller nanoparticles. The particle size was measured using ImageJ® and particle size distribution modelled using a log normal distribution. Using the log normal distribution, the average particle size after a reaction time of 60 minutes was determined to be 32.2 ± 21.7 nm. However, it can be seen that the particle size distribution does not look like a simple log-normal distribution, but rather a superposition of a number of log-normal distributions. The obtained particle size distribution may not be a result of poor mixing of the solution (by hand) during the synthesis of the nanoparticles as this was a unique outcome for this surfactant combination and reaction time.

In order to investigate the role of the surfactants, the surfactant combination was changed to trioctylamine and octylamine for the synthesis of cobalt nanoparticles keeping all other synthesis variables constant. The cobalt nanoparticles were sampled after a reaction time of 20, 40 and 60 minutes. The TEM images of the cobalt nanoparticles synthesized with trioctylamine and octylamine as surfactants are shown in Figure 4-2. The cobalt nanoparticles sampled after a reaction time of 20 minutes can be seen to have a cubical and spherical morphology. ImageJ® was used to measure the particle size for the cobalt nanoparticles sampled after 20 min of synthesis. The size of each nanoparticle was measured across the longest distance between its corners. A minimum of 150 nanoparticles were measured. A log-normal distribution was used to model the particle size distribution, determine the average particle size and standard deviation. The average particle size for the cobalt nanoparticles after a reaction time of 20 minutes was determined to be 4.6 ± 1.3 nm indicating a narrow size distribution. It was observed that some particles appeared to be darker on the TEM images. This could as a result of higher electron density which was caused by a number of particles on top of each other.

The TEM images of the cobalt nanoparticles sampled after a reaction time of 40 minutes shows that there are both cubical and spherical particles. Using the log-normal distribution the average particle size after a reaction time of 40 minutes was determined to be 6.0 ± 1.8 nm. A slight, but significant increase in the average particle size after a reaction time of 40 minutes compared to the average particle size after a reaction time of 20 minutes may imply either a slow growth of the crystallites, e.g. via Ostwald ripening during synthesis.

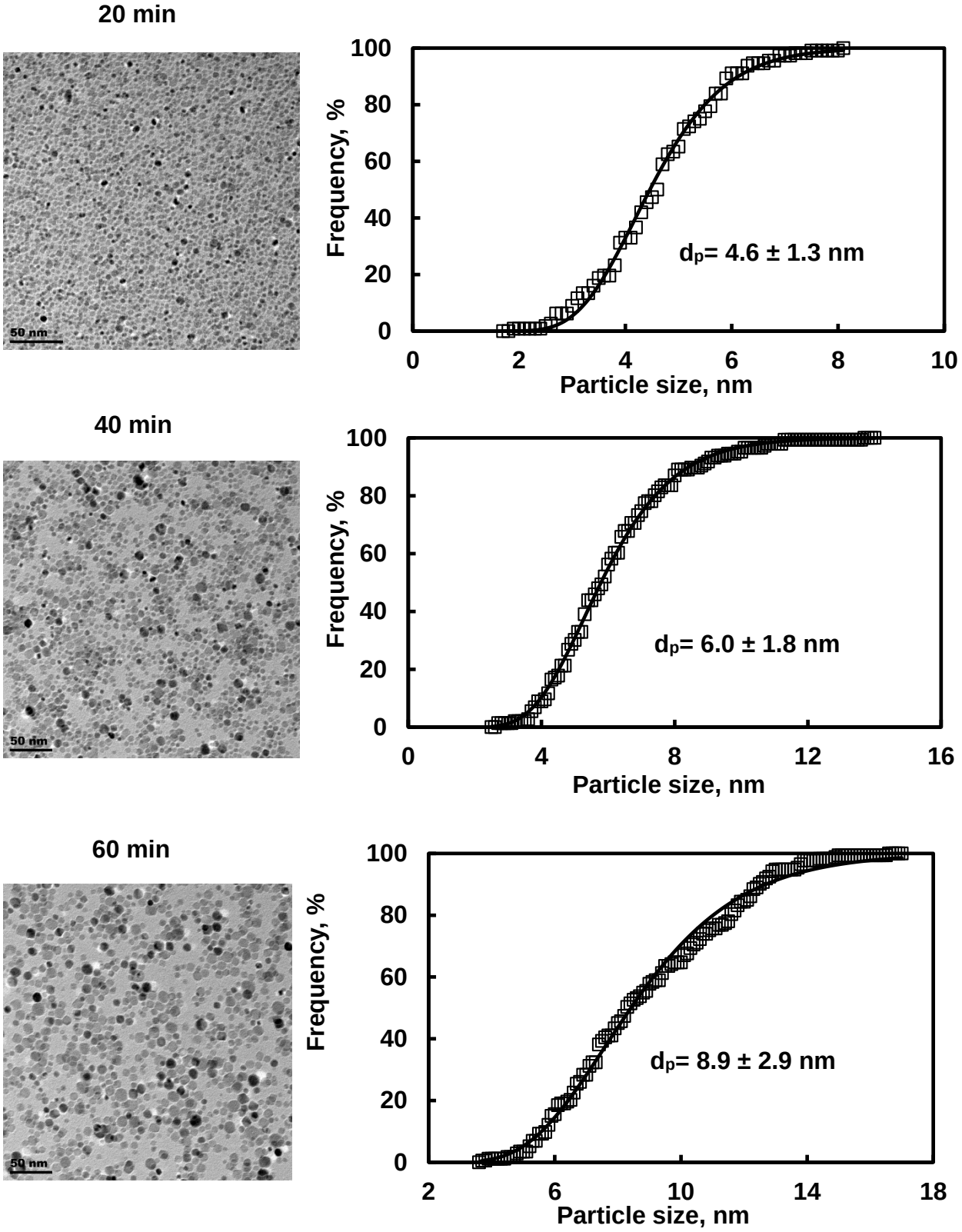

Figure 4-2**:** TEM images of cobalt nanoparticles synthesized with trioctylamine (TOA) and octylamine (OA) as surfactants sampled after various reaction times (20, 40 and 60 minutes)

After a reaction time of 60 minutes in the presence of trioctylamine and octylamine spherical and cubic nanoparticles are obtained as shown by the TEM-image (see Figure 4.2). The cubic nanoparticles were observed to be the dominant morphology. The particle size was measured using ImageJ® and particle size distribution modelled using a log-normal distribution. From the log-normal distribution, the average particle size after a reaction time of 60 minutes was determined to be 8.9 ± 2.9 nm indicating further growth.

The surfactant combination was then changed to oleylamine and octylamine for the synthesis of cobalt nanoparticles. The cobalt nanoparticles were again sampled after a reaction time of 20, 40 and 60 minutes. The TEM images of the cobalt nanoparticles synthesized with oleylamine and octylamine as surfactants are shown in Figure 4-3. The morphology of the cobalt nanoparticles sampled after 20 min could not be determined as the particles were too small. ImageJ® was used to measure the particle size for the cobalt nanoparticles sampled after 20 min of synthesis. A minimum of 50 nanoparticles were measured. A log-normal distribution was used to model the particle size distribution, from which the average particle size after a reaction time of 20 minutes was determined to be 2.4 ± 0.7 nm indicating a narrow size distribution.

The TEM images of the Co nanoparticles sampled after a reaction time of 40 minutes shows that there are both cubical and spherical particles. The particle size was measured using ImageJ® and particle size distribution modelled using a log normal distribution. Using the log-normal distribution the average particle size after a reaction time of 40 minutes was determined to be 4.9 ± 2.1 nm. The increase of 1.4 mm in the standard deviation of the particle size from a reaction time of 20 minutes to a reaction time of 40 minutes suggests that Ostwald ripening occurred during synthesis.

After a reaction time of 60 minutes, the TEM images show both spherical and cubic nanoparticles. The cubic nanoparticles were observed to be the dominant morphology. The particle size was measured using ImageJ® and particle size distribution modelled using a log-normal distribution. However, it can be noted that the particle size distribution deviates somewhat from the log-normal distribution. Using the log-normal distribution the average particle size after a reaction time of 60 minutes was determined to be 7.4 ± 2.3 nm.

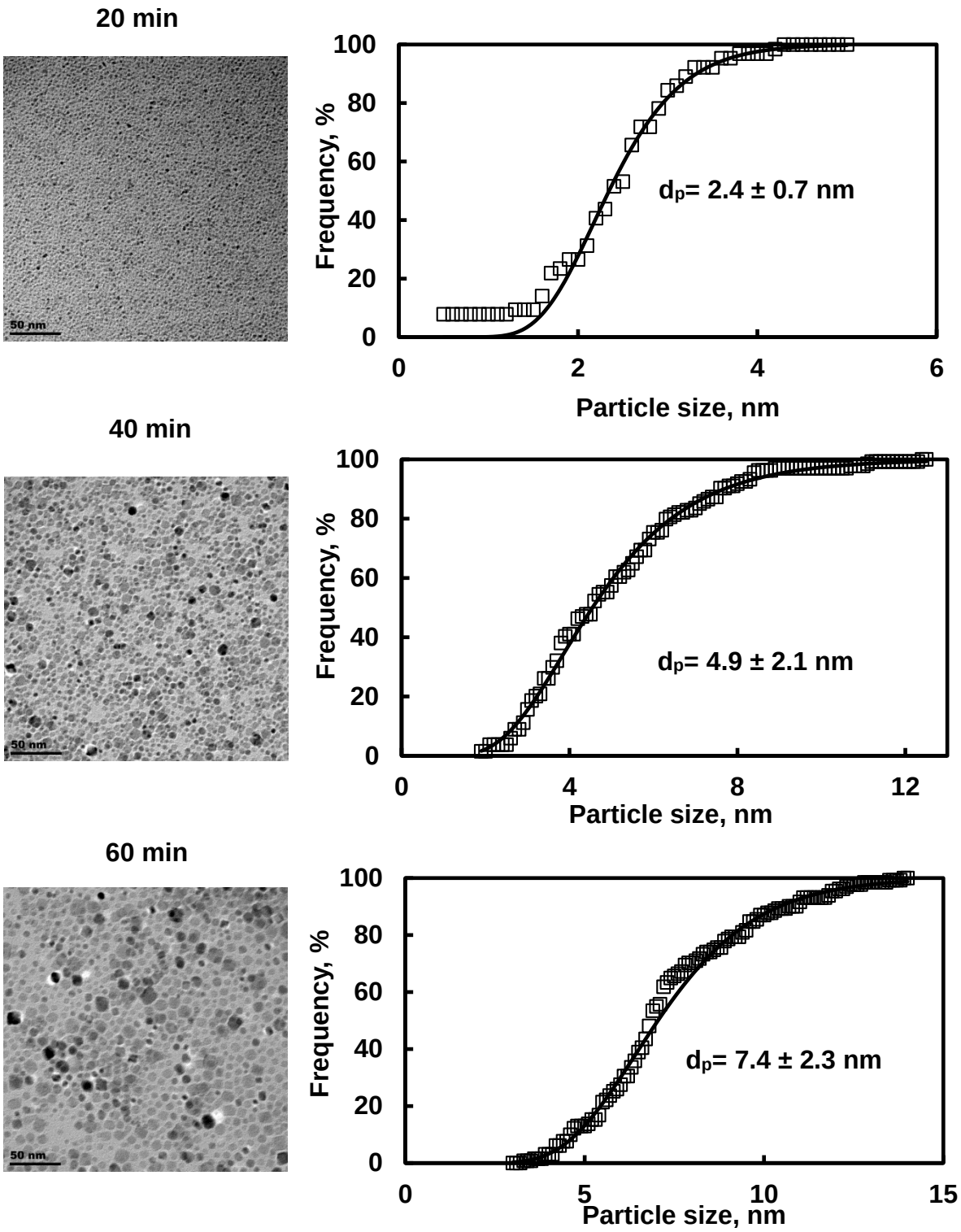

Figure 4-3: TEM images of cobalt nanoparticles synthesized with oleylamine (OA_m) and octylamine (OA) as surfactants sampled after a reaction time of 20, 40 and 60 minutes.

The surfactant combination used has been observed to affect the growth rate of the cobalt nanoparticles after nucleation as well as facile separation between the nucleation and growth stage (see in Figure 4-1 to Figure 4-3).

The use of organic solvents and surfactants during nanoparticle synthesis has the advantages of good control over crystal size and shape, easier controllability of growth parameters, good redispersibility and low agglomeration tendency (Pinna and Niederberger, 2008; Jun *et al.*, 2006). The low agglomeration tendency was due to the improved colloidal stability in the presence of surfactants. Although the agglomeration tendency was reduced by the surfactants, a large amount of organic impurities remain which restrict accessibility of the nanoparticle surface (Pinna and Niederberger, 2008).

Surfactants with high binding affinity can remain on the surface of the nanoparticles even after several washes. In order to understand the binding affinity of the used surfactants, FTIR spectrum of the surfactants and the as-synthesized cobalt nanoparticles was recorded (see Figure 4-4; note the as-synthesized cobalt nanoparticles were washed 6 times with methanol).

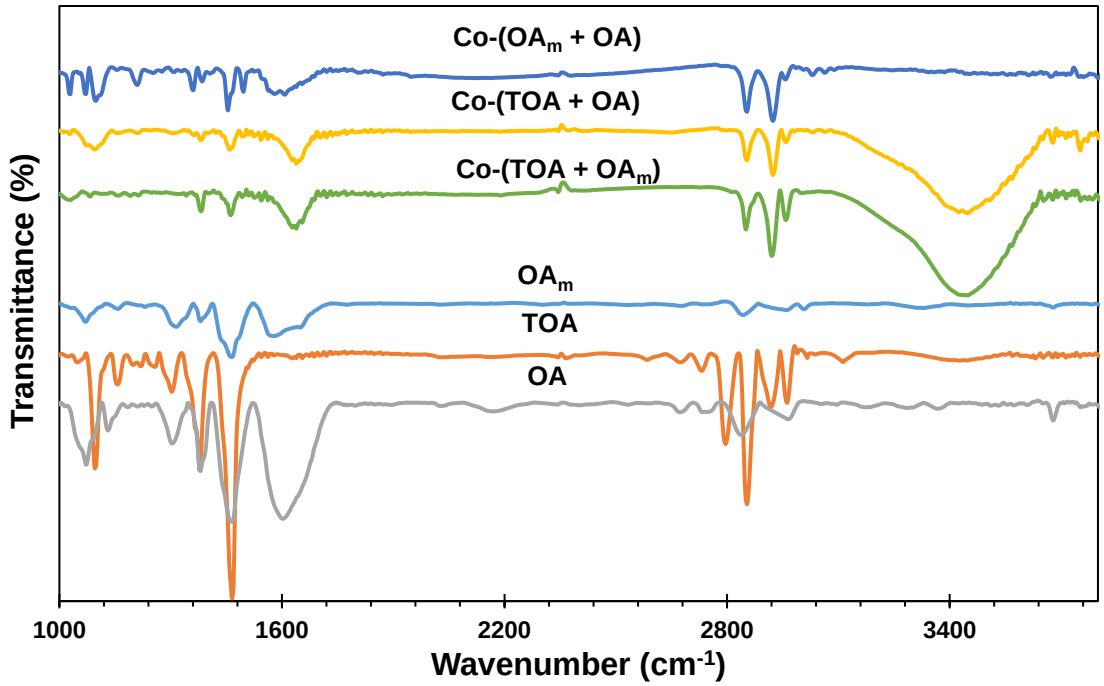

Figure 4-4: FTIR spectra of surfactants and cobalt nanoparticles synthesized with various binary mixtures of surfactants after a reaction time of 20 minutes after washing with 6 times with methanol (OA: octyl amine; TOA: trioctylamine; OA_m: oleylamine)

Oleylamine and octylamine are primary amines with asymmetrical, symmetrical and bending NH_2 vibrations (see Fig. 4-4 and Table 4-1). These vibration frequencies were not observed with the tertiary amine, trioctylamine. Oleylamine has a double bond, which shows its characteristic vibrational frequencies at 1647 cm^{-1} and 3006 cm^{-1}. There vibrations were unique to oleylamine.

Table 4-1**:** FTIR vibrational modes (cm^{-1}) and their assignment for the surfactants oleylamine, octylamine and trioctylamine.

Vibrational modes	Oleylamine	Octylamine	Trioctylamine
$\boldsymbol{v_{as}(NH_2)}$ **and** $\boldsymbol{v_s(NH_2)}$	3376 cm^{-1} 3300 cm^{-1}	3367 cm^{-1}, 3305 cm^{-1}	
$\boldsymbol{\delta(=C-H)}$	3006 cm^{-1}		
$\boldsymbol{v_{as}(C-H)}$ **and** $\boldsymbol{v_s(C-H)}$	2922 cm^{-1} 2854 cm^{-1}	2681-2970 cm^{-1}	2731-2966 cm^{-1}
$\boldsymbol{\delta(-C=C)}$	1647 cm^{-1}		
$\boldsymbol{\delta(NH_2)}$	1593 cm^{-1} 795 cm^{-1}	1612 cm^{-1}	
$\boldsymbol{\delta(CH_3)}$	1465 cm^{-1}	1458 cm^{-1}	1466 cm^{-1}
$\boldsymbol{\delta(C-N)}$	1071 cm^{-1}	1076 cm^{-1}	1095 cm^{-1}
$\boldsymbol{\delta(C-C)}$	722 cm^{-1}		

v_{as} = asymmetric stretching vibrations; v_s = Symmetrical stretching vibration; δ = bending vibration

In Figure 4-4 also shows the FTIR-spectra of synthesized cobalt nanoparticles with a combination of surfactants after washing with methanol. The nanoparticles prepared with a mixture of trioctylamine and octylamine or a mixture of trioctylamine with oleylamine show a clear absorption bands at ca. 1600 cm^{-1} and 3440 cm^{-1}.These bands are characteristic of N-H bending and stretching, but could also be attributed to OH bending and stretching. The amines do not show a strong absorption band at 3440 cm^{-1}. Hence, this band may be attributed to O-H stretching. It might thus be concluded

that these nanoparticles contain surface OH species on the surface of the nanoparticles. During the synthesis of the cobalt nanoparticles there are no O-H or O containing species in the reaction medium therefore it was not anticipated that there would be O-H species on the surface of the catalyst. However, even short time exposure of these particles to air may result in oxidation, which upon exposure to water vapour may result in the formation of surface O-H species on the surface of the nanoparticles.

The FTIR spectrum of the cobalt nanoparticles synthesized with oleylamine and octylamine shows absorption bands at 1600 cm^{-1} and a shoulder at 1645 cm^{-1} but no absorption bands at around 3440 cm^{-1}. This was indicative of the presence of NH_2 and C=C vibrations. This suggests that oleylamine was present on the surface of the cobalt nanoparticles.

The presence of NH_2 absorption bands on the synthesized cobalt nanoparticles after 6 washes indicates the presence of either octylamine or oleylamine on the surface of the particles. It indicates the presence of oleylamine, if this was associated by the presence of absorption bands attributable to C=C bending, but it does not negate the presence of either octylamine or trioctylamine on the surface of the nanoparticles.

The nanoparticle surface needs to be free of surfactants and have low agglomeration tendency in order to effectively modify it with silicates. A surfactant-free nanoparticle surface that has low agglomeration tendency could not be achieved with this synthesis method. However, it was decided that 6 washes with methanol should have removed the surfactants on the nanoparticle surface to a sufficiently low concentration allowing surface modification while minimizing agglomeration.

4.1.2 Effect of synthesis time

Cobalt nanoparticles were synthesized using three binary surfactant combinations. In all three cases, the reactor was sampled after a reaction time of 20, 40 and 60 minutes to elucidate the effect of reaction time on the crystallite size and shape. The effect of reaction on the average crystallite size is shown in Figure 4-5. The crystallite size increases linearly with increasing reaction time for all surfactant combinations, with the exception between a reaction time of 40 and 60 minutes for the nanoparticles synthesized with a mixture of trioctylamine (TOA) and oleylamine (OA_m) during which time agglomeration was observed. The linear growth rate constant, k, can thus be

obtained from the slope of the average particle size as a function of reaction time. The intercept, I, might be a measure for the size of the nucleus. The surfactant mixture affects both the linear rate constant, k, and the intercept, I (see Table 4-2). The linear growth constant, k, was the smallest during the initial phase of growth for cobalt nanoparticles synthesized in the presence of trioctylamine (TOA) and oleylamine (OA_m), whereas the linear growth constant was approximately the same for cobalt nanoparticles synthesized with combination of trioctylamine (TOA) and octylamine (OA) as well as octylamine (OA) and oleylamine (OA_m). Interestingly, the intercept was the largest for the growth for cobalt nanoparticles synthesized in the presence of trioctylamine (TOA) and oleylamine (OA_m). This may imply that the initial nuclei are rather large, but do not grow fast (until agglomeration sets in after a reaction time of 40 minutes). The replacement of one of these amines with octylamine results in a smaller intercept (possibly indicating smaller nuclei), but faster linear growth rates.

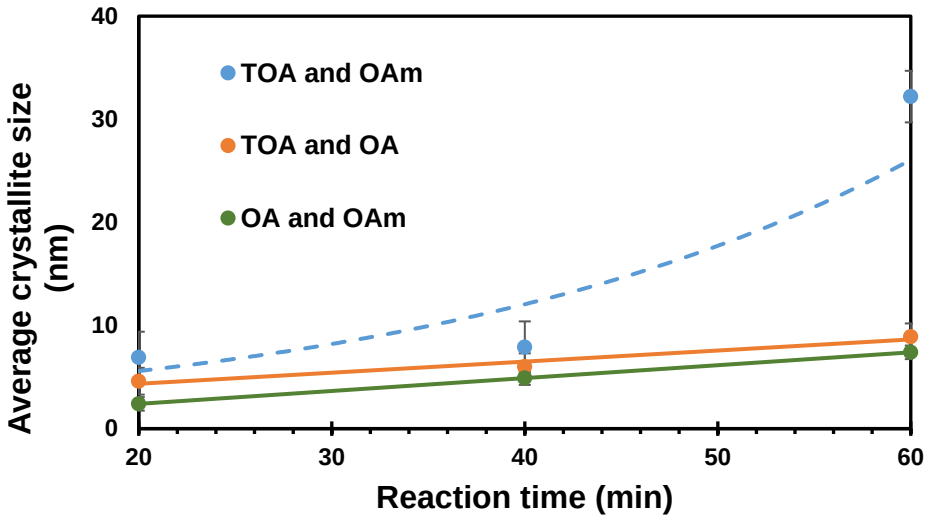

Figure 4-5**:** Effect of reaction time on the average particle size of cobalt nanoparticles

Table 4-2**:** Growth kinetics of cobalt nanoparticles in the presence of surfactants.

Surfactant mixture	k, nm/min	I, nm	R^2
Trioctylamine (TOA) + oleylamine (OA_m)[1]	0.05	5.9	-[1]
Trioctylamine (TOA) + octylamine (OA)	0.11	2.2	0.9610
Octylamine (OA) + oleylamine (OA_m)	0.12	0	0.9997

[1]: Only taking into account the data after a reaction time of 20 and 40 minutes and hence R^2 is meaningless

4.2. Characterization of as-synthesized cobalt nanoparticles

The as-synthesized cobalt nanoparticles were synthesized using organic surfactants and surfactant. It had been observed that not all of the organic surfactants can be removed from the surface of the particles by washing as shown in 4.1.1. The used organic surfactants are hydrophobic as they contain non-polar long carbon chains which repel water molecules. A nanoparticle surface, which was partially covered with the organic surfactant, will become more hydrophobic.

Tetraethoxysilane (TEOS) is a hydrophilic compound. When TEOS interacted with the hydrophobic oxidized cobalt nanoparticles during modification, the formation nanoparticles clusters were seen (see Figure 4-20). The silica precursor was changed to non-polar compound triphenylethoxysilane (TPEOS) and the modification technique was changed for the as-synthesized cobalt nanoparticles to prevent agglomeration during modification.

4.2.1 Silylation of as-synthesized cobalt nanoparticles

The silylation of as-synthesized cobalt nanoparticles using triphenylethoxysilane, TPEOS, was conducted at room temperature. The as-synthesized cobalt nanoparticles were kept in contact with the modifying agent TPEOS for three hours through vigorous mixing in a sonicator while suspended in chloroform. The resultant Si/Co ratio after modification of the as-synthesized cobalt nanoparticles was determined using EDX. The minimum detection limit typically varies for different elements however it was generally understood that the detection limit was 0.1 wt %.

The as-synthesised cobalt nanoparticles after modification in an infinite dilute TPEOS solution with initial concentration of 0.9 mmol/l were observed using scanning electron microscopy (SEM) (see Figure 4-6). The nanoparticles are observed to be in flakess of different shapes and sizes. Five area on the flakess were selected for elemental analysis and the average species wt% was reported. The Si content in the as-synthesised cobalt nanoparticles after modification in an infinite dilute TPEOS solution with initial concentration of 0.9 mmol/l was below the detection limit of the scanning electron microscope.

The as-synthesised cobalt nanoparticles after modification in an infinite dilute TPEOS solution with initial concentration of 0.34 mmol/l were observed using scanning electron microscopy (SEM) (see Figure 4-6). The nanoparticles are observed to be in

filings of different shapes and sizes. Five area on the flakess were selected for elemental analysis and the average species wt% was reported. The Si/Co ratio in the as-synthesised cobalt nanoparticles after modification in an infinite dilute TPEOS solution with initial concentration of 0.34 mmol/l was 13 ± 2 mmol/mol.

The as-synthesised cobalt nanoparticles after modification in an infinite dilute TPEOS solution with initial concentration of 0.51 mmol/l were observed using scanning electron microscopy (SEM) (see Figure 4-6). The nanoparticles are observed to be in flakes with a rough topical surface. At the edge of the flakes there are fillings of different sizes and shapes. Five area on the flakess were selected for elemental analysis and the average species wt% was reported. The Si content in the as-synthesised cobalt nanoparticles after modification in an infinite dilute TPEOS solution with initial concentration of 0.51 mmol/l was below the detection limit of the scanning electron microscope.

The as-synthesised cobalt nanoparticles after modification in an infinite dilute TPEOS solution with initial concentration of 1.64 mmol/l were observed using scanning electron microscopy (SEM) (see Figure 4-6). The nanoparticles are observed to be agglomerates of various sizes and shapes. Five area on the stub were selected for elemental analysis and the average species wt% was reported. The Si/Co ratio in the as-synthesised cobalt nanoparticles after modification in an infinite dilute TPEOS solution with initial concentration of 1.64 mmol/l was 18 ± 1.8 mmol/mol.

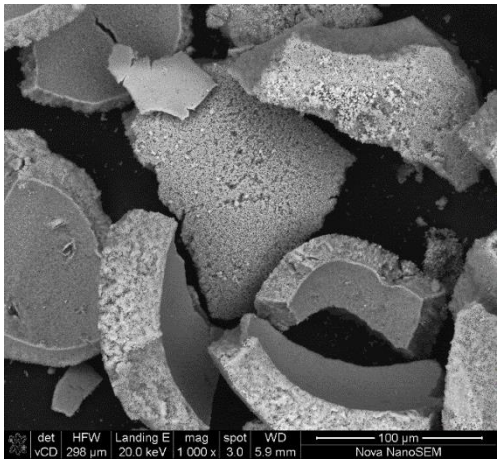

$[TPEOS]_{initial}$ = 0.9 mM

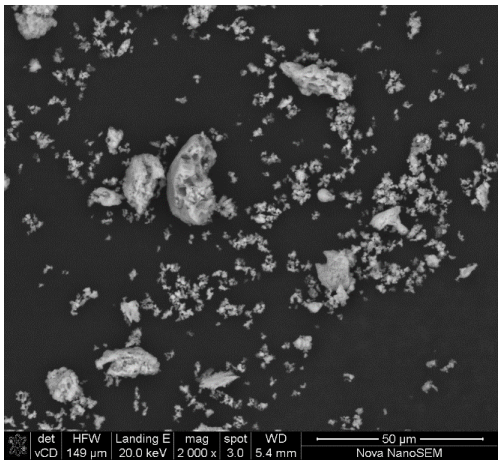

$[TPEOS]_{initial}$ = 0.34 mM

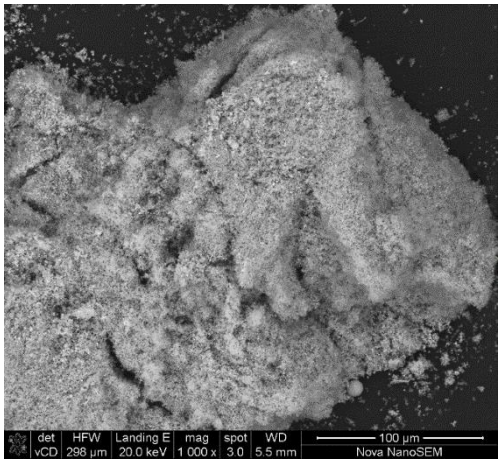

$[TPEOS]_{initial}$ = 0.51 mM

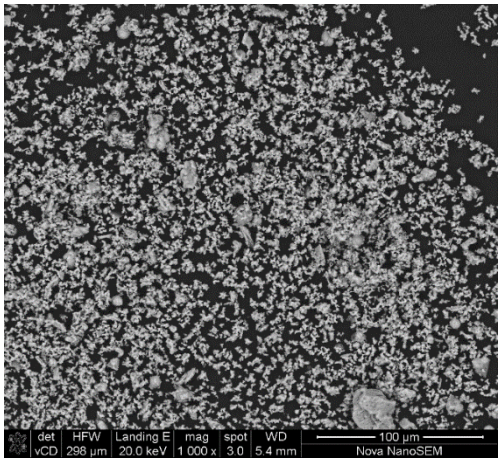

$[TPEOS]_{initial}$ = 1.64 mM

Figure 4-6: SEM images of as-synthesized cobalt nanoparticles on which EDX analysis was conducted, in brackets the Si/Co (mmol/mol)

4.2.1 XRD analysis of modified as-synthesized cobalt nanoparticles

X-ray diffraction (XRD) was used to determine the crystallite size or phase composition of the TPEOS modified as-synthesized cobalt nanoparticles. The XRD diffraction spectra for the cobalt nanoparticles modified by exposing to a solution of TPEOS in chloroform of 0.19 mmol/L shows diffraction lines at 40°,42°, 49° and 73°. The diffraction line at 40°, 42° and 49° can be ascribed to the maximum diffraction line for CoO, Co_3O_4, Co^0 respectively. Whereas the diffraction lines at 73° could not be ascribed.

The XRD diffraction spectra for the cobalt nanoparticles modified by exposing to a solution of TPEOS in chloroform of 0.34 mmol/L shows diffraction lines at 40°,42°, 49°

and 73°. The diffraction line at 40°, 42° and 49° can be ascribed to the maximum diffraction line for CoO, Co_3O_4, Co^0 respectively. Whereas the diffraction lines at 73° could not be ascribed.

The XRD diffraction spectra for the cobalt nanoparticles modified by exposing to a solution of TPEOS in chloroform of 0.51 mmol/L shows diffraction lines at 40°,42°, 50° and 73°. The diffraction line at 40°, 42° and 50° can be ascribed to the maximum diffraction line for CoO, Co_3O_4, Co^0 respectively. Whereas the diffraction lines at 73° could not be ascribed.

The XRD diffraction spectra for the cobalt nanoparticles modified by exposing to a solution of TPEOS in chloroform of 1.6 mmol/L shows diffraction lines at 40°,42°, 50° and 73°. The diffraction line at 40°, 42° and 50° can be ascribed to the maximum diffraction line for CoO, Co_3O_4, Co^0 respectively. Whereas the diffraction lines at 73° could not be ascribed.

These phases where identified using reference pattern included in Figure 4-7. There was a shift in the peak maximum from 52° in the as-synthesised cobalt nanoparticles to 50° in the TEOS modified as-synthesised cobalt nanoparticles. This could possibly be due to strain induced by the modification of the surface. There are no diffraction lines that could be identified as crystalline or amorphous silica (broad diffraction line at 20°). This could be because it could not be detected as it was in small quantities.

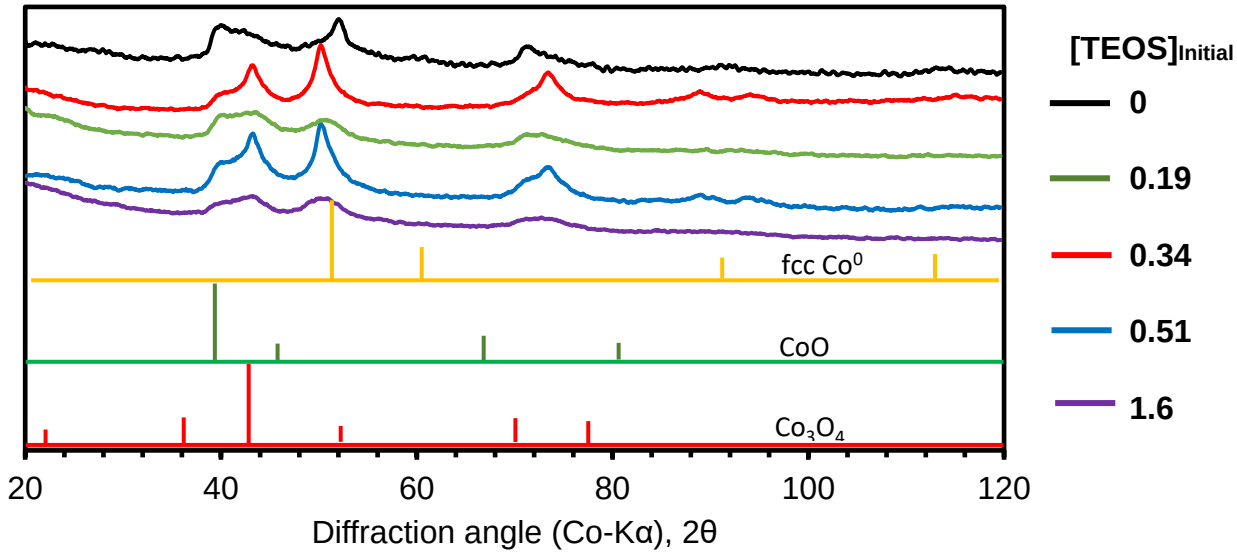

Figure 4-7: X-ray diffraction pattern of TPEOS modified and unmodified as-synthesized cobalt nanoparticles

The average crystalline size of the modified as-synthesized cobalt nanoparticles was determined using the Debye-Scherrer equation and was reported in Table 4-3. The most intense diffraction line at ca 50°. was used in the determination of the average crystallite size. There was no apparent effect of the modification on the crystallite size. The variation in the crystallite size could be due to the varying rates of oxidation of the NPs upon exposure to air.

Table 4-3: Average crystallite size for TPEOS modified nanoparticles

$[TPEOS]_{Initial}$	**0**	**0.19**	**0.34**	**0.51**	**1.6**
Size (nm)	8.6	9	7.5	10.0	5.6

4.2.2 Spectroscopic analysis of as-synthesized cobalt nanoparticles modified with TPEOS

The surface composition of the as-synthesized cobalt nanoparticles was modified with triphenylethoxysilane (TPEOS) diluted in chloroform. The functional groups of TPEOS where evaluated using FTIR (see Figure 4-8). There are eight distinctive peaks in the between 880 cm^{-1} and 1300 cm^{-1}, which in the region of interest because the Si-Co vibration frequency had been reported in to be in the region. These vibrational frequencies are 949 cm^{-1} (C-H rocking in CH_3), doublet 999 cm-1 & 1026 cm-1 (in-plane bending of phenyl ring), 1080 cm^{-1} (Si-O stretch in Si-O-C), 1119 cm^{-1} (C-O asymmetric stretching in C-O-Si) and doublet 1157 cm^{-1} & 1188cm^{-1} (ring torsion).

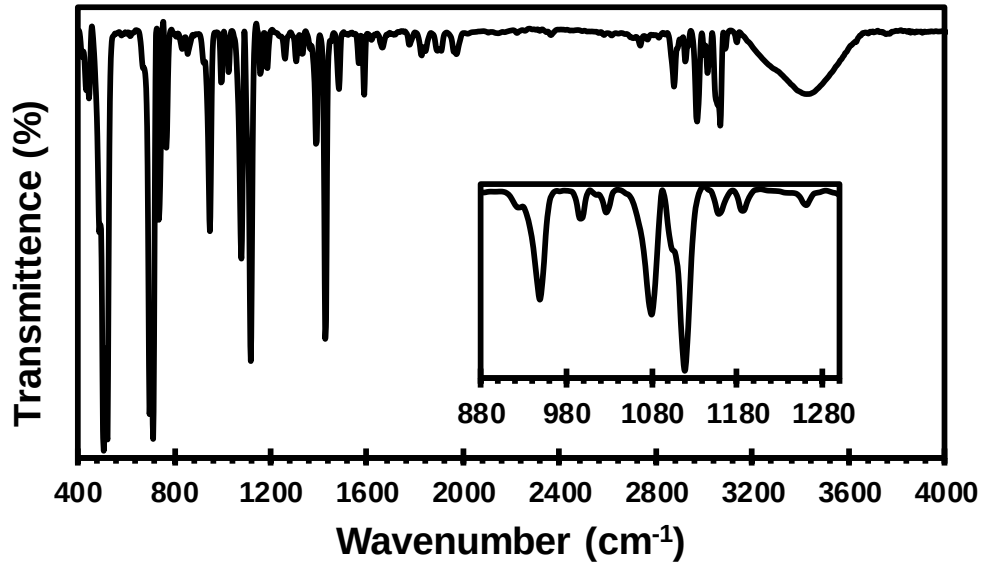

Figure 4-8: FTIR spectra of triphenylethoxysilane

The introduction of new functional groups on the surface of the as-synthesized cobalt nanoparticles through TPEOS modification was evaluated using FTIR. The FTIR spectra of the unmodified and modified nanoparticles are shown in Figure 4-9. The three distinctive peaks in the region of interest are at 1060 cm^{-1}, 1120 cm^{-1} and 1165 cm^{-1} wavenumbers.

The FTIR spectrum for the cobalt nanoparticles modified by exposing to a solution of TPEOS in chloroform of 0.19 mmol/L shows a small absorption band at 890 cm^{-1} followed by a broad, asymmetric absorption feature with a maximum at ca. 1040 cm^{-1} followed by minor bands at 1120 and 1170 cm^{-1}.

The FTIR spectrum of the cobalt nanoparticles modified by exposing to a solution of TPEOS in chloroform of 0.34 mmol/L shows again a broad, asymmetric absorption feature with a maximum at ca. 1040 cm^{-1}, but the weak feature at ca, 890 cm^{-1} could not be observed.

The FTIR spectrum of the cobalt nanoparticles modified by exposing to a solution of TPEOS in chloroform of 0.51 mmol/L shows a broad, asymmetric adsorption feature with a maximum at ca. 1040 cm^{-1} but the feature at ca. 890 cm^{-1} and the minor bands at 1120 and 1170 cm^{-1} could not be observed.

The FTIR spectrum for the cobalt nanoparticles modified by exposing to a solution of TPEOS in chloroform of 1.6 mmol/L shows an asymmetric absorption feature with a maximum at ca. 1040 cm^{-1} followed by minor bands at 1120 and 1170 cm^{-1}

According to literature the Co-O-Si bond vibrations are reported to be between 1020 cm^{-1} and 1030 cm^{-1} (Kababji *et. al.*, 2009; Shukla *et. al.*, 2011). For the TPEOS modified Co^0 NPs the Co-O-Si band vibrations shifted to 1060 cm^{-1}. This could have been as a result of the presence of the bulk phenyl groups that cause steric hindrance. The presence of the phenyl groups in the nanoparticles after modification was shown by the ring torsion bending vibrations at 1120 cm^{-1} and 1165 cm^{-1}.

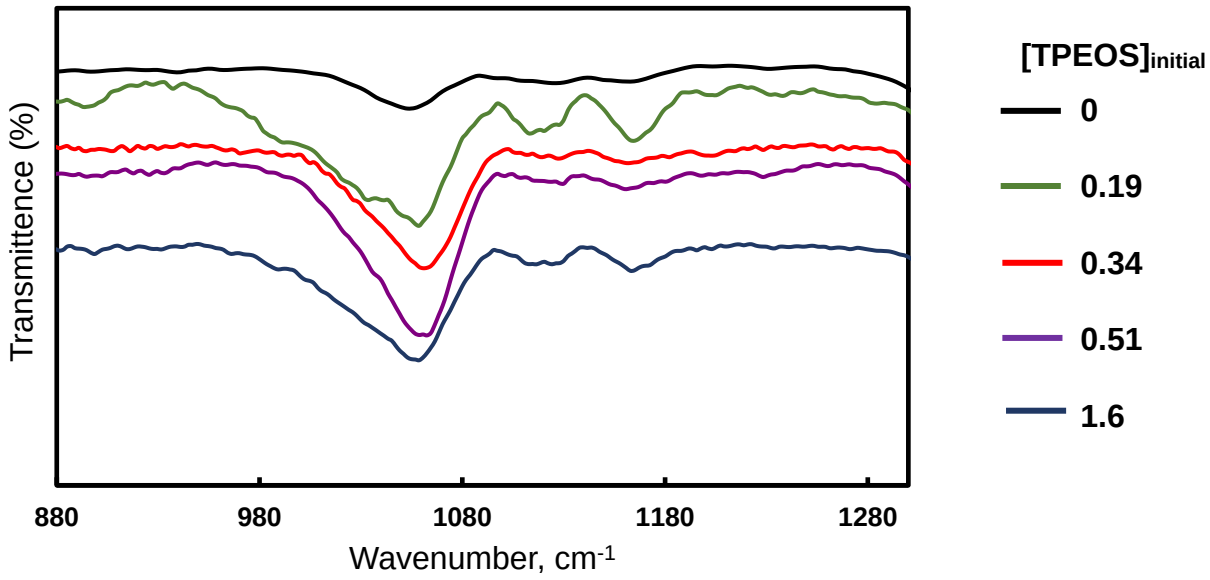

Figure 4-9: FTIR spectra for unmodified and TPEOS modified as-synthesized cobalt nanoparticles in the range of 880-1300 cm^{-1}

4.2.3 TEM analysis of TPEOS modified as-synthesised nanoparticles

After the as-synthesized cobalt nanoparticles where modified with TPEOS they are analysed with TEM to observe the effect of modification on the dispersion, size and shape of the nanoparticles. The nanoparticles maintained their cubic morphology and size after modification. It can be observed from Figure 4-10 that after modification most of the particles are present in clusters in what seems to be a solvent/surfactant/ modifying agent. Within this cluster the particles remain well-dispersed and defined. It is to be seen if this substance would affect the ability of the nanoparticles to adhere to the support, carbon black.

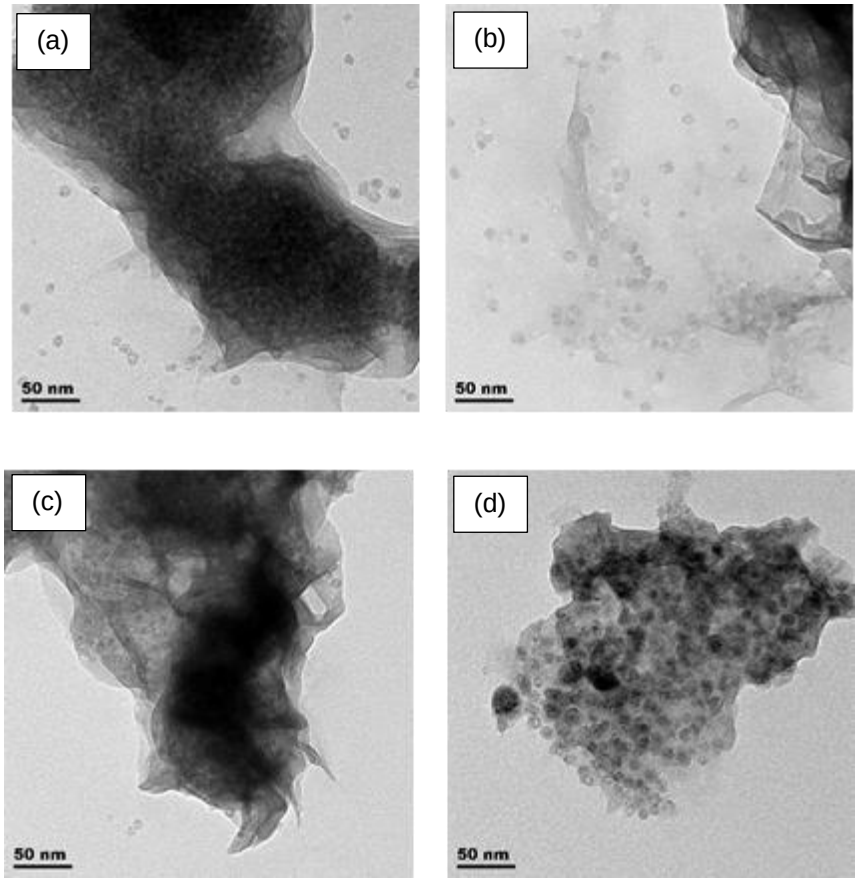

Figure 4-10: TEM micrographs of as-synthesized cobalt nanoparticles initially exposed to solution of TPEOS in Chlorofom with an initial concentration of TEOS of (a) 0.19, (b) 0.34, (c) 0.51 and (d) 1.6

4.3. Oxidation of as-synthesised cobalt nanoparticles

Co_3O_4 is the thermodynamically favoured form of cobalt oxide in air at standard temperature and pressure (Petitto *et al.*, 2008). Therefore, metallic cobalt and even CoO may readily oxidize to Co_3O_4 under ambient conditions. The cobalt nanoparticles synthesized with trioctylamine (TOA) and oleylamine (OA_m) as surfactants using a reaction tine of 20 minutes were exposed to air under ambient conditions in a fume hood for a period of 48 hours to oxidize them to Co_3O_4

One of the main concerns was whether complete oxidation of the metallic cobalt to Co_3O_4 was achieved upon exposure to ambient condition. Three cobalt oxides exist, namely: CoO, Co_3O_4 and Co_2O_3 (Gulbransen and Andrew, 1951). The formation of Co_2O_3 can only occur by precipitation of a solution containing Co^{3+} with OH^- and cannot be formed by dry oxidation. It had been observed experimentally that during oxidation of metallic cobalt by dry oxidation a layer of CoO in contact with cobalt metal was formed, but a thin layer comprising of Co_3O_4 was observed on the surface. The

thickness of the Co_3O_4 layer increases with decreasing temperature at which oxidation was conducted (Gulbransen and Andrew, 1951).

4.3.1 Phase analysis using X-ray diffraction (XRD)

The phase composition of the model catalyst was determined using X-ray diffraction (see Figure 4-11). The diffraction pattern from the cobalt nanoparticles synthesized with trioctylamine and oleylamine as surfactants shows broad reflections with the main reflections at $2\theta = 39.9^o$, $41,7^o$ (shoulder), 49.9^o (shoulder), 51.9^o and 71.3^o. Comparing the diffraction pattern of the as-synthesized nanoparticles with the reference spectra, it appears that the sample still contains some fcc-cobalt as evidenced by the relatively sharp diffraction line at $2\theta = 51.9^o$. Furthermore, the sample also contains some Co(II)O as exemplified by the reflection at $2\theta = 39.9^o$. Co_3O_4 does not seem to be present in these samples seeing the lack of a diffraction line at $2\theta = 36.6^o$. Hence, it may be concluded that the outer core of the cobalt nanoparticles oxidized during the purification of the particles in the multiple washing steps with methanol (Verelst *et al.*, 1999). The average size of the crystalline domain of fcc-cobalt was determined to be 8.6 nm applying the Debye-Scherrer equation to the reflection at $2\theta = 51.9^o$. This was slightly larger than determined using TEM, since XRD yields a volume-based average particle size and TEM a number based average particle size

The diffraction pattern of the cobalt nanoparticles after oxidation shows broad reflections at $2\theta = 21.1^o$, 36.6^o, 43.2^o, 52.7^o, 70.4^o and 77.7^o, which are characteristic of spinel Co_3O_4 when using a Co-K_α source. The average size of the crystalline domain of Co3O4 in the nanoparticles after oxidation was determined to be 3.4 nm applying the Debye-Scherrer equation to the reflection at $2\theta = 36.6^o$. This implies that the oxidation of the cobalt nanoparticles was associated with particle break-up possibly via the Kirkendahl effect as seen previously (Weststrate *et al.*, 2011). This implies the oxidized samples after reduction may contain smaller metallic cobalt nanoparticles (Hauman *et al.*, 2012).

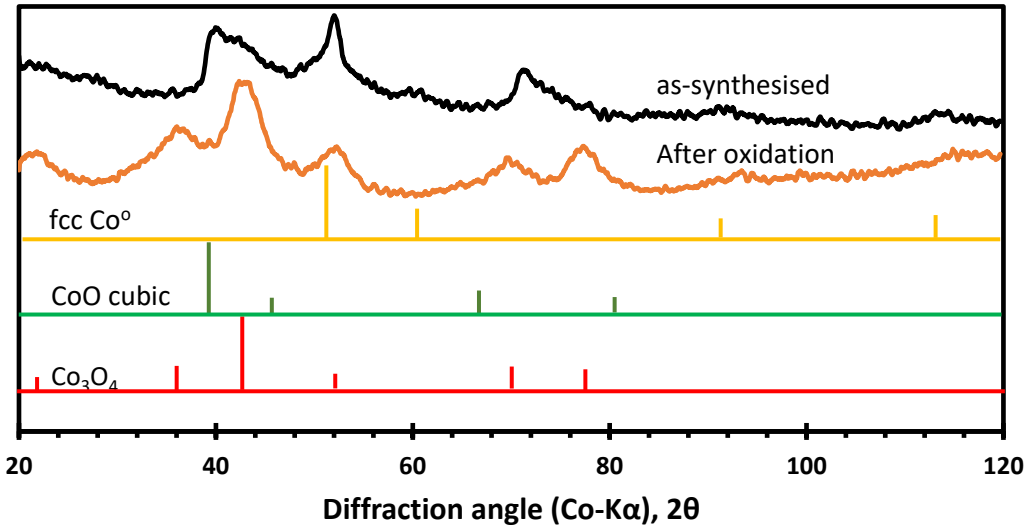

Figure 4-11: X-ray diffraction pattern for as-synthesized cobalt nanoparticles with trioctylamine (TOA) and oleylamine (OA_m) as surfactants and a reaction time of 20 minutes and the cobalt nanoparticles after exposure to air for 48 hours.

4.3.2 FTIR analysis

The FTIR spectrum of the as-synthesized cobalt nanoparticles using trioctylamine and oleylamine as surfactants and a reaction time of 20 minutes and the FTIR-spectrum of these cobalt nanoparticles after oxidation are shown in Figure 4-12. The absorption bands observed at around 2900 cm^{-1} and 1200-1800 cm^{-1} can be ascribed to C-H, C-C and N-H bond stretches from the residual of the surfactants used. The oxidized cobalt nanoparticle FTIR spectra show two distinctive bands at 582 cm^{-1} and at 663 cm^{-1}, which are attributed to the stretching frequency of the metal-oxygen bond. The vibrational frequency at 582 cm^{-1} was distinctive to the OB_3 vibrations in the spinel lattice, where B denotes Co^{3+} in an octahedral hole, while the vibrational frequency at 663 cm^{-1} denotes the ABO_3 vibration, where A denotes the Co^{2+} in a tetrahedral hole (Tang *et al*., 2008). It can thus be concluded that exposure of the as-synthesized cobalt nanoparticles to air for 48 hrs results in the formation of cobalt in a spinel lattice.

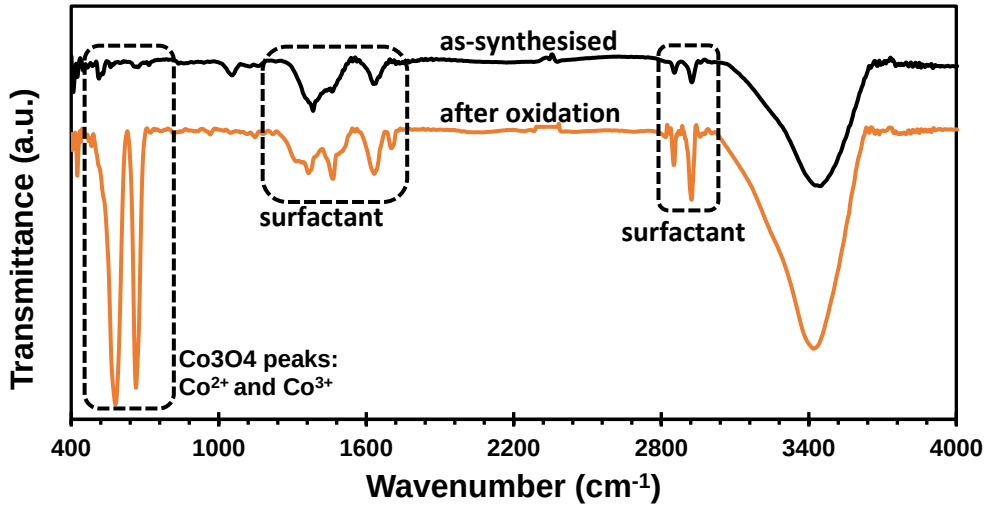

Figure 4-12: FTIR spectra of as-synthesized cobalt nanoparticles using trioctylamine and oleylamine surfactants and a reaction time of 20 minutes and their oxidized counterparts

4.4. Characterization of oxidised cobalt nanoparticles

4.4.1 Silylation of oxidized cobalt nanoparticles with tetraethoxysilane (TEOS)

The surface of the oxidized cobalt nanoparticles was modified using tetraethoxysilicate (TEOS). This modification was thought to proceed via a chemical reaction between functional groups on the catalyst surface to form Si-O-Co bonds. It had been suggested that the presence of surface hydroxyl groups on the catalyst surface are necessary for the silylation process (Mogorosi, 2012; Qing *et al*., 2011). The presence or absence of these hydroxyl groups may result in differences in the bonding of the alkoxy silane on the as-synthesized and oxidized cobalt nanoparticles. During the modification process, the oxidized cobalt nanoparticles (0.175 g) were suspended in a solution of TEOS in hexane (250 mL) for 24 hours through continual mixing with a magnetic stirrer at 500 rpm. The initial TEOS concentration was varied between 0.9-7.2 mmol/L to elucidate the effect of initial concentration on the uptake of TEOS by the solid. In order to avoid the self-condensation of TEOS to SiO_2 the initial concentration of the TEOS solution was kept low.

The oxidized cobalt nanoparticles were modified with a dilute TEOS solution to monitor the development and quantify the amount of TEOS adsorbed on the oxidized cobalt nanoparticles. The amount of TEOS that adsorbed on the surface of the oxidized cobalt nanoparticles was determined using two different methods, i.e. a difference

analysis based on the concentration of TEOS in the liquid and analysis of the recovered solid using EDX.

The first method involved sampling of 10 ml aliquot during the silylation process and determining the TEOS content in the aliquot using a gas chromatograph equipped with an FID. The amount of TEOS absorbed can then be determined from the difference in the concentration in the aliquot taking assuming that the number of moles of TEOS removed due to sampling was negligible:

$$TEOS\ uptake = \frac{n_{TEOS,uptake}}{n_{Co}} = \frac{C_{TEOS,initially} \cdot V_{initial} - C_{TEOS,t} \cdot V_t}{\frac{m_{Co\ in\ solution}}{M_{Co}}}$$

Equation 4-1

It was assumed that the amount of material removed from the suspension does not significantly affect the number of was assumed that all cobalt carbonyl initially used to make the nanoparticles are converted into cobalt nanoparticles. The concentration of TEOS can be determined from the relative area of TEOS and *n*-hexane in the solution (see Figure 4-8). In the very dilute region (as here was the case), a linear relationship between the ratio of the peak area of TEOS relative to the peak area of n-hexane and the concentration of TEOS in the solution was obtained. It can be further deduced that the molar response of the FID for the detection of TEOS relative to the detection of n-hexane was 0.581.

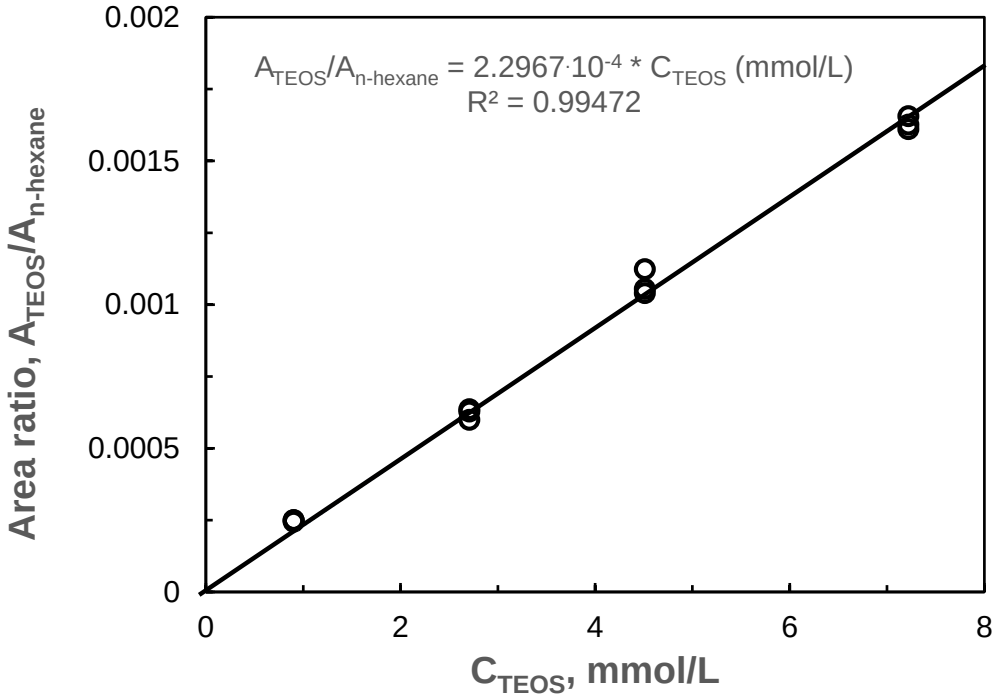

Figure 4-13: Calibration curve of the peak ratio of tetraethoxysilane (TEOS) to n-hexane as a function of the concentration of tetraethoxysilane in the solution

The uptake of TEOS on Co_3O_4 was determined from the difference in the concentration of TEOS in the solution as a function of time (see Fig. 4.9). This was achieved by sampling the solution to observe the uptake of TEOS with time as depicted in Figure 4-18. The obtained uptake data show a relatively large amount of scatter. This may be attributed to the storage of samples and possible evaporation of n-hexane as the amount of TEOS adsorbed was determined from the ratio of the peak area of TEOS to the peak area of n-hexane in the GC-trace. The system seems to approach with time an equilibrium state, which was dependent on the concentration of tetraethoxysilane in the mixture. The final uptake of tetraethoxysilane seems to increase with an increasing concentration of TEOS in the solution.

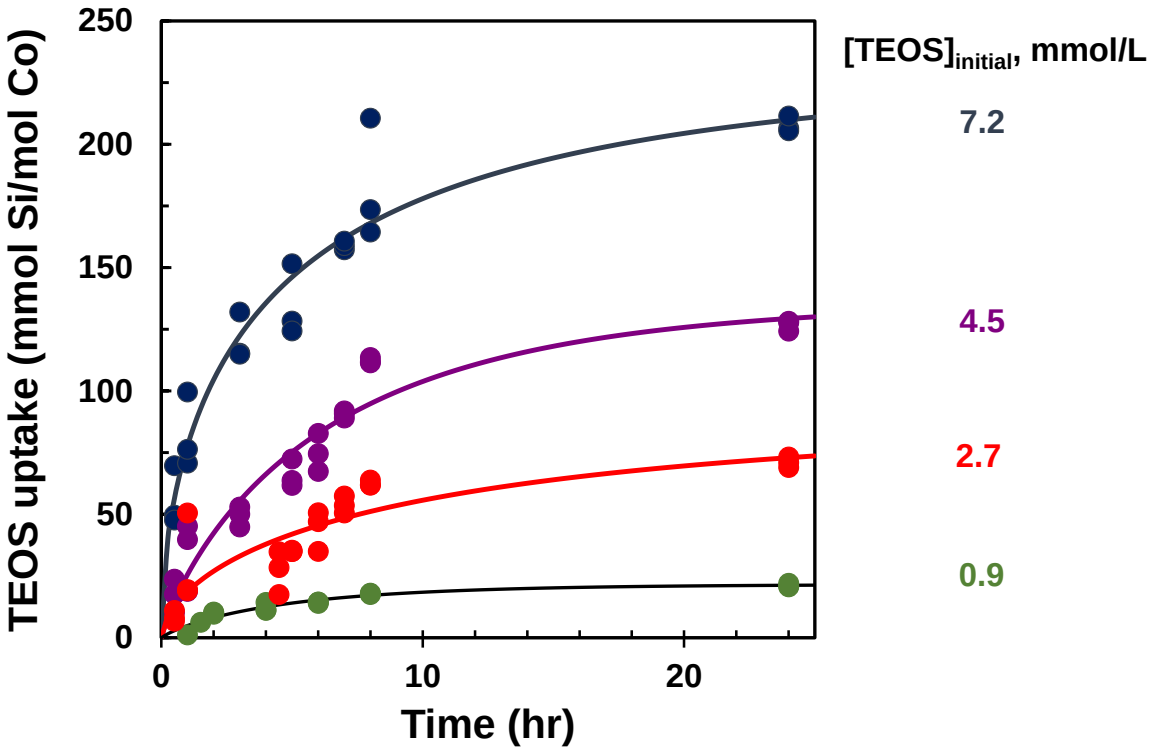

Figure 4-14: The resulting Si/Co ratio on the oxidised cobalt nanoparticles (trioctylamine and oleylamine used as surfactants, reaction time of 20 min and oxidised for 24 hrs) as determined using gas chromatography equipped with an FID as a function of the exposure time (see equation 4-1; solid lines represent fit to a kinetic growth model - see text)

It was shown that upon modifying the surface of cobalt with a metal oxide precurser, metal oxide may be present as islands on the surface of the cobalt(Morales *et al*., 2005; Macheli *et al*., 2018; Petersen *et al*., 2018). The growth of these islands on the surface of the cobalt nanoparticles may be modelled using island growth kinetics. The empirical form of the Johnson-Mehl-Avami-Kolmogorov (JMAK) equation had been used to model phase changes of materal at constant temperature (Avrami, 1941; the derivation of the Johnson-Mehl-Avami-Kolmogorov (JMAK) equation is in Appendix A6).

This kinetic model for the growth of particles may be adapted to an empirical form as:

$$\left({}^{Si}/_{Co}\right)_t = \left({}^{Si}/_{Co}\right)_{eq} * \left(1 - \exp\left[-\left(\frac{t}{\tau}\right)^m\right]\right)$$

where,

τ: time constant of the process

m: shape dependent parameter

The parameters for the fit of the experimental data of the TEOS uptake on the oxidsed cobalt nanoparticles to the empirical Johnson-Mehl-Avrami-Kolgomorov expression are shown in Table 4-4. In general, the data was reasonably described by the Johnson-Mehl-Avrami-Kolgomorov as indicated by the goodness of fit (R2).

The maximum uptake depends linearly on the intitial concentration of TEOS in the solution (see Figure 4-15). The value for the shape dependent parameter (m) was low and seems to decrease even further with increasing concentration of TEOS in the solution. The low value of m would indicate that mainly one dimensional growth of the silicates was occuring on the surface of the oxidised cobalt nanoparticles. There does not seem to be a clear correlation between the time constant for the deposition process and the concentration of TEOS in the solution.

Table 4-4**:** Parameters for the fit of the TEOS uptake on the oxidised cobalt nanoparticles to the empirical Johnson-Mehl-Avrami-Kolgomorov equation (Avrami, 1941)

Initial TEOS conc. (mmol/l)	**0.9**	**2.7**	**4.5**	**7.2**
$(Si/Co)_{eq}$, mol/mol	33.4	90.3	136.2	231.1
m	1.21	0.62	0.84	0.55
τ (hrs)	2.20	10.70	6.50	5.00
R^2	0.9436	0.7783	0.9302	0.9479

The uptake of TEOS on Co_3O_4 was also monitored using EDX (see Figure 4-15). It can be seen that the uptake of TEOS correlates linearly with the initial concentration of TEOS in the solution. It was clear that the Si/Co-ratio determined using EDX on the recovered solids are much lower than the Si/Co-ratio determined using a difference analysis (see equation 4-1). After exposing the oxidized cobalt nanoparticles to the silane containing solution, these particles were washed with methanol prior to the EDX analysis. This may have resulted in the removal of physisorbed TEOS on the surface of the nanoparticles. A difference in the obtained Si/Co ratio from these two methods was therefore anticipated.

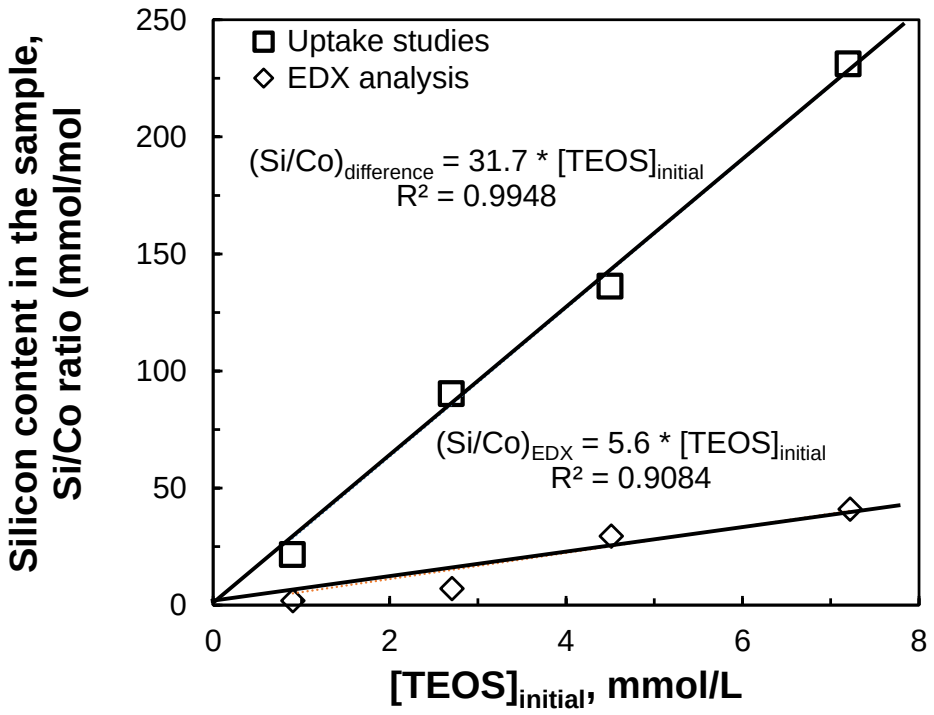

Figure 4-15: The maximum uptake of tetraethoxysilane as a function of the concentration of tetraethoxysilane in the initial solution as determined from a difference analysis (see equation 4-1) and from the EDX analysis of the modified samples

The time constant of the uptake of TEOS on the oxidized cobalt nanoparticles seems to fluctuate as a function of the initial concentration of TEOS. This may be a consequence of the inaccuracy in the determination of the amount of TEOS adsorbed, in particular at low concentrations, due to the use of a difference analysis.

4.4.2 XRD analysis of oxidized cobalt nanoparticles after TEOS modification

It was known that the nanoparticle preparation method, the support material used and the calcination temperature may affect the average size of crystallites. The nanoparticles were synthesized by chemical reduction of cobalt carbonyl. The average crystallite size and phase composition of the TEOS modified oxidized cobalt nanoparticles was characterized using X-ray diffraction (XRD). All the TEOS modified nanoparticles had a single phase, i.e. spinel Co_3O_4 as identified using the reference pattern. This indicates that the modification of the oxidized cobalt nanoparticles with TEOS did not induce a phase composition upon modification.

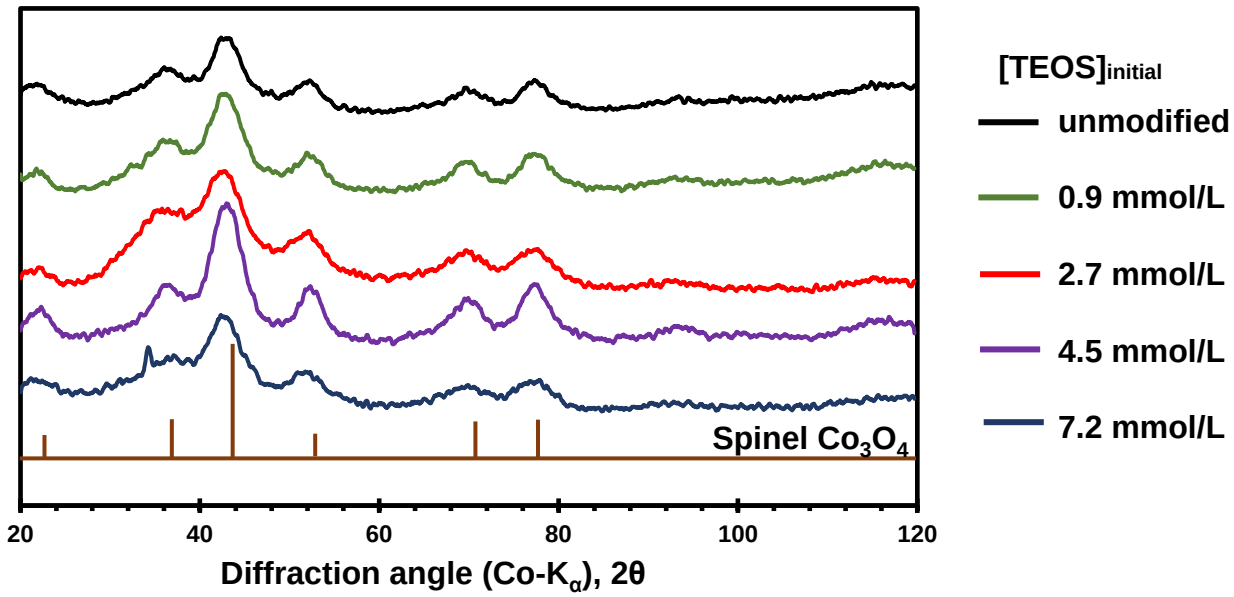

Figure 4-16: X-ray diffraction pattern of TEOS modified cobalt oxide nanoparticles

The average crystalite size of the nanoparticles was determined using the Debye-Scherrer equation using the most intense difraction line, 2θ = 43.6º (see Table 4-5) was used to determine the average cystallite size of Co_3O_4 in the as-prepared catalysts using the oxidized, modified nanoparticles The average crystalline domain of Co_3O_4 in these materials was ca. 3 nm for both modified and unmodified nanoparticles implying theat the modification step did not affect the average crystallite domain size of Co_3O_4 in these materials.

It was known that the nanoparticle preparation method, the support material used and the culcination temperature may affect the average size of crystallites. The nanoparticles were synthesised by chemical reduction of a cobalt complex. No support was used and the particles were not calcined. The TEOS content was the only factor could attributed to the observed changes in the as-sythesised cobalt nanoparticles crystallite size variation. A similar phenomenon has been reported for iron catalyst modified with TEOS (Mogorosi, 2012).

Table 4-5: Average crystallite size of the Co_3O_4 domain in oxidized cobalt nanoparticles exposed to solutions containing TEOS

[TEOS]initial, mmol/L	**unmodified**	**0.9**	**2.7**	**4.5**	**7.2**
Size (nm)	3.4	3.1	3.0	3.1	3.2

4.4.3 Spectroscopic analysis of oxidised cobalt nanoparticles modified with TEOS

The effect of the metal-support interaction has been investigated using the inverse method where ligand bonds could be formed on the surface of the active metal or its precursor to resemble the interface between the metal and the support. It has been postulated that the formation of the ligand bonds on the active metal, metallic cobalt, and its precursor, cobalt oxide, occurs differently. The confirmation of the presence of these ligand bonds (Co-O-Si) was evaluated with infrared spectroscopy.

The infrared spectra for TEOS was for comparison shown in Figure 4-17. The absorption bands have been assigned based on the work done by Mondragón *et al*. (1995) and Tejedor-Tejedor *et al.* (1998). In the range between 880 cm^{-1} to 1300cm^{-1}, there are four characteristic vibrational modes of tetraethoxysilane (TEOS), i.e. at 964 cm^{-1} (C-H rocking in CH_3), at 1076 cm^{-1} (Si-O stretch in Si-O-C), at 1115 cm^{-1} (C-O asymmetric stretching in C-O-Si) and at 1173 cm^{-1} (C-H rocking in CH_3).

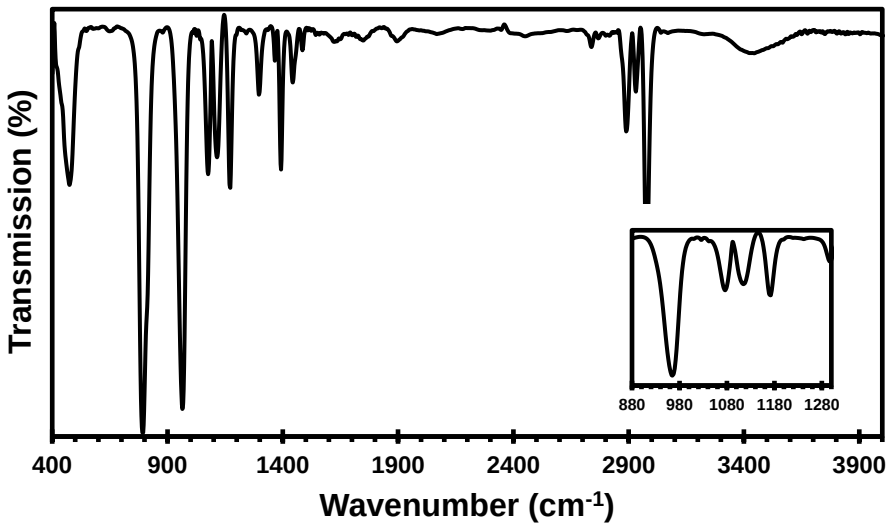

Figure 4-17**:** FTIR spectra of tetraethoxysilane (TEOS)

The precise allocation of the observed frequencies for TEOS was not paramount as a quantitative determination of the presence of TEOS on the surface of the cobalt nanoparticles.

The spectra of the oxidised cobalt nanoparticles before and after modification by exposing them to solutions of TEOS in n-hexane with varying concentrations (between 0.9 and 7.2 mM) are shown in Figure 4-18. All spectra show a broad absorption band

at 1600 cm^{-1} and 3400 cm^{-1} which was characteristic of OH on the surface of the nanoparticles. This absorption band was also present in the as-synthesized sample and the oxidized sample (see Figure 4.7).

The FTIR spectrum of the unmodiffied cobalt nanoparticles shows two distictive bands at 582 cm^{-1} and 663 cm^{-1} which are attributed to the stretching frequency of the metal-oxide bond (Tang *et al.*, 2008). These bands are followed by vibrational frequencies at 1360 cm^{-1}, 1466 cm^{-1} (bending vibrations of CH_3) and 1701 cm^{-1}. The possitive peak at 2400 cm^{-1} shows that the background was overcorrected for during analysis. The adsorption bands at 2850 cm^{-1} and 2920 cm^{-1} are attributed to the asymetrical and symmetrical stretching vibration of C-H bond respectively. These are indicative of the presence of surfactants on the surface of the nanoparticles. The modified oxidized cobalt nanoparticles have the same adsoption bands as the unmodified oxidised cobalt nanoparticles with additional adsoption bands in the region on 880 cm^{-1} and 1300 cm^{-1}.

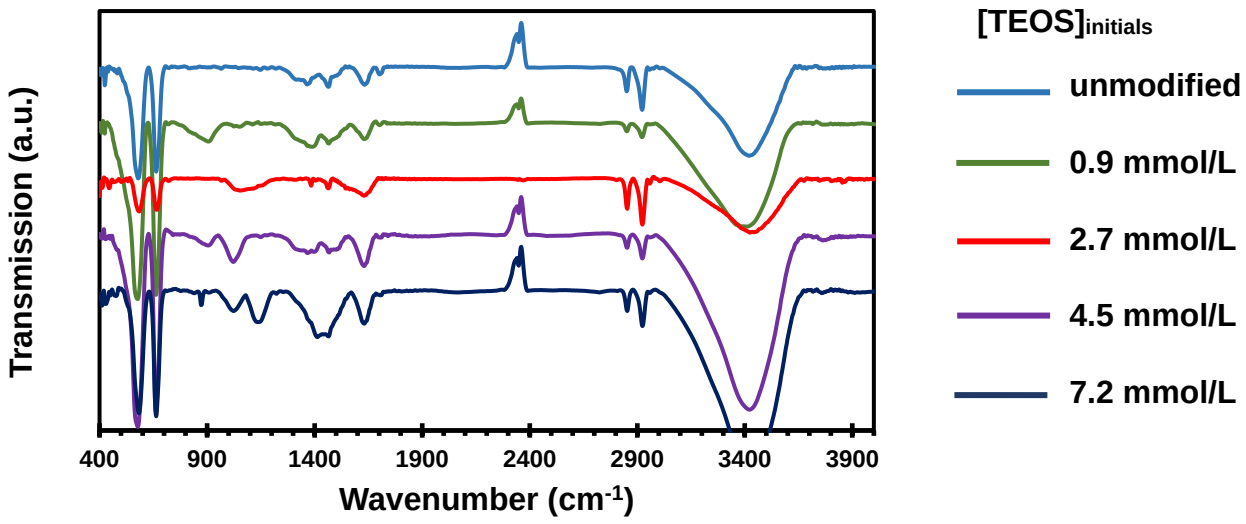

Figure 4-18**:** FTIR spectra of the oxidized cobalt nanoparticles modified by exposing them to solutions containing TEOS in n-hexane at different concentrations.

Figure 4-19 shows the FTIR spectra for the unmodified and modified oxidised cobalt nanoparticles in the range of 880-1300 cm^{-1}. The unmodified, oxidized cobalt nanoparticles do not show any major absorption feature in this range. The modified samples do show some absorption features in this range, but the characteristic absorption bands for tetraethoxysilane (TEOS) in the range of 880- 1300 cm^{-1} are

absent. This suggests that molecular TEOS on the surface of the nanoparticles was at the most in insignificant amounts present.

The sample exposed to a solution of TEOS in n-hexane initially containing 0.9 mmol/L shows a weak and broad absorption band at 910 cm^{-1}. The major bands for cobalt orthosilicates have been reported to be at 900 cm^{-1} and 935 cm^{-1} (Jong and Cheng, 1995). Hence, the sample exposed to a solution of TEOS in n-hexane with a low concentration may have bonds similar to the bonds in cobalt orthosilicates.

The sample exposed to a solution of TEOS in n-hexane initially containing 2.7 mmol/L should a broad absorption band at ca. 1020 cm^{-1}. This feature becomes more defined for the samples exposed to a solution of TEOS in n-hexane of 4.5 and 7.2 mmol/L. The absorption band at 1020-1036 cm^{-1} has been attributed to stretching vibrations of the ligand bond, Co-O-Si (Kababji *et al*., 2009), although Shukla *et al.* (2011) reported it at 1066 cm^{-1}.

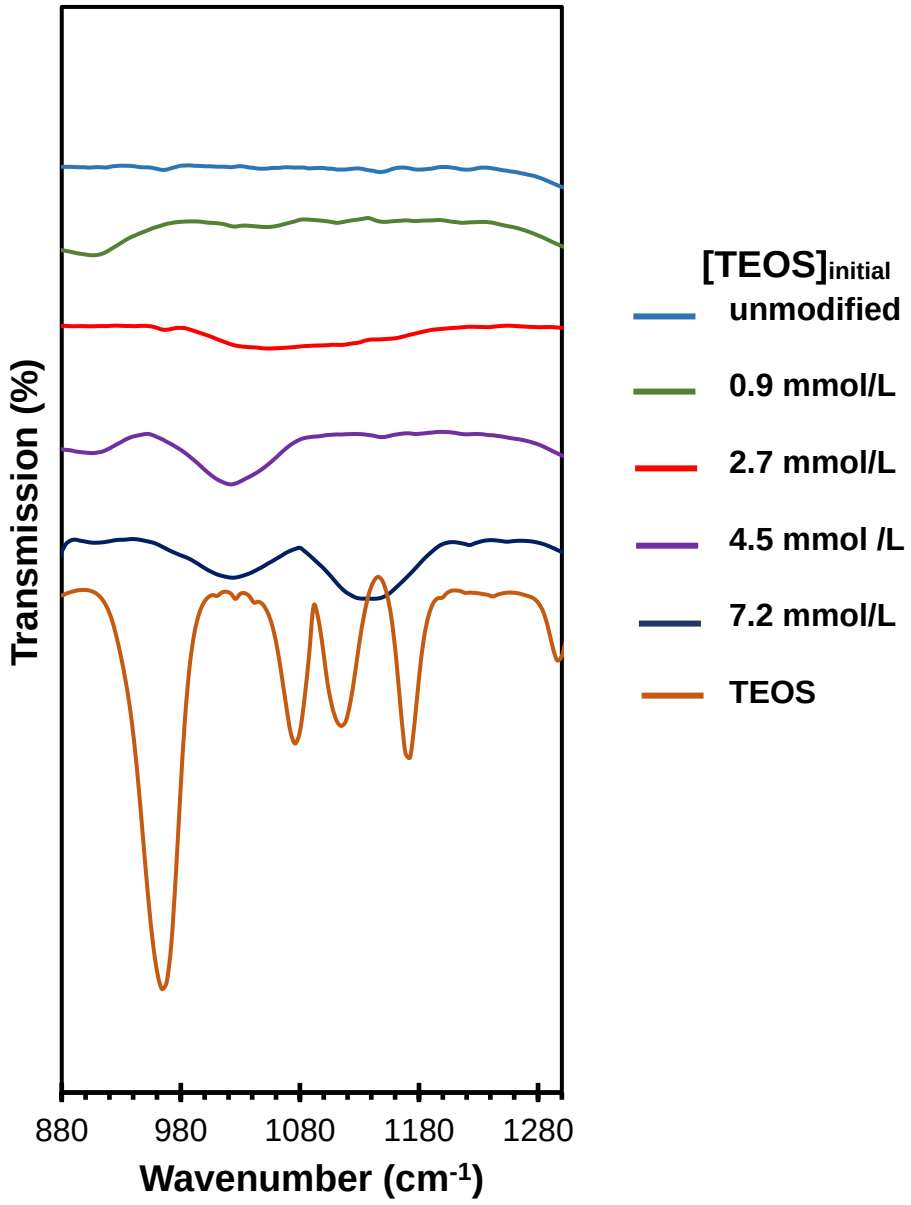

Figure 4-19: FTIR spectra in the range of 880-1300 cm^{-1} for oxidised cobalt nanoparticles modified by exposing them to solutions containing TEOS in n-hexane.

An absorption band at 1130 cm^{-1} and at 880 cm^{-1} was observed for the sample with oxidized cobalt nanoparticles exposed to a solution of TEOS in n-hexane of 7.2 mmol/L. During silylation TEOS may condense to form SiO_2 which has been reported to have asymmetrical and symmetrical stretching adsorption bands at 1090 cm^{-1} and 800 cm^{-1} respectively (Huang & Chen, 2004; Yin *et al*., 2009; Fouad *et al*., 2011).

Hence, the presence of the absorption bands at 1130 cm^{-1} and at 880 cm^{-1} may indicate that TEOS condensation has occurred on the surface of the nanoparticles. The absence of these absorption bands ascribed to the Si-O-Si bond stretching in the spectra of the oxidised nanoparticles contacted with a TEOS solution with lower concentration indicates that self-condensation of the TEOS may not have occurred to a large extent when exposing the cobalt nanoparticles to the dilute TEOS solutions ([TEOS]< 4.5mM).

4.4.4 TEM analysis of oxidized cobalt nanoparticles after TEOS modification

The TEM micrographs of the oxidized cobalt nanoparticles before and after modification with TEOS using the infinite dilution method with n-hexane as a solvent is shown in Figure 4-20. The unmodified oxidized cobalt nanoparticles where observed to be cubical and spherical morphology. There does not seem to be a dominant morphology. The large dark nanoparticles could possibly be agglomerated oxidized cobalt nanoparticles. ImageJ® was used to determine the particle size distribution for the nanoparticles. The size of each nanoparticle was measured across the longest distance between its corners. A minimum of 150 nanoparticles were measured and the average particle size was determined to be 6.9 ± 2.5 nm.

The oxidized cobalt nanoparticles after modification in an infinite dilute TEOS solution with initial concentration of 0.9 mmol/l were observed to be clustered. The clusters are comprised of small nanoparticles that form dark clusters. This was indicative of nanoparticles being entrained within an organic compound. This suggests that during modification the oxidized cobalt nanoparticles were clustered and entrained within an organic compound.

After modification with infinite dilute TEOS solution with initial concentration of 2.7 mmol/l the oxidized cobalt nanoparticles were observed using TEM to determine the average crystallite size, particle size distribution and morphology. The particles remain well dispersed and the particles size has decreased significantly from the unmodified cobalt oxide nanoparticles. This could be as a result of attrition during modification.

The oxidized cobalt nanoparticles after modification in an infinite dilute TEOS solution with initial concentration of 4.5 mmol/l had an appearance of large spherical shapes comprising of smaller particles. This was indicative of nanoparticles being entrained

within an organic compound. This suggests that during modification the oxidized cobalt nanoparticles were clustered and entrained within an organic compound. The particle size of the large spherical shapes ranges from 50 – 210 nm. The particle size of the smaller particles within the large spherical shapes could not be measured because the modification was too large and no other magnifications are not available. When the oxidized cobalt nanoparticles were modified with TEOS solution of initial concentration 7.2 mmol/l the large spherical structures seemed to grow further having a size range between 100 – 325 nm. The was no evidence that the cobalt nanoparticles grew in size during modification.

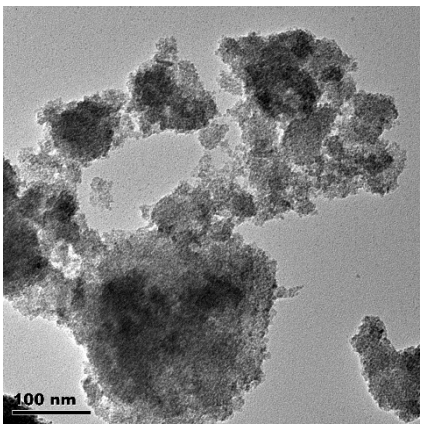

$[TEOS]_{initial}$ = 0.9 mM

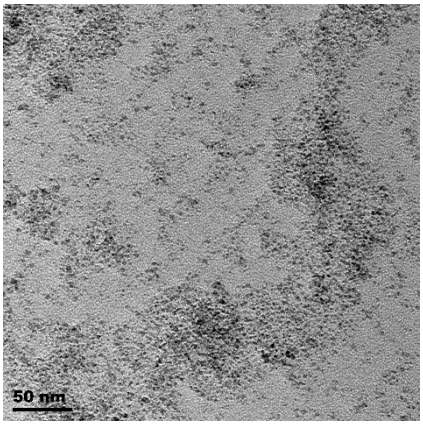

$[TEOS]_{initial}$ = 2.7 mM

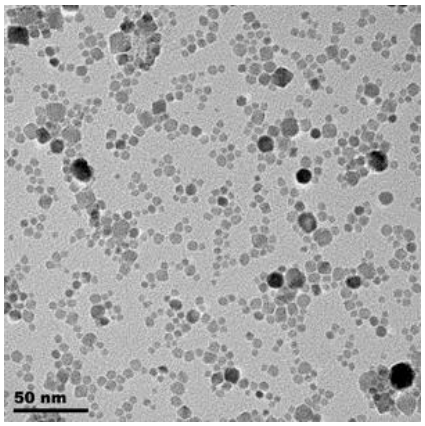

$[TEOS]_{initial}$ = 0 mM

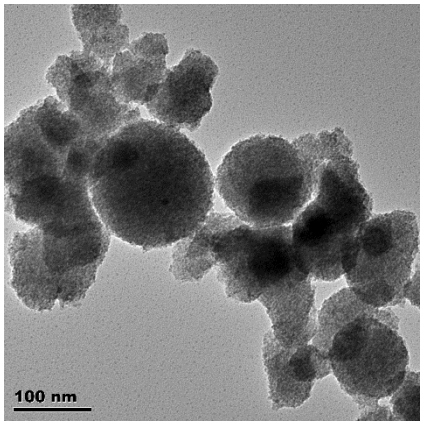

$[TEOS]_{initial}$ = 4.5 mM

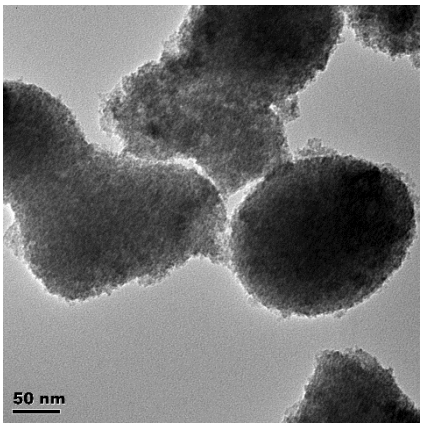

$[TEOS]_{initial}$ = 7.2 mM

Figure 4-20: TEM micrographs of oxidized cobalt nanoparticles after surface modification with TEOS

4.5. Charecterization of supported material

Catalysts are typically supported in order to achieve high metal dispersion, anchoring the active metal to limit sintering. A number of supports have been used for the cobalt catalyst in the Fischer-Tropsch synthesis which include silica, alumina, titanium and

carbon. These supports can interact strongly with the catalyst forming hardly reducible materials like $CoAl_2O_4$ and $CoSiO_4$ which results in limiting the activity of the Fischer-Tropsch synthesis. In this work, the effect metal-support interaction (MSI) between the cobalt catalyst and silica support on the Fischer-Tropsch process was investigated using the inverse method. In order to achieve high dispersion of the cobalt catalyst synthesized using the inverse method, we supported them on carbon material.

Carbon materials can be divided into two main categories: amorphous carbon and crystalline carbon (Fu and Li, 2015). Furthermore, there are more unconventional carbon supports, such as carbon nanofibers (CNFs), nanotubes (CNTs), carbon spheres (CSs) and mesoporous carbons. These have inert surfaces and hence the formation of hardly reducible materials becomes negligible (Fu *et al.*, 2013). The pore size of the carbon material used as a support for cobalt catalyst in the Fischer-Tropsch synthesis was important as it may affect the cobalt particle size (Jiang *et al.*, 2018). Microspores could lead to the formation of particles below 6-8 nm. However, the pore size of the carbon material used in this study was not of significant importance as the cobalt NPs where synthesized before being supported.

Carbon black (Vulcan XC 72R) was chosen to support the synthesized, oxidized and modified cobalt nanoparticles as it was least susceptible to form additional metal-support interactions (MSI). A 10 wt% carbon black supported catalyst was synthesized by dispersing 0.1 g of the (modified) cobalt nanoparticles in chloroform. Once the nanoparticles were dispersed completely in the chloroform, 0.9 g of carbon black was added. The mixture was then sonicated for 20 min at room temperature. The solvent was then evaporated in a fume hood overnight.

A TEM micrograph of the supported unmodified oxidized cobalt nanoparticles is shown in Figure 4-21. The nanoparticles adhere to the support as all particles that were observed were located on the support. The dispersion of the catalyst on the carbon black support was good. Because of the carbon black support had small pore sizes the nanoparticles attach to the surface of the support and not within in the pore structure.

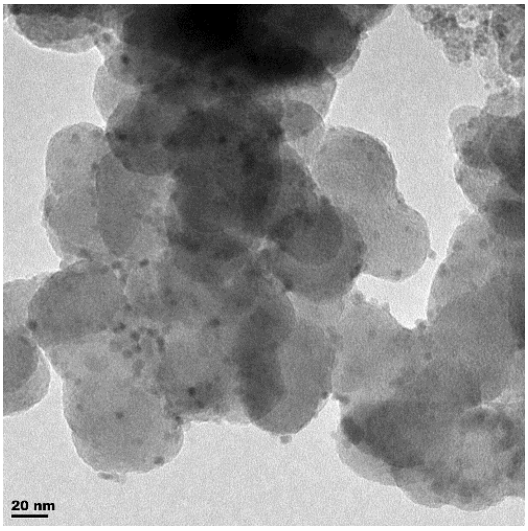

Figure 4-21**:** TEM micrograph of oxidized cobalt nanoparticles supported on carbon black (Vulcan XC 72R)

Studies of the reduction behaviour of the oxidized and as-synthesized cobalt nanoparticles supported on carbon black was conducted using temperature programmed reduction (TPR). A quartz reactor was loaded with 30 mg of catalyst and was subsequently degassed in helium (50 mL/min(NTP)) at 120 °C removing excess moisture and contaminants on the catalyst, which can desorb at these temperatures. The reactor was cooled to 60 °C before the gas was changed to 5% H_2/Ar at a flow rate of 50 mL/min (NTP). The temperature was ramped from 60 °C to 900 °C using a constant heating rate of 10 °C/min.

4.5.1 Reduction of as-synthesized cobalt nanoparticles

Cobalt nanoparticles where synthesized by chemical reduction using surfactants, washed with methanol and modified with TPEOS. It was observed through XRD measurements that some oxidation occurred during the process of washing resulting in the formation of a CoO layer. The effect of the silylation process on the reduction of this CoO layer was examined using temperature programmed reduction (TPR). The TPR analysis was conducted on carbon supported material.

The TPR profile of the as-synthesized and TPEOS modified cobalt nanoparticles is shown in Figure 4-22. The unmodified sample sow a small peak with a maximum at 320 °C. The peak appears to be asymmetric possibly due to the presence of less accessible cobalt oxide. The modification of the as-synthesized cobalt nanoparticles with a solution containing TPEOS in 0.34 mM results in a hydrogen consumption 3.94 mol H_2/mol Co. The hydrogen consumption can be attributed to two processes, one

with a maximum at ca. 330 °C and one with a maximum at ca. 415 °C. The second peak was smaller than the first. The first peak was the transformation of CoO to Co^0. The consecutive peak can be ascribed to reduction of CoO in the vicinity of the silicates on the surface of the nanoparticles.

The modification of the as-synthesized cobalt nanoparticles with a solution containing TPEOS in 1.6 mM results in a hydrogen consumption 4.01 mol H_2/mol Co. The hydrogen consumption was attributed to the first process of the transformation of CoO to Co^0 at a peak maximum of 350 °C as well as the second process of the reduction of CoO in the vicinity of silicates on the surface having a peak maximum at 510 °C.

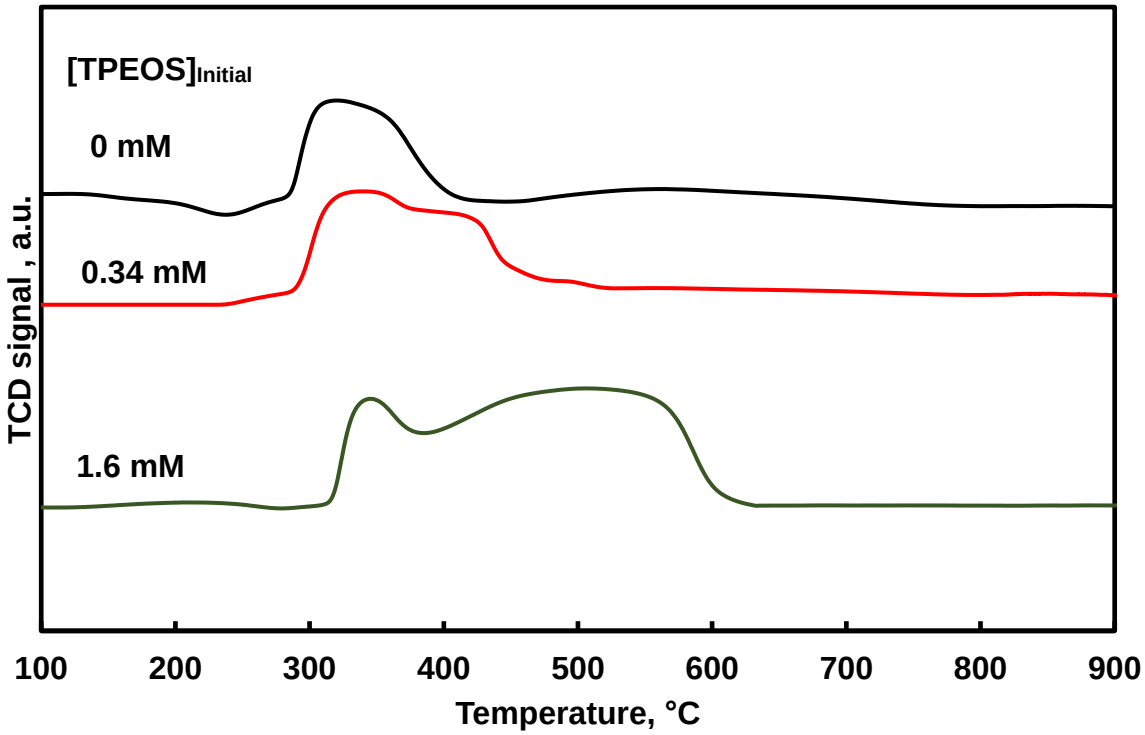

Figure 4-22: TPR profile of as-synthesised cobalt samples modified with TPEOS using a heating rate of 10 °C/min

4.5.2 Reduction of oxidized cobalt nanoparticles

The TPR profile for the unmodified and TEOS modified oxidized cobalt nanoparticles supported on carbon black is shown Figure 4-23. In the unmodified oxidised cobalt nanoparticles the first reduction peak was observed at 405 °C and was attributed to the reduction of Co_3O_4 to CoO. Another other peak was identified at 440 °C. Cobalt (II, III) oxide has been reported to have two reduction peaks for the reduction of Co_3O_4 to CoO and Co to Co^0 (Sabat *et al.*, 2014). It was postulated that because of the

ramping rate of 10 °C/min the two reduction peaks were not separated completely resulting in the appearance the first peak as a shoulder or as a single peak (Petersen *et al.*, 2018).

For oxidized cobalt nanoparticles after modification in an infinite dilute TEOS solution with initial concentration of 0.9 mmol/l and supported on carbon black the first reduction peak was observed at 270 °C this could be as a result of the desorption of ethoxide on the TEOS as catalyst was not calcined prior to reduction. This was followed by a reduction peak at 350 °C which was attributed to the reduction of Co_3O_4 to CoO and the final reduction peak at 430 °C.

For oxidized cobalt nanoparticles after modification in an infinite dilute TEOS solution with initial concentration of 2.7 mmol/l and supported on carbon black the first reduction peak was observed at 270 °C this could be as a result of the desorption of ethoxide on the TEOS as catalyst was not calcined prior to reduction. This was followed by a reduction peak at 360 °C which was attributed to the reduction of Co_3O_4 to CoO and the final reduction peak at 460 °C.

For oxidized cobalt nanoparticles after modification in an infinite dilute TEOS solution with initial concentration of 4.5 mmol/l and supported on carbon black the first reduction peak was observed at 320 °C this could be as a result of the desorption of ethoxide on the TEOS as catalyst was not calcined prior to reduction. This was followed by a shoulder at 460 °C with a reduction peak maximum at 490 °C. A shoulder at 540 °C was observed.

For oxidized cobalt nanoparticles after modification in an infinite dilute TEOS solution with initial concentration of 7.2 mmol/l and supported on carbon black the first reduction peak was observed at 270 °C this could be as a result of the desorption of ethoxide on the TEOS as catalyst was not calcined prior to reduction. This was followed by a reduction peak at 370 °C which was attributed to the reduction of Co_3O_4 to CoO and the final reduction peak at 460 °C.

There was a shift in the peak temperatures with increasing initial concentration of TEOS solution and the presence of high temperature peaks suggest the presence of metal-support interactions in the modified oxidised cobalt nanoparticles (Petersen *et al.*, 2018).

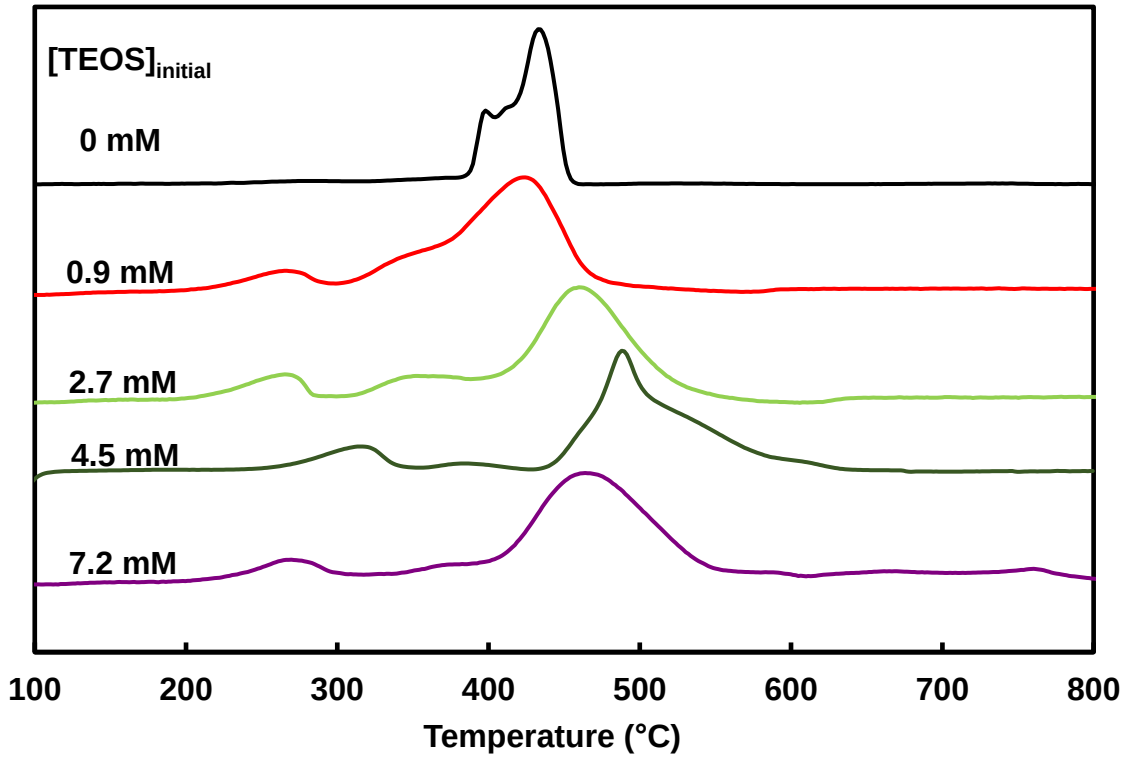

Figure 4-23: TPR profile for unmodified oxidized cobalt nanoparticles and oxidized cobalt nanoparticles modified using TEOS

The degree of reduction (DOR) and hydrogen consumption for the modified and unmodified cobalt oxide nanoparticles is shown in Table 4-6. The hydrogen consumption for the unmodified oxidized cobalt nanoparticles was 0.58 mol H_2/mol Co. As the silicon content on the surface of the particles increased the hydrogen consumption was observed to increase. The increase in the hydrogen consumption could be the result of the reduction or hydrolysis of that ethoxy group

Table 4-6: DOR and H_2 consumption per mole of cobalt for the oxidised cobalt nanoparticles

$[TEOS]_{Initial}$ (mM)	Degree of Reduction	H_2 consumption (mol H_2/mol Co)
0	81.8	0.58
0.9	44.4	0.59
2.7	66.6	0.89
4.5	100	1.42
7.2	33	0.44

4.5.3 Surface chemical properties of as-synthesized cobalt nanoparticles

The activity and selectivity of a Fischer-Tropsch catalyst wasis dependent on its ability to adsorb and dissociate CO and H_2. CO-TPD studies were conducted to elucidate the effect of the TEOS modification on the adsorption behaviour of CO on the reduced materials (T_{red} = 350 °C, t_{red} = 30 min). The as-synthesized cobalt nanoparticles were supported on carbon black before the CO-TPD studies were conducted. The adsorption of CO on the support may obscure the results obtained from the CO-TPD.

To eliminate this possibility a CO-TPD analysis of the carbon black support was conducted. A broad signal was obtained in the CO-TPD for the carbon support in the temperature range between 300 °C and 900 °C (see Figure 4-24). However, after normalization of the CO-TPD signal with the mass used during analysis it was observed that the signal of the carbon support was small in comparison to the signal from Co desorption on the unmodified oxidized cobalt nanoparticles after reduction. Hence, the obtained signal can be ascribed to the desorption of CO from the modified and unmodified as-synthesized cobalt nanoparticles and the signal attributable to the support represents merely background noise.

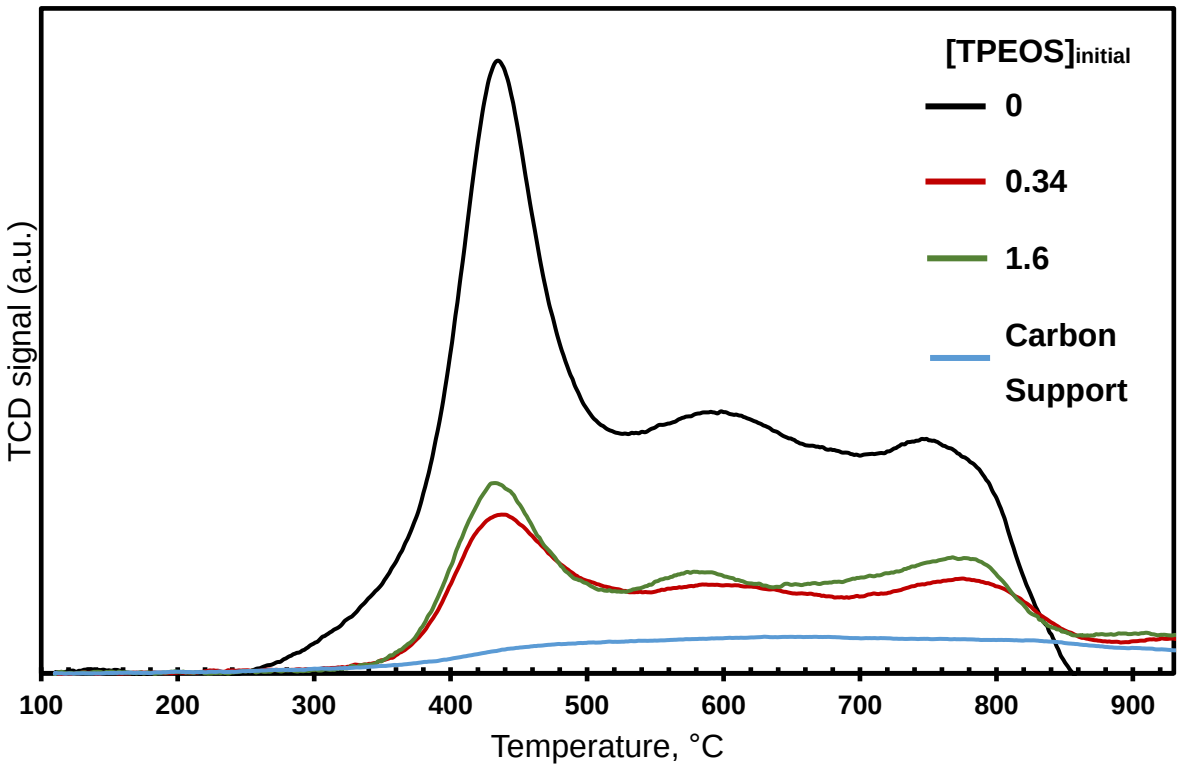

Figure 4-24: CO-TPD from the as-synthesized cobalt nanoparticles modified with TPEOS supported on activated carbon after reduction in H_2 at 350 °C

The unmodified as-synthesized cobalt nanoparticles exhibited CO desorption peaks at 440, 614 and 760 °C which suggest that there are at least 3 distinct sites from which CO can desorb or pathways for CO desorption. The first CO desorption peak at ca. 440 °C may be attributed to desorption of adsorbed CO on bridge sites and the CO desorption peak at 614 °C to desorption of CO on atop sites (Carlsson *et al.*, 2003). The third CO desorption peak at 760 °C peak was attributed to dissociatively adsorbed CO. The CO-TPD spectrum was deconvoluted using Gaussian functions (see Fig. 4.23). The area of the first peak was larger than that of the consecutive peaks which indicates that a significant amount of CO was associatively adsorbed on bridge sites on the surface of the catalyst. The ratio of the amount of CO desorbed ascribed to associatively desorbed CO (desorbing at ca. between 400 °C and 610 °C) and the amount of Co desorbed ascribed to dissociatively adsorbed CO (desorbing at ca. 760 °C) was ca. 3.7 over the unmodified sample (see Table 4-7).

The cobalt nanoparticles modified by exposing to a solution of TPEOS in chloroform of 0.34 mmol/L exhibit CO desorption peaks at 440, 614 and 780 °C. This was indicative of at least 3 distinct sites from which CO can desorb or pathways for CO

desorption. The first CO desorption peak at ca. 440 °C may be attributed to desorption of adsorbed CO on bridge sites and the CO desorption peak at 614 °C to desorption of CO on atop sites (Carlsson *et al.*, 2003). The third CO desorption peak at 780 °C peak was attributed to dissociatively adsorbed CO.

The cobalt nanoparticles modified by exposing to a solution of TPEOS in chloroform of 1.6 mmol/L exhibit CO desorption peaks at 440, 614 and 780 °C. This was indicative of at least 3 distinct sites from which CO can desorb or pathways for CO desorption. The first CO desorption peak at ca. 440 °C may be attributed to desorption of adsorbed CO on bridge sites and the CO desorption peak at 614 °C to desorption of CO on atop sites (Carlsson *et al.*, 2003). The third CO desorption peak at 780 °C peak was attributed to dissociatively adsorbed CO.

There were minor shifts in the desorption temperature before and after TPEOS modification which may indicate that the was nor major shift in the Co-C bond strength. The CO desorption area for the modified as-synthesized cobalt nanoparticles decreases to less than 30% of the CO desorption area of the unmodified as-synthesized cobalt nanoparticles indicating that the number of active sites decreased (Xiaoping *et. al.* 2006).

The ratio between the amount of Co desorbed ascribed to associatively desorbed CO (desorbing at ca. between 400 °C and 610 °C) and the amount of Co desorbed ascribed to dissociatively adsorbed CO on weaker sites (desorbed at ca. 760 °C) decreases with increasing Si/Co ratio (see Table 4-7). This suggest than the presences of silicates enhances dissociative adsorption of CO.

Table 4-7: TPD Peak ratio analysis for modified as-synthesized cobalt nanoparticles

$[TEOS]_{Initial}$	Associative/dissociative
0	3.70
0.34	2.80
1.6	2.67

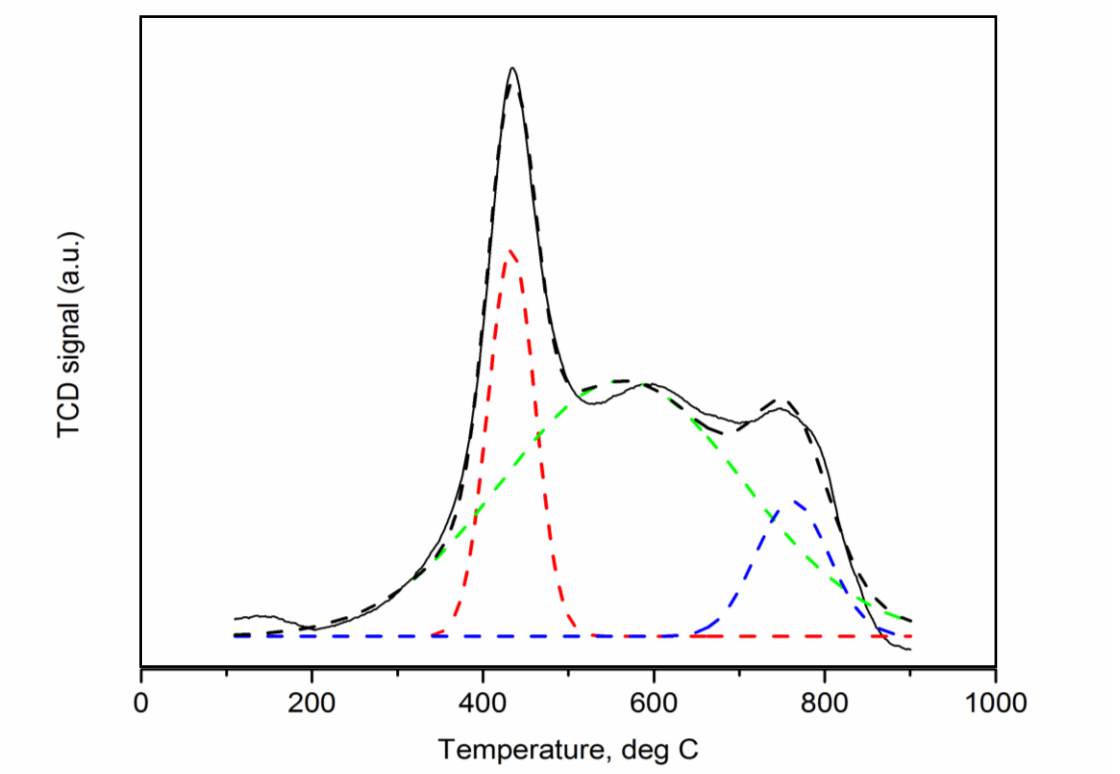

Figure 4-25: Modelling CO-TPD profile of unmodified as-synthesized cobalt nanoparticles supported on carbon back (10 wt. %) with Gaussian function (heating rate was 10 °C s^{-1})

4.5.4 Surface chemical properties of oxidised cobalt nanoparticles

The activity and selectivity of a Fischer-Tropsch catalyst was dependent on its ability to adsorb and dissociate CO and H_2. CO-TPD studies were conducted to elucidate the effect of the TEOS modification on the adsorption of CO on the reduced materials (reduction in H_2, T_{red} = 350 °C, t_{red} = 30 min). The oxidised cobalt nanoparticles were supported on carbon black before the CO-TPD studies were conducted.

The adsorption of CO on the support can obscure the results obtained from the CO-TPD. To eliminate this possibility a CO-TPD analysis of the carbon black support was conducted. A broad signal was obtained in the CO-TPD for the carbon support in the temperature range between 300 °C and 900 °C (see Figure 4-26). However, after normalization of the CO-TPD signal with the mass used during analysis it was observed that the signal of the carbon support was small in comparison to the signal from CO desorption from the unmodified oxidized cobalt nanoparticles after reduction. Hence, the obtained signal can be ascribed to the desorption of CO from the modified

and unmodified oxidized cobalt nanoparticles and the signal attributable to the support represents merely background noise

The CO-TPD spectrum of the unmodified oxidized cobalt nanoparticles supported on activated carbon showed various desorption peaks. The low desorption temperature peak with a maximum at ca. 185 °C was relatively small. CO desorbing at these temperatures may be attributed to weakly adsorbed CO entrained in the catalyst pores or physisorbed CO (Carlsson *et. al.,* 2003; Wang *et. al.,* 2006). The large desorption peak with a maximum at ca. 450^{o}C was preceded by a distinct feature appearing at ca. 400 ^{o}C. Carbon monoxide desorbing at these temperatures is, based on FTIR studies, attributed to adsorbed CO on bridge sites (400 °C) and CO on atop sites (450 °C) (Carlsson *et al.,* 2003). Deconvoluting the CO-TPD profile using Gaussian functions (see Fig. 4.16) shows that the ratio of CO adsorbed on bridge sites relative to CO adsorbed on atop sites was ca. 0.9. This number should be interpreted with care seeing that the modelled peak width for CO desorbed from atop sites was significantly less than the peak width for CO desorbed from the bridge sites, and hence the obtained result may be an artefact due to the deconvolution process than actual representation of the relative number of different amounts of CO adsorbed. The dominant CO desorption peak at 450 ^{o}C was also accompanied by a desorption peak at a higher temperature (ca. 520 ^{o}C). The fourth desorption peak (blue) at 520 °C may be attributed to the decomposition of superficial oxygen complexes formed during carbon black preparation or subsequent oxidation (Wang *et al.,* 2006).The CO-TPD spectrum of the unmodified oxidised cobalt nanoparticles supported on activated carbon after reduction shows evidence of a high temperature CO desorption peak with a maximum at ca. 650 ^{o}C. This may be attributed to the desorption of recombined, previously dissociated CO.

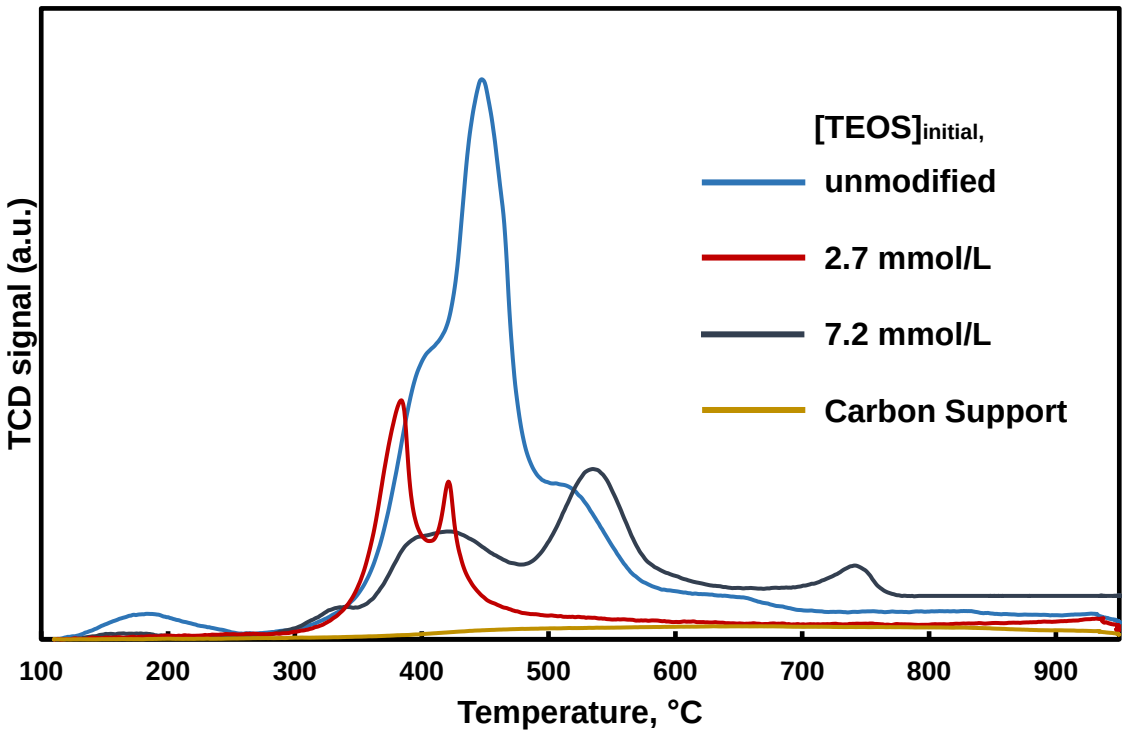

Figure 4-26**:** CO-TPD on the oxidized cobalt nanoparticles modified with TEOS supported on activated carbon after reduction in H_2 at 350 ^oC for 30 min

The CO-TPD spectra of modified oxidised cobalt nanoparticles exposed to solutions containing 2.7 mM and 7.2 mM TEOS in n-hexane shows marked deviations from the CO-TPD spectrum of the unmodified oxidised cobalt nanoparticles. The modified oxidised cobalt nanoparticles exposed to a solution containing 2.7 mM TEOS in n-hexane was observed to have two CO desorption peaks at ca. 385 °C and 420 °C respectively. The CO-TPD spectrum of the unmodified oxidised cobalt nanoparticles supported on activated carbon show desorption peaks at similar or slightly upward shifted temperatures ascribed to the desorption of CO adsorbed on bridge sites and on atop sites (Carlsson *et al.,* 2003). It was interesting to note that the ratio of CO adsorbed on these sites have shifted in comparison to the unmodified oxidised cobalt nanoparticles towards more CO desorbing from bridge sites

The modified oxidised cobalt nanoparticles exposed to a solution contain in 7.2 mM TEOS in n-hexane was observed to have four CO desorption peaks at ca. 340 °C, 420 °C, 540 °C and 750 °C. The CO-TPD spectrum of the unmodified cobalt nanoparticles supported on activated carbon showed a similar desorption peaks at slightly downward shifted temperatures these were attributed to weakly adsorbed CO entrained in the

catalyst pores or physisorbed CO (340 °C), adsorbed CO on bridge sites (420 °C), CO on atop sites (540 °C) and previously dissociated CO (750 °C) (Carlsson *et. al.,* 2003; Wang *et. al.,* 2006).

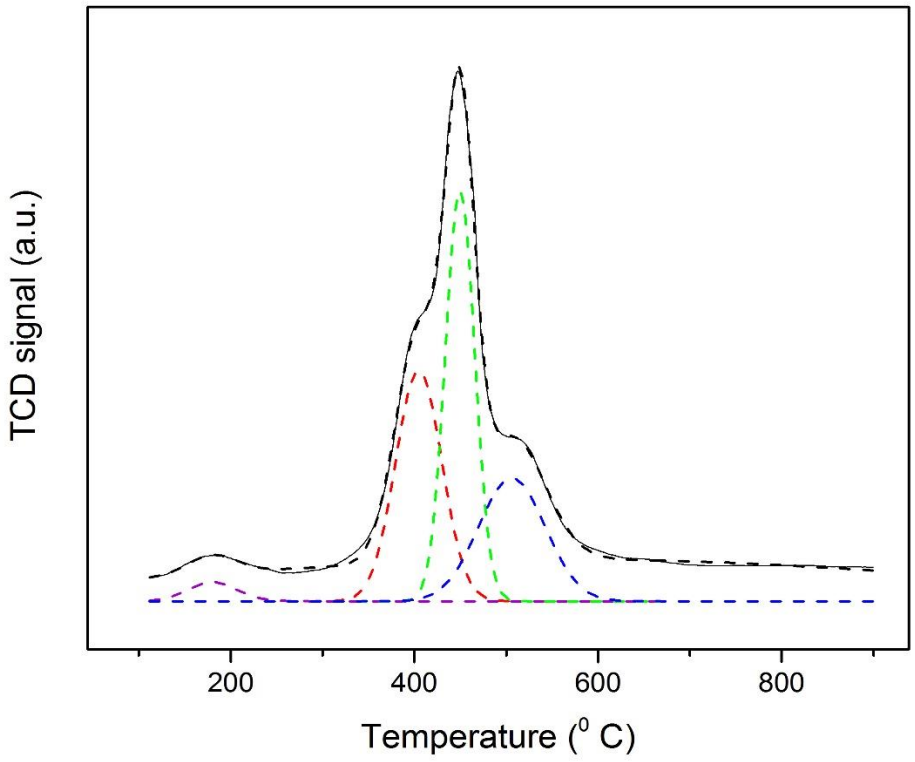

Figure 4-27: Modelling CO-TPD profile for unmodified, oxidized cobalt nanoparticles supported on carbon black (10 wt. %) with Gaussian functions (heating rate was 10 °C s^{-1}).

At low Si/Co ratio the CO desorption peaks shift to lower temperatures indicating that the Co-C bond strength decreased, while at high Si/Co ratio's the CO desorption peaks shift to higher temperatures indicating Co-C bond strength increases (Xiaoping *et. al.,* 2006). The peak area decreased for all modified oxidised cobalt nanoparticles which suggests that the number of actives sites decreased (Xiaoping *et al.,* 2006).

4.6. Fischer-Tropsch synthesis

The Fischer-Tropsch synthesis was conducted for the unmodified and TEOS modified oxidised cobalt nanoparticles. The Fischer-Tropsch synthesis was attempted on the as-synthesised cobalt nanoparticles as well, but these reactions could not be completed due to mechanical fault in the reactor that could not repaired.

The oxidised cobalt nanoparticles were supported on carbon black to ensure good dispersion and were reduced a 350 °C in the presence of hydrogen for 16 hours before synthesis was started. The Fischer-Tropsch synthesis was conducted in a fixed bed reactor under industrially relevant low temperature Fischer-Tropsch conditions of: 220 °C, 20 bar 40 ml/min H_2, 20 ml/min CO and 0.5 g of catalyst with 10 wt% Co. A space velocity of 17.9 mmol CO/min/g Co was applied over the catalysts that were tested. The analysis of the reaction products was conducted using an online GC equipped with a TCD to determine the CO conversion and methane selectivity and an offline GC equipped with an FID to determine the organic product distribution.

4.6.1 Fischer-Tropsch synthesis activity

The “activity” of the Fischer-Tropsch synthesis quantifies the rate at which the CO hydrogenation reaction occurs on the model catalysts that were synthesized. When a fixed set of process conditions were used, the CO conversion can be used as a measurement of the Fischer-Tropsch synthesis activity, that is, a higher conversion implies higher activity (Bukur *et. al.*, 1990).

The CO conversion over the unmodified, oxidised cobalt nanoparticles supported on carbon black (VULCAN XC 72R) has been observed to decrease on the first 1000 minutes on stream (see Figure 4-28). Oddly, the CO-conversion seems to increase after this period reaching some kind of steady-state after ca. 1500 minutes on stream (ca. 24 hrs on stream). The average rate of CO conversion between 1500 and 3000 minutes on stream was 5.5 ± 0.6 %, which corresponds to a rate of CO consumption of 0.10 ± 0.01 mmol CO/min/$g_{catalyst}$. This correspond to a cobalt time yield of 1.0 ± 0.1 mmol CO/min/mol Co. The reduction of this catalyst will yield metallic cobalt particles of a size of 2.7 nm, if it can be assumed that the catalyst in its synthesized state contains only Co_3O_4 particles with an average size of 3.4 nm and these particles reduce without sintering. Using this assumption turnover frequency of $3 \cdot 10^{-3}$ s^{-1} can be estimated. This low turnover frequency, and thus the low measured activity may be linked to the small cobalt particles in this sample (Bezemer *et al.*, 2006; Fischer *et al.*, 2013).

The CO-conversion obtained over the oxidised cobalt nanoparticles contacted with a solution containing TEOS in n-hexane ($[TEOS]_{initial}$ = 0.9 mmol/L) shows initially a high conversion and after 420 minutes on line (7 hrs), the CO-conversion was still larger

than 50% (not shown in Figure 4-28 because of the scale). However, the conversion drops as a function of time on stream and the CO-conversion between 1500 and 3000 minutes on line was 4.7 ± 0.5 %. This implies that the CO-conversion at steady state over this catalyst containing oxidised cobalt nanoparticles exposed to a solution containing TEOS in n-hexane with ($[TEOS]_{initial}$ = 0.9 mmol/L was statistically not different from the CO conversion obtained over the catalyst containing the unmodified, oxidised cobalt nanoparticles.

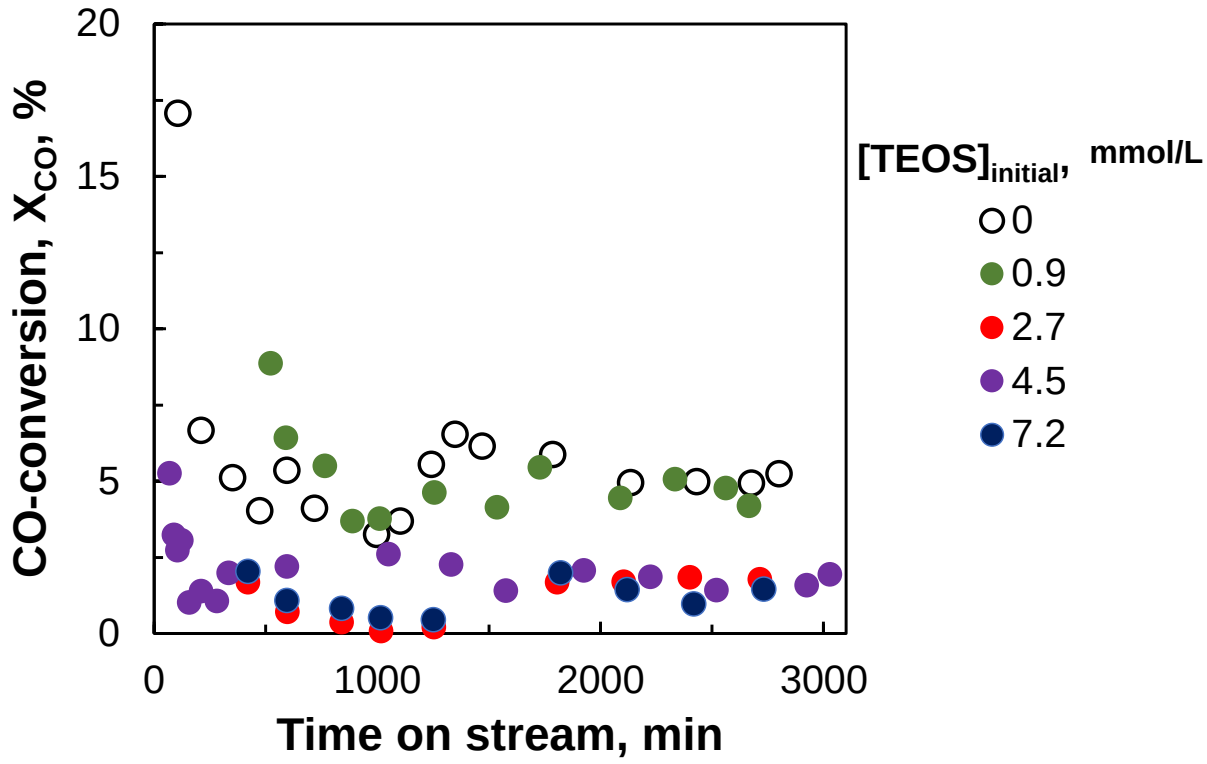

Figure 4-28: CO-conversion obtained over the oxidized cobalt catalyst in the Fischer-Tropsch synthesis (220 °C, 20 bar, 40 ml/min H_2, 20 ml/min CO and 0.5 g of catalyst with 10 wt% Co) as a function of time after reduction in H_2 (50 ml(NTP)/min) at 350 °C for 16 hrs

The CO-conversion obtained over the catalysts containing oxidised cobalt nanoparticles exposed to solutions of TEOS in n-hexane with a higher initial concentration of TEOS shows a significantly lower conversion. The CO-conversion as a function of time on stream seems to pass a minimum for the catalysts containing oxidised cobalt nanoparticles exposed to solutions of TEOS in n-hexane with an initial concentration of TEOS of 2.7 and 7.2 mmol/L. The average CO-conversion obtained at time on stream between 1500 and 3000 minutes on stream with the catalysts containing oxidised cobalt nanoparticles exposed to solutions of TEOS in n-hexane

with an initial concentration of TEOS of 2.7, 4.5 and 7.2 mmol/L was 1.8 ± 0.1 %, 1.7 ± 0.3 % and 1.5 ± 0.4 %, respectively.

Figure 4-29 shows the obtained CO-conversion in the Fischer-Tropsch synthesis after 1500-3000 minutes on stream as a function of the initial concentration of TEOS in the n-hexane solution used to modify the oxidised cobalt nanoparticles. Despite the low conversion levels, it can be concluded that the modification of the oxidised cobalt nanoparticles with TEOS resulted in a decrease in the catalytic activity after depositing the resulting materials on carbon black. This may be taken as an indication that the presence of silicates on the surface of the catalyst inhibits the Fischer-Tropsch activity.

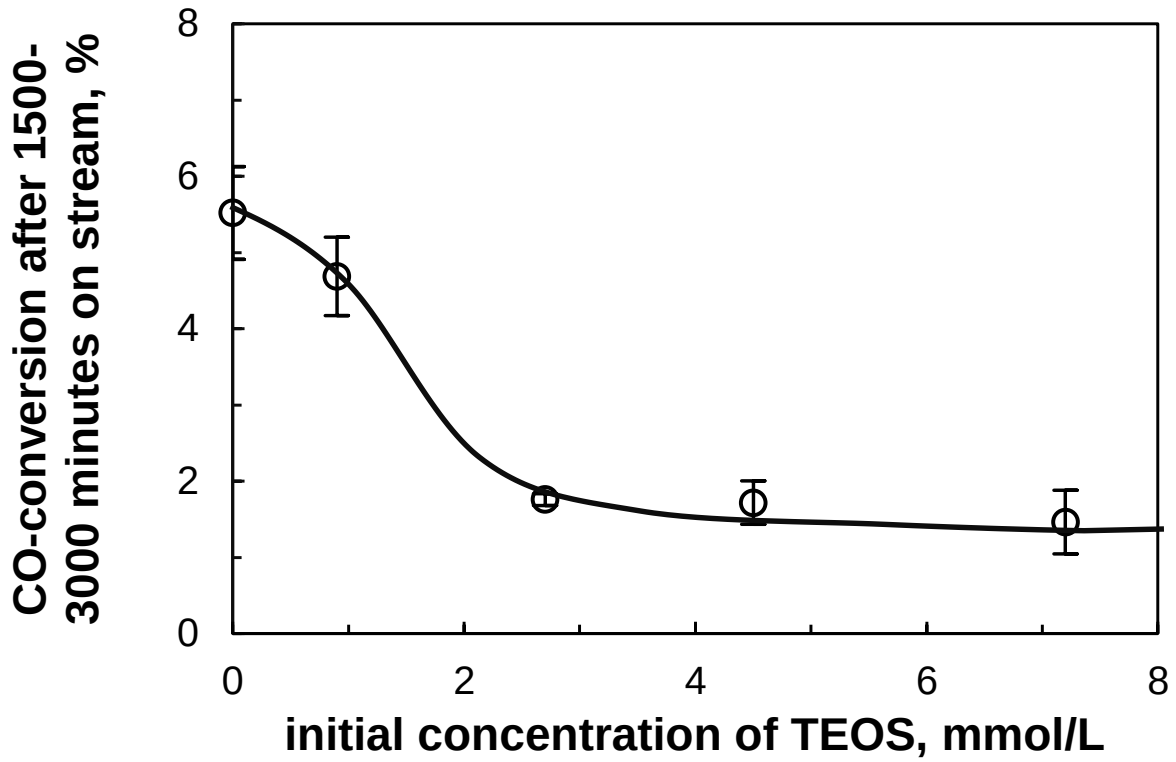

Figure 4-29: The effect of initial concentration of TEOS in n-hexane during the modification of oxidised cobalt nanoparticles on the obtained conversion in the Fischer-Tropsch synthesis after 1500-3000 minutes on stream for the materials supported on carbon black

4.6.2 Fischer-Tropsch synthesis selectivity

Part of the main objectives of the Fischer-Tropsch synthesis was to obtain high selectivity of desired C_{5+} products and reduce methane selectivity. An analysis into the organic compounds after 2600 minutes on stream, especially the olefin content, the 1-olefin content and the alcohol content allows for the understanding of the delicate

interplay between the kinetics of various parallel reaction (Fischer-Tropsch synthesis, water gas shift and olefin secondary reactions) (Todic *et. al.*, 2016).

4.6.2.1. Methane and C_{5+} selectivity

Methane was the least valuable but thermodynamically most favoured organic product in the Fischer-Tropsch synthesis making it necessary that its formation should be inhibited. It was formed when a methyl surface species and a surface hydrogen interact to associatively desorb. The ratio of methyl species, which are chain starters, to hydrogen surface species may affect the rate at which methane forms and thus be chain growth probability.

Figure 4-30 shows the methane selectivity obtained in the Fischer-Tropsch synthesis as a function of time on stream. The variation in the methane selectivity can be quite large since it was determined from the ratio of the amount of methane formed (relative to the internal standard nitrogen) and the amount of CO converted. The catalyst containing the unmodified, oxidised cobalt nanoparticles show the expected methane selectivity of a cobalt catalyst tested in a fixed bed reactor of 11.5 ± 0.9 C-% between 1500 and 3000 minutes on stream. The catalysts containing oxidised cobalt nanoparticles, which had been modified by exposing them to a solution of TEOS in n-hexane, all show a much reduced methane selectivity. It should be noted that the methane selectivity of catalysts tested may also be affected by the different levels of conversion at which the catalysts were tested.

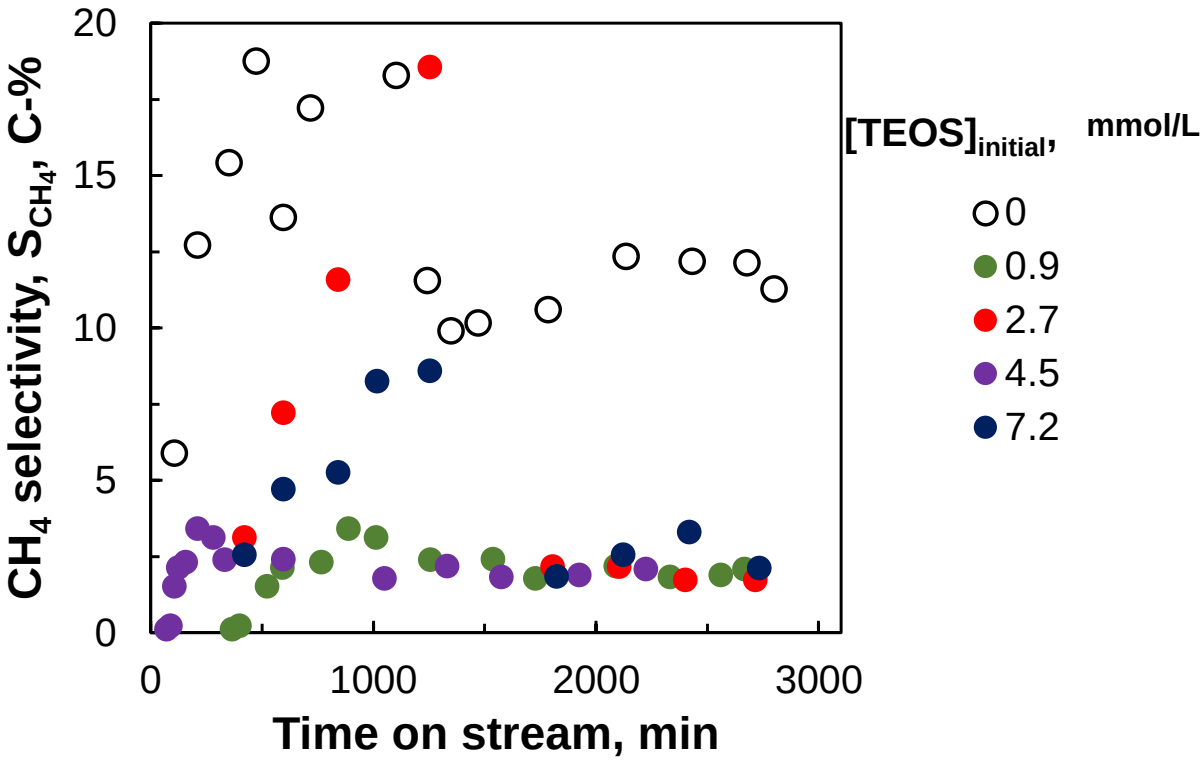

Figure 4-30: Methane and C5+ selectivity as a function of time on stream for oxidized cobalt nanoparticles

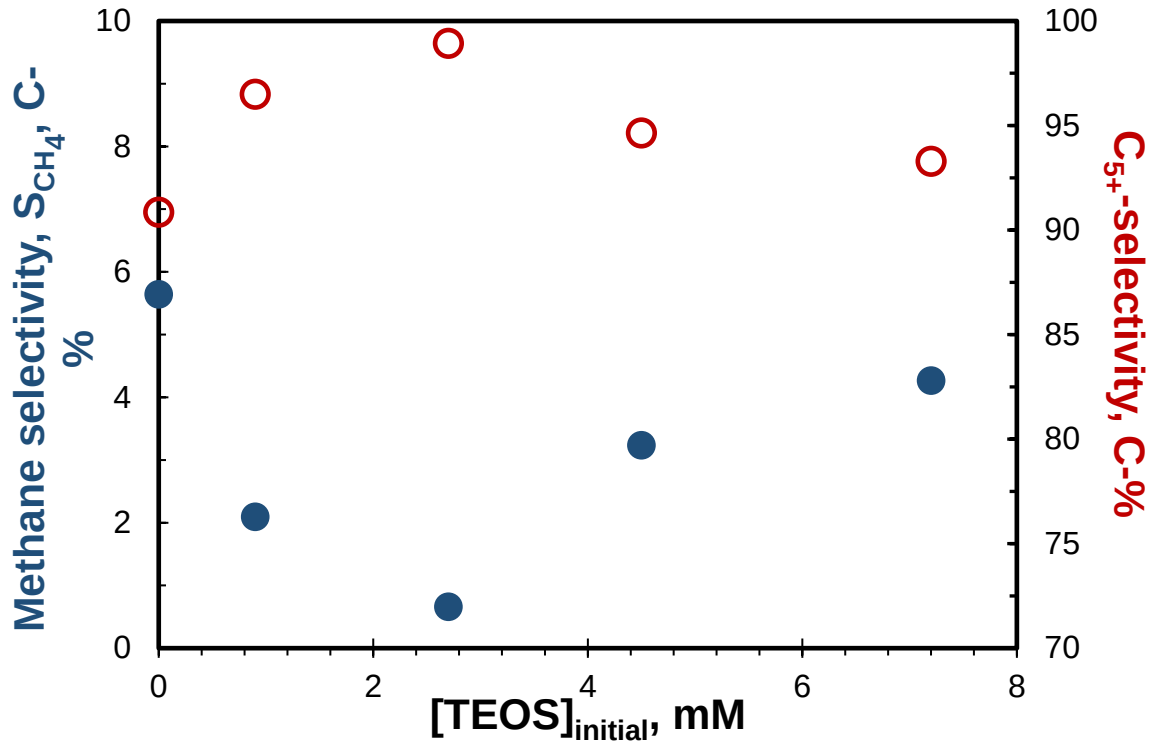

Figure 4-31: Methane and C_{5+} selectivity as a function of silicon content in oxidized cobalt nanoparticles

The methane selectivity for the (un)modified cobalt oxide NPs in the Fischer-Tropsch process is reported in Figure 4-31. The methane selectivity decreases to a minimum at a $[TEOS]_{Initial}$ of 2.7 mM. The C_{5+} selectivity mirrors the methane selectivity. Typical value for methane selectivity over cobalt based catalyst is 5 C-%. In fixed bed reactors, the value of 8-20 C-% is more typically measured (depending on the conversion) (Jahangiri *et al., 2014)*. The C_{5+} selectivity mirrors the methane selectivity. This is typically accompanies by selectivity of C_2-C_4 that is approximately constant (Keyser *et al.*, 1998).

4.6.2.2. Chain growth probability

The product composition of the Fischer-Tropsch synthesis is versatile yet manifests distinct pattern/regularities (Schulz & Claeys, 1999a). The main products of the Fischer-Tropsch synthesis is a polymerisation reaction resulting in the formation of alkanes (paraffins) and alkenes (olefins) of varying carbon chain length. The chain growth probability (α) is the parameter that is used to model the propagation and termination of the polymerization reaction occurring in the Fischer-Tropsch synthesis. It is defined as the fraction of chain growth rate to the total turnover rate and is dependent on carbon chain length, n, and reaction conditions (Förtsch *et al.*, 2015).

The Anderson-Schulz-Flory distribution is obtained when it is assumed that the chain growth probability, α, is independent of carbon chain length (Schulz, 2003):

$$x_n = (1 - \alpha) * \alpha^{n-1} \qquad (4.\ 1)$$

Where x_n is the mole fraction of products having n carbon atoms.

The ASF is an idealized distribution function due to the assumption of a constant chain growth probability. Experimental results have shown deviations from the ideal ASF distribution with products with a higher carbon numbers (C_{10+}) products and methane are present in higher amounts than predicted while the opposite effect is reported for C_2 carbon number products (Todic *et al.*, 2016).

Figure 4-32 shows the experimentally obtained molar product distribution as a function of carbon number on a semi-logarithmic plot. The graph shows the characteristic distribution with higher than expected methane content, a lower than expected content in C_2- product compounds, a gradual increase in the slope of the curve with increasing carbon number. As a result of the expected deviations, the ASF distribution was only applied for carbon number with in the range $4 \leq n \leq 8$, where the chain growth probability α was obtained from the slope.

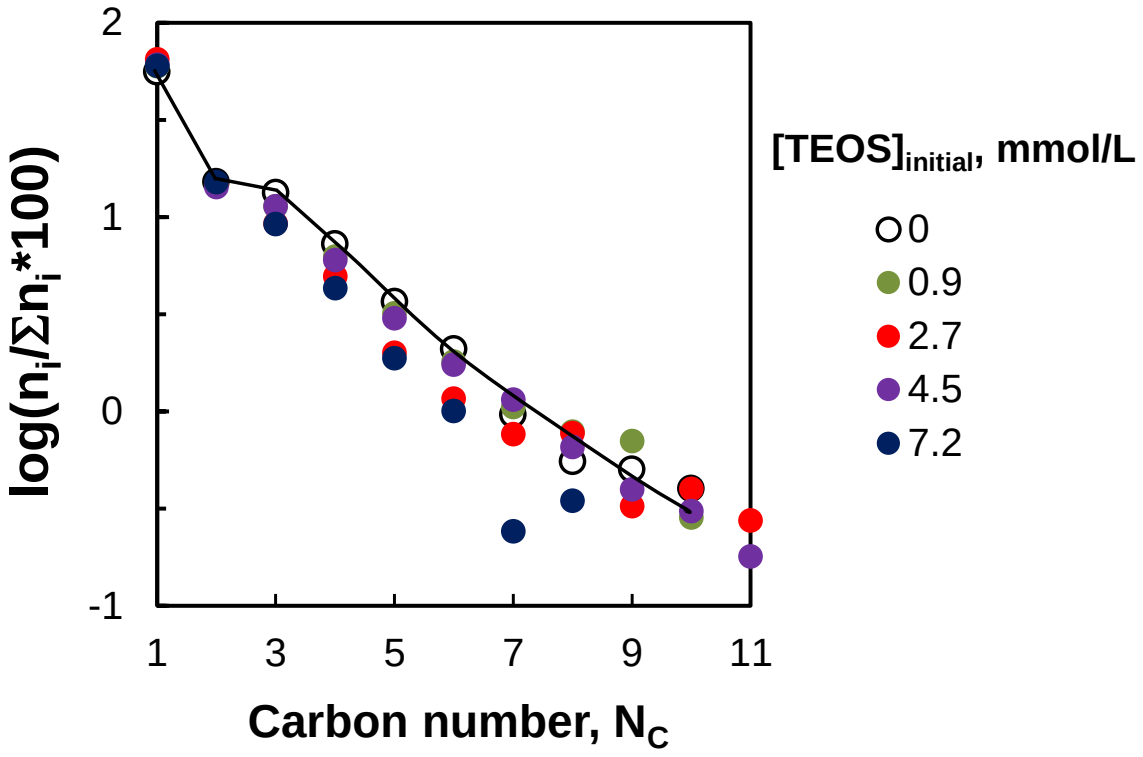

Figure 4-32: Semi-logarithmic of the mole fraction of product compounds as a function of carbon number for modified oxidized cobalt nanoparticles supported on carbon black having a $[TEOS]_{initial}$ of 0, 0.9, 2.7, 4.5, and 7.2 mmol/L The reactor was sampled after 40 hours on stream,

The effect of initial concentration of TEOS in n-hexane to which the oxidised cobalt nanoparticles were exposed on chain growth probability as determined in the range C_4-C_8 was shown on in. The chain growth probability initially increases for the catalysts containing oxidised cobalt nanoparticles, which were exposed to a solution of TEOS in n-hexane up to an initial concentration of 2.7 mmol/L. It may be deduced that the presence of some silicate on the surface of the cobalt nanoparticles in low concentration increases the propagation of the polymerization reaction relative to chain termination in the Fischer-Tropsch synthesis. The chain growth probability decreases again for the catalysts containing oxidised cobalt crystallites exposed to TEOS solutions in n-hexane with a higher concentration

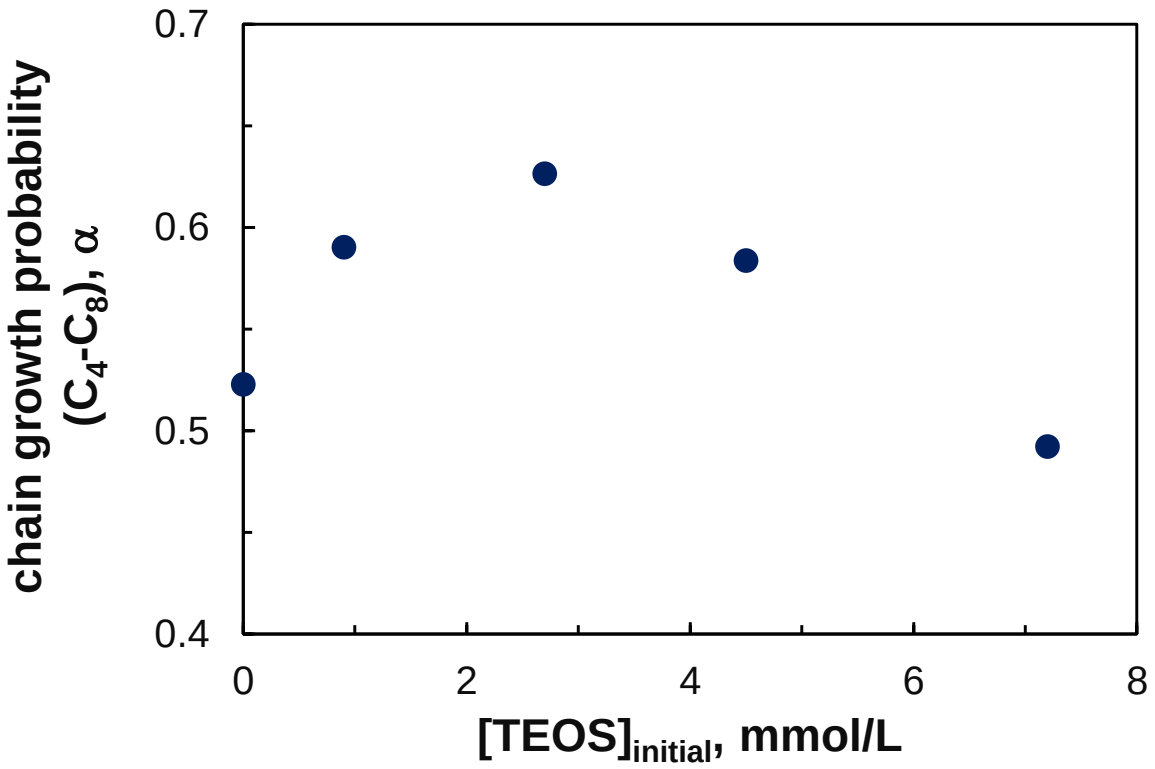

Figure 4-33: The chain growth probability in the Fischer-Tropsch synthesis obtained over oxidised cobalt nano-particles supported on carbon black

4.6.2.3. Olefin content

Primary products of the Fischer-Tropsch synthesis are olefins and paraffins. The olefin content in the fraction of linear hydrocarbons as a function of carbon number was a

useful indicator to assess possible secondary conversion of olefins into paraffins. (see Figure 4-34)

The olefin content obtained over the reduced, unmodified oxidised cobalt nanoparticles supported on carbon black shows the classical trend with a low olefin content in C_2, a maximum at C_3/C_4 and a decrease in the olefin content with increasing carbon number. The low olefin content in C_2 has been attributed to the high reactivity of ethene for secondary hydrogenation under Fischer-Tropsch conditions (Schulz and Gokcebay, 1985). The reactivity of higher olefins was thought the be less dependent on carbon number and the olefin content decreases with increasing carbon number due to the higher solubility of these product compounds in the liquid wax in the reactor. The maximum may shift from C_3 to C_4, if double bond isomerization occurs to a large extent since internal olefins are less susceptible to secondary hydrogenation.

The olefin content over reduced, oxidised cobalt nanoparticles exposed to solutions of TEOS in n-hexane with an initial concentration of TEOS of 0.9 mmol/l and supported on supported on carbon black shows the classical trend with a low olefin content in C_2, a maximum at C_3/C_4 and a decrease in the olefin content with increasing carbon number. The modification of the oxidised cobalt nanoparticles with initial concentration of TEOS of 0.9 mmol/l resulted in a greater than 20% increase in olefin content

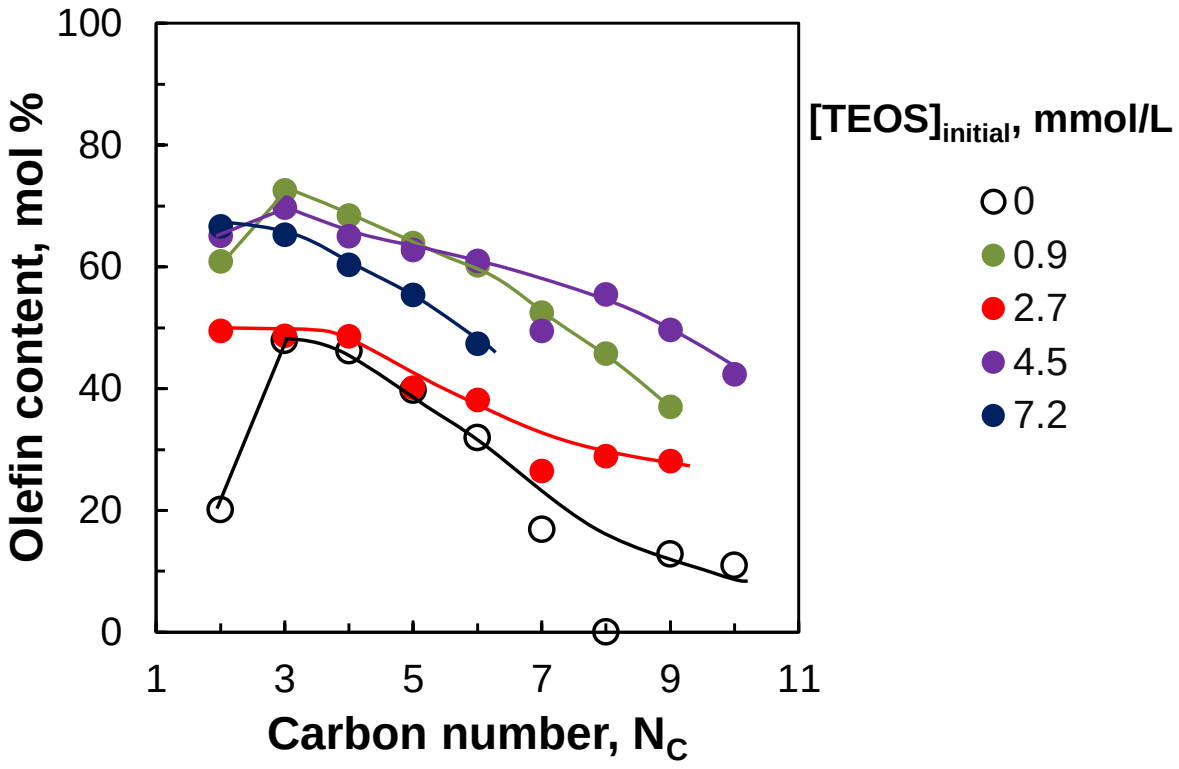

Figure 4-34: The effect of $[TEOS]_{initial}$ on the olefin content in the fraction of linear hydrocarbons as a function of carbon number

The primary product of the Fischer-Tropsch synthesis are linear α-olefins which are formed by the reductive elimination of surface alkyl species from the surface (Schulz & Claeys, 1999b). These terminal olefins are used in the production of valuable industrial and consumer product. Obtaining a high selectivity to α-olefins in the raw Fischer-Tropsch synthesis product had substantial economic benefits as it would decrease the cost of product separation (Bukur *et al.*, 1997).

High selectivity to α-olefins may be limited as it can re-adsorb on the surface of the catalyst and undergo secondary reactions. Alpha olefins can either undergo hydrogenation producing n-paraffin or undergo isomerization where a double bond shift occurs or even participate in further chain growth. Reaction conditions, the catalyst used, and the olefin chain length are the parameters that affect the rate at which the α-olefin secondary reactions occur (Schulz & Claeys, 1999b). In this work the reaction conditions were kept constant for all catalysts that were tested.

The 1-olefin content in fraction of linear olefins is reported in Figure 4-35. The 1-Olefin content decreases with increasing carbon number for all oxidized cobalt catalyst that were tested. Secondary reactions increase with increasing carbon number due to

increase solubility of the olefins in the liquid phase. When the amount of silicates on the surface was increased the 1-olefin content in fraction of linear olefins increased. This suggest that secondary double bond isomerization was hindered by the presence of silicates on the catalyst surface.

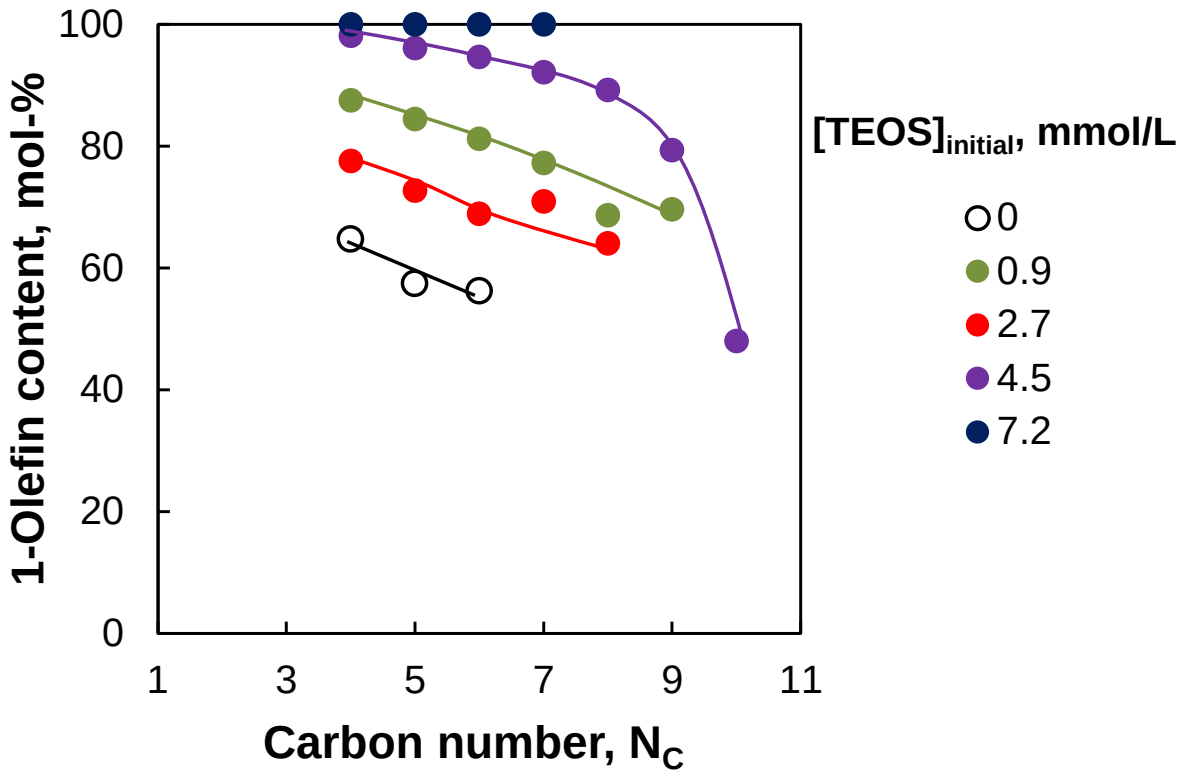

Figure 4-35: The effect of $[TEOS]_{initial}$ on 1-olefin content in fraction of linear olefins for C_4-C_8

An adsorbed species on the surface of the catalyst can desorb as a paraffin, olefin or oxygenate in the Fischer-Tropsch synthesis. The selectivity in the fraction of C_2-products is reported in Figure 4-36.The olefin and aldehyde content were observed to increase with increasing Si/Co ratio. The opposite trend was observed for paraffins and alcohols. The total oxygenate content remained fairly constant for both the unmodified and modified cobalt oxide catalyst. The dehydrogenation of alcohols to aldehydes increases with $[TEOS]_{initial}$ used to modify the catalyst.

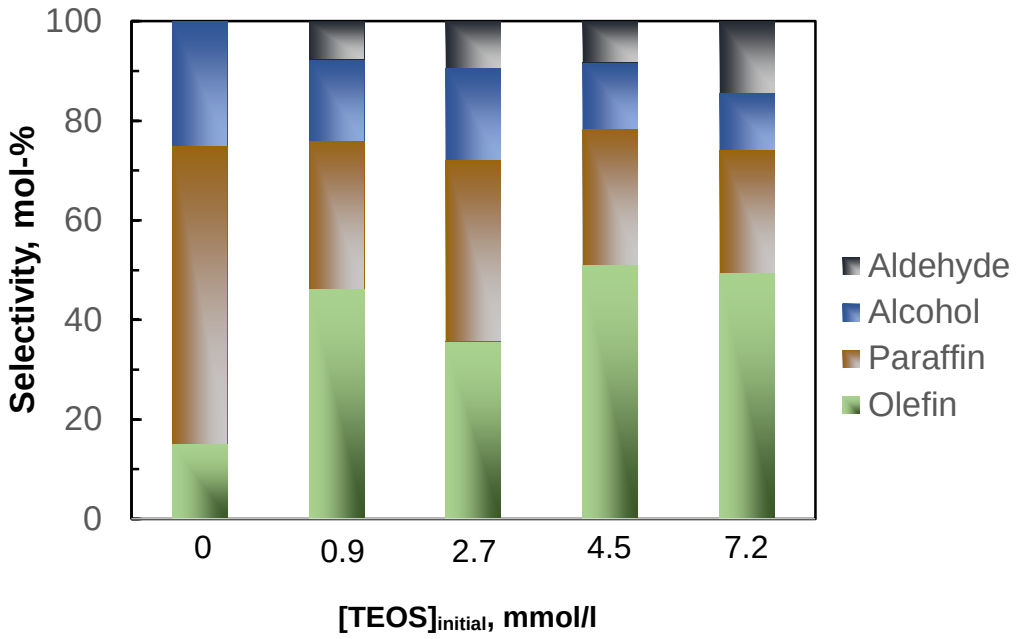

Figure 4-36: Selectivity in the fraction of C2-products as a function of silicon content

4.6.3 Analysis of spent catalyst

After 44 hours on-line, the fixed bed reactor was shutdown. The shutdown procedure required the turning off of all feed gasses with the exception of argon. The argon flow was used to purge the system while the temperature of the reactor was allowed to decrease via conduction. The spent catalyst was removed from the fixed bed reactor by shacking to contents onto a weighting boat and using compressed air to blowout any catalyst that may have attached to the walls of the reactor.

A 150 µm sieve was used to separate the catalyst from the diluent, SiC, prior to analysis. The change in the shape and particle size of the catalyst during Fischer-Tropsch was analysed using TEM. The effect of silylation on the dispersion of the catalyst was investigated using H_2 chemisorption. The dispersion will be attained from the direct information obtained on number of active sites from H_2 chemisorption.

TEM micrographs of the cobalt oxide spent catalysts are shown in Figure 4-37. The particle size increased from 5.8 ± 1.3 nm to 11.0 ± 2.7 nm for the unmodified nanoparticles which indicates that some sintering occurred for the unmodified nanoparticles. There appears to be clustering of nanoparticles for the modified nanoparticles. It was not clear from the TEM images whether the nanoparticles have sintered or migrated to form agglomerates on the catalyst.

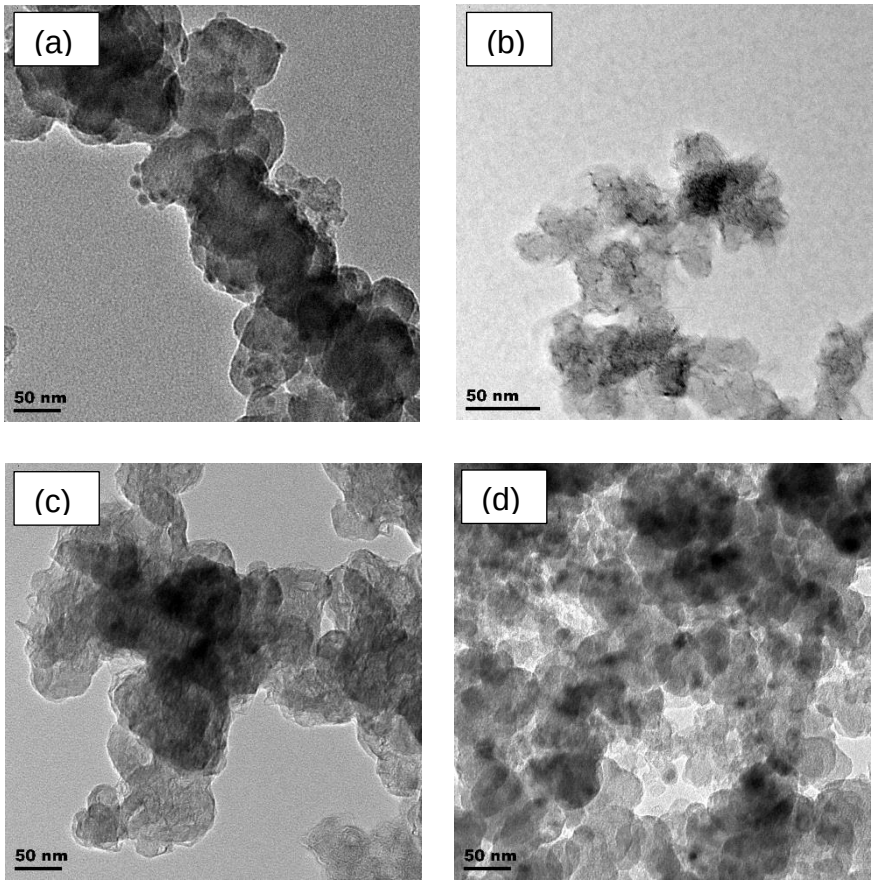

Figure 4-37: TEM micrographs of spent catalyst of the catalysts containing initially oxidised cobalt nanoparticles exposed to solution of TEOS in n-hexane with an initial concentration of TEOS of (a) 0, (b) 0.9, (c) 4.5 and (d) 7.2

H_2 chemisorption studies of the spent catalysts was conducted to obtain the dispersion. A negative metal dispersion and surface area was obtained. This suggested that there was wax in the pores of the catalyst. In order for the dispersion to be determined the wax need to be removed from the pores. Soxhlet extraction could be used to remove the wax in the pores of the catalyst. Wax is highly soluble in xylene hence it was the ideal extraction solvent to use. The catalysts was placed in a filter paper thimble during the extraction process. The catalyst adheres to the filter paper making the recoverability of the catalyst in the wax removal process very low. Since 0.5 g of catalyst are used during Fischer-Tropsch synthesis and at least 0.2 grams of catalyst are needed for H_2 chemisorption the use of Soxhlet extraction became unfeasible. Therefore, it was not possible to determine the dispersion.

Chapter 5 Discussion of results

Oxidized cobalt nanoparticles were synthesized by reducing cobalt carbonyl to cobalt nanoparticles. The as-synthesized cobalt nanoparticles were then left in the fume hood to oxidize to Co_3O_4. The oxidized cobalt nanoparticles were then modified in dilute TEOS solutions in n-hexane. A study on the rate of uptake of the TEOS with varying initial TEOS concentration was conducted. In this study it was observed that the Si/Co ratio generated by the uptake studies was higher than the Si/Co ratio determined by the elemental analysis technique, EDX. The washing of the cobalt nanoparticles after modification may have resulted in some of the physisorbed TEOS to be removed from the nanoparticles. If this was the case, it suggests that TEOS was only weakly bonded to the surface of the oxidized cobalt nanoparticles. This resulted on them being removed during the washing process after modification. More investigation is required to understand if the different bond strengths of TEOS on the surface could amount to the difference in the bonding that constitutes electron sharing (chemisorption) or van de Waal forces (physisorption).

The X-ray diffraction (XRD) pattern of the modified oxidized cobalt nanoparticles showed that the crystalline structure was not affected by the modification with TEOS. No other crystalline structures were observed suggesting that the silicates on the surface of the catalyst are amorphous or too small to be detected using XRD. The Debye-Scherrer equation was used to determine the crystallite size of the oxidized cobalt nanoparticles. The calculated crystallite size was smaller than the observed particle size from the transmission electron microscopy (TEM) suggesting there maybe two oxide phases still present in the catalyst. TEM analysis of the TEOS modified particles showed that they formed clusters resulting in poor dispersion. It was postulated that the TEOS modification results in a strong attraction between the nanoparticles leading to the formation of these clusters. Sintering of the oxidized cobalt nanoparticles during modification was ruled out as the particles were well dispersed upon supporting them on carbon black.

The unmodified and TEOS modified oxidized cobalt nanoparticles were reduced in a fixed bed Fischer-Tropsch reactor. Syngas was reacted over the reduced (un)modified oxidized cobalt nanoparticles. It was observed that the activity of the catalyst decreases with increasing silicon content on the surface of the catalyst. A comparison

of the turnover frequency (TOF) of the small NPs (d_p= 5.8 ± 1.3 nm) used in this work with that of larger NPs (d_p 25 nm) (Macheli, 2014) is shown in Figure 5-1. The turnover frequency was determined by dividing the number of moles of CO consumed with the product of the mole of Co^0 in the catalyst and time on stream. Time on stream was 40 hours.

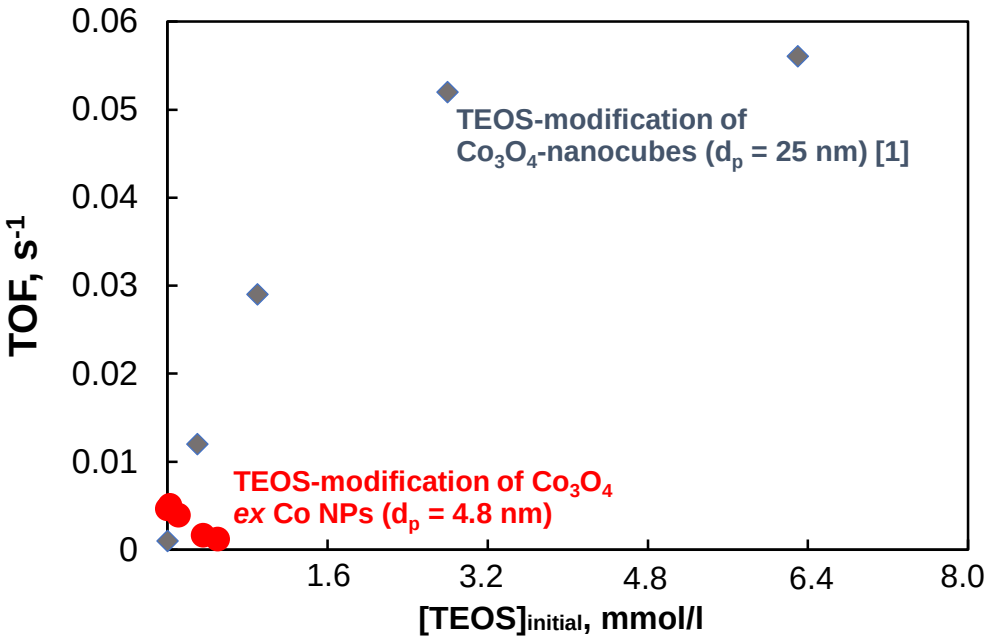

Figure 5-1: Effect of silicate content in cobalt catalyst surface on the TOF in the Fischer-Tropsch synthesis.

The TOF increases with increasing silicates per surface cobalt for large cobalt oxide nanoparticles. For small oxidized cobalt nanoparticles small increases of the surface silicates leads to a decrease in the TOF. The presence of silicates on the surface of cobalt oxide nanoparticles can increase or decrease the TOF, hence activity, of the catalyst depending on the particle size.

The cobalt particle size effect on the Fischer-Tropsch activity was reported by Bezemer *et al.* (2006). The activity behaves like a volcanic curve were it initially increases with decreasing particle size until a maximum activity was reached. When this maximum was reached further decrease in particle size results in a rapid decline in the activity. The maximum Fischer-Tropsch activity for cobalt based catalyst when operating at 1 bar and 35 bar was reached at the average particle size of 6 nm and 8nm respectively (Bezemer et al., 2006). It has been argued through SSITKA experiments that this was due to the increase in irreversibly adsorbed CO on the

surface, increase in surface residence time for reversibly bonded CH_x intermediates and decrease in the surface coverage of CH_x and CO intermediates for particles smaller than 6 nm (den Breejen *et al.*, 2009). Small particles promote strong adsorption of CO on the catalyst surface in cobalt based Fischer-Tropsch.

The surface modification of cobalt catalyst with transition metal oxide precursors has been investigated (Morales *et al*., 2005; Johnson, Werner & Bell, 2015; Macheli *et al.*, 2018; Petersen *et al.*, 2018). In these studies, it has been shown that upon contacting the catalyst with the precursor, metal oxide islands were formed on the cobalt oxide surface. Further evidence was given to show that the islands acted as Lewis acids which elongates the CO bond resulting in a more facile CO bond cleavage. A DFT study conducted on the effect of alumina ligand on a Co surface on the adsorption and dissociation of carbon monoxide also revealed that the ligand acts as a Lewis acid which result in lowering the energy for the cleavage of the CO bond (van Heerden & van Steen, 2017). Therefore, silicates present on the catalyst surface may facilitates the dissociation of adsorbed CO.

The rates of CO consumption, hence the catalyst activity, in the Fischer-Tropsch reaction is dependent on the surface coverage of carbon on the catalyst as depicted in Figure 5-2. Large cobalt nanoparticles have a low surface coverage of carbon(den Breejen *et al.*, 2009). When surface silicates are increased a facile CO bond cleavage is facilitated. Higher carbon surface coverage is achieved leading to an improve activity as observed for the large cobalt oxide nanoparticles. Small cobalt nanoparticles have a high CO/Co_{surf} due the large amount of edge/corner sites (den Breejen *et al.*, 2009). Increasing the surface silicates in small particles would result in a decrease in the activity of the catalyst due to high surface carbon coverage.

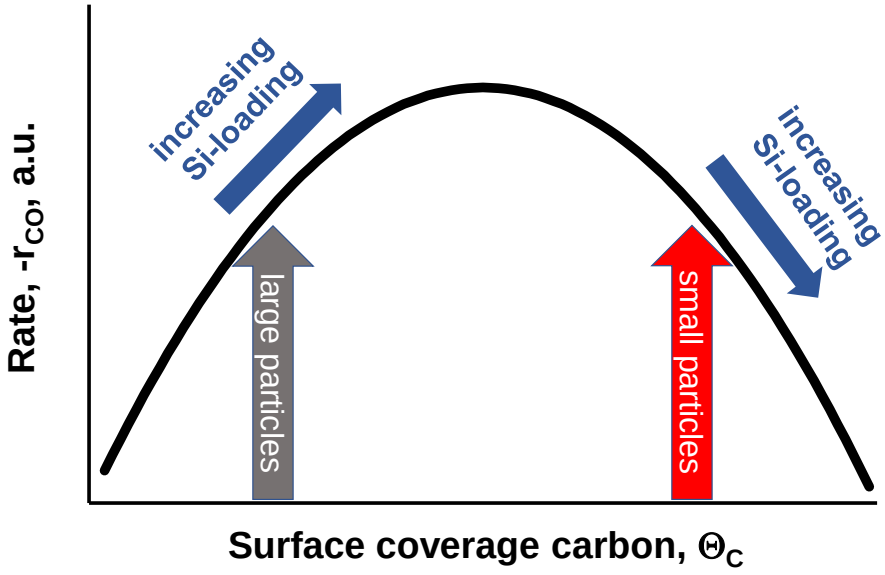

Figure 5-2: The rate of CO consumption as a function of the surface coverage of carbon

The desired products in low temperature Fischer-Tropsch are long chain hydrocarbons. The production of methane is undesired as it has a low market value. For the tested oxidized cobalt nanoparticles it was observed that with that the methane selectivity was low and passed through a minimum. The methane selectivity depends on the carbon coverage/hydrogen availability on the surface of the catalyst. Low carbon coverage leads to high methanation due to too much hydrogenation. High carbon coverage results in a slow supply of the CH_x intermediate for chain growth leading to high levels of methanation (Schulz, van Steen & Claeys, 1994; van Santen *et al.*, 2011). As the Si/Co_{surf} increases, the carbon coverage is thought to increase, since the surface silicates are thought to facilitate CO dissociation, thus lowering methane selectivity. However, further increase in the Si/Co_{surf} leads to high carbon coverage which increases methane selectivity. The overall low methane selectivity maybe as a result of the low conversions that were obtained.

An analysis on the selectivity in the fraction of C_2-products showed that the olefin and aldehyde content increased with increasing surface silicates. This was as a result of less hydrogenation due to the presence of silicates on the surface of the catalysts. The 1-olefin content in the fraction of linear olefins increased with increasing Si/Co ratio between carbon numbers 4 and 8. 1-Olefins can reabsorb on the catalyst surface and can be either hydrogenated to n-paraffins or undergo secondary double bond

isomerization to form 2-olefins. The increase in 1-olefine content with increasing silicates suggests that a lower hydrogen availability leading to less secondary double bond isomerization.

As-synthesized cobalt nanoparticles were synthesized using the same protocol as used for the oxidised cobalt nanoparticles, however the oxidation step was omitted. The catalysts did however get oxidised during the washing process forming a CoO layer as was detected by XRD studies. In order to prevent agglomeration of the nanoparticles during modification, as observed with the oxidized cobalt nanoparticles, the modification medium was changed to chloroform. This required that the organo-silane used during silylation be soluble in chloroform. Triphenylethoxysilane was chosen as it was highly soluble in organic solvents. Furthermore, it contains an ethoxy group that can react with surface hydroxyl groups. After modification, the catalysts were washed with methanol followed by EDX elemental analysis. The Si/Co ratio of the two catalysts was below the detection level of 0.1 wt%. This suggested that either there are only a few sites on which the formation of the silicate islands can form on the catalyst surface or the organosilane used during modification exhibits steric hindrance due to the large phenyl groups therefore limiting the silicate adsorption. The presence of silicates in the catalysts was confirmed by the presence of Si-O-Co bond for all modified catalysts in FTIR studies.

The adsorption sites on the surface of the catalyst were observed through CO chemisorption. This leads to more CO molecules undergoing dissociative adsorption as evidenced by the peak ratio shifts. The reducibility of the catalyst decreased with increasing Si/Co ratio as observed by the shift of the TPR peak maximum to higher temperatures. The presence of a shoulder peak in the modified nanoparticles further suggested that there a parts of the catalyst which are reduce at higher temperatures due to their proximity to the silicate island.

Chapter 6 Conclusion

The objective of this work was to elucidate the effect of oxidation state of cobalt on the formation of metal-support interactions (MSI) on silica support and how this would affect the activity and selectivity of the Fischer-Tropsch synthesis. The inverse method of catalyst preparation was adopted in order to isolate MSI from other support parameters that influence the activity and selectivity of the Fischer-Tropsch synthesis. The preparation of an inverse catalyst involves the bonding of a support like ligand to the active metal precursor. The bonding of a support like ligand to the active metal precursor has been shown in literature to form amorphous support islands on the surface on the support.

As-synthesized and oxidised cobalt nanoparticles were modified with triphenylethoxysilane (TPEOS) and tetraethoxysilane (TEOS), respectively. The formation of amorphous support islands, silicate islands in this case, was evaluated using FTIR measurements. The signature functional group observed in FTIR for the silicates bonded to the cobalt surface was Si-O-Co. The Si-O-Co band was observed at wavenumbers of 1020 cm^{-1} and 1060 cm^{-1} for oxidised and as-synthesized cobalt nanoparticles respectively. The silicate islands have been reported to be stable during reduction and Fischer-Tropsch synthesis. This was however not tested in this work.

Complete reduction of the cobalt nanoparticles to the active form, Co^0, in Fischer-Tropsch is essential for the effective use of this expensive resource. The reduction temperature of both as-synthesized and oxidised cobalt nanoparticles increased with increasing Si/Co ratio. This suggests that the surface silicates hinder the reduction process by hindering activation and nucleation of reduced cobalt phases.

The inverse catalysts were supported on carbon black for Fischer-Tropsch analysis. The Fischer-Tropsch activity decrease sharply with increasing Si/Co ratio. This was not anticipated as surface silicates act as Lewis acids which make the CO bond facile, reducing the energy of CO dissociation. However, the understanding of the particle size effect revealed that for nanoparticles with less than 8 nm there was high carbon coverage due to the large presence of step/corner sites. Since surface silicates also increase carbon deposition it led to a decrease in activity due to high carbon surface coverage. The methane selectivity passed through a minimum with increasing Si/Co ratio. The C_{5+} selectivity mirrored the methane selectivity.

Chapter 7 Recommendation

In order to understand to stability of the surface silicates during reduction, in situ XPS studies could be performed with reduction oxidation cycles. TEM elemental mapping for both modified as-synthesized and oxidised cobalt nanoparticles could also be used to observe if the formation of the surface silicates occurs differently on them.

The Fischer-Tropsch synthesis of the as-synthesized cobalt could also be done to observe how the modification would affect the activity and selectivity of the Fischer-Tropsch synthesis. The Fischer-Tropsch synthesis could also be conducted with larger amounts of catalyst. This experiment could also be performed with larger cobalt crystallites.

References

Adesina, A.A. 1996. Hydrocarbon synthesis via Fischer-Tropsch reaction: trials and triumphs *Applied Catalysis A: General*. **138**: 345-367

Ahmadi, M., Mistry, H. & Cuenya, B.R. 2016. Tailoring the catalyst properties of the metal nanoparticle via support interaction. *The Journal of Physical Chemistry Interaction* **7**: 3519-3533.

Arsalanfar, M., Mirzaei, A.A., Bozorgzadeh, H.R. & Samimi, A. 2014. A review of Fischer-Tropsch synthesis on the cobalt based catalysts. *Physical Chemistry Research* **2(2)**: 179-201.

Avrami, M. 1941.Kinetics of phase change III. Granulation, phase change and microstructure. *Journal of Chemical Physics* **9(2)**: 177-184.

Bellido, J.D.A. & Assaf, E.M. 2009. Effect of the Y_2O_3-ZrO_2 support composition on nickel catalyst evaluated in dry reforming of methane. *Applied Catalysis A: General* **352**: 179-187.

Bernal, S.,Calvino, J.J., Cauqui, M.A., Gatica, J.M., Larese, C., Perez Omil, J.A., Pintado, J.M. 1999. Some recent results on metal/support interaction effects in NM/CeO_2 (NM: noble metal) catalysts. *Catalysis Today* **50(2)**: 175-206.

Bezemer, G.L., Bitter, J.H., Kuipers, H.P., Oosterbeek, H., Holewijn, J.E., Xu, X., Kapteijn, F., van Dillen, A.J. & de Jong, K.P. 2006. Cobalt particle size effect in the Fischer-Tropsch reaction studied with carbon nanofiber supported catalyst . *Journal of American Chemical Society* **128**: 3956-3964.

Blyholder, G. & Wyatt, W.V. 1966. Infrared spectra and structures of some CxHyO compounds Adsorbed on silica-supported Iron, Cobalt, and Nickel. *The Journal of Physical Chemistry* **70(6)**: 1745-1750.

Bukur, D.B., Lang, X., Mukesh, D., Zimmerman, W.H., Rosynek, M.P. & Li, C. 1990. Binder/support effect on the activity and selectivity of iron catalysts in the Fischer-Tropsch synthesis. *Industrial & Engineering Chemistry Research* **29(8)**: 1588-1599.

Bukur, D.B., Lang, X., Akgerman, A. & Feng, Z. 1997. Effect of process conditions on olefin selectivity during conventional and supercritical Fischer− Tropsch synthesis. *Industrial & Engineering Chemistry Research* **36(7)**: 2580-2587.

Camargo, P.H.C., Rodrigues, T.S., da Silva, Anderson G. M. & Wang, J. 2015. Controlled synthesis: nucleation and growth in solution. In *metallic nanostructures: from controlled synthesis to applications (*Y. Xiong & X. Lu, Eds) Springer International Publishing pp. 49-74.

Cargnello, M., Fornasiero, P. & Gorte, R.J. 2012. Opportunities for tailoring catalytic properties through metal-support interactions. *Catalysis Letters* **142**: 1043-1048.

Carlson, A.F., Naschitzki, M., Baumer, M., Freund, H. J. 2003. The structure and reactivity of Al_2O_3-supported cobalt-palladium particles: A CO-TPD, STM, and XPS study. *Journal of Physical Chemistry* **107**: 778-785

Che, M. 1993. Interfacial coordination chemistry: concepts and relevance to catalysis phenomena. *Studies in Surface Science and Catalysis* ***75***: 31-68.

Chen, Y., Liew, K.Y. & Li, J. 2009. Size controlled synthesis of Co nanoparticles by combination of organic solvent and surfactant*. Applied Surface Science* **255(7)**: 4039-4044.

Chonco, Z.H., Lodya, L., Claeys, M., van Steen, E. 2013. Copper ferrites: A model for investigating the role of copper in the dynamic iron-based Fischer-Tropsch catalyst. *Journal of Catalysis* **308**: 363-373

Cuenya, B.R. 2010. Synthesis and catalytic properties of metal nanoparticles: size, shape, support, composition, and oxidation state effects. *Thin Solid Films* **518**: 3127-3150.

Davis, B.H. 2001. Fischer–Tropsch synthesis: current mechanism and futuristic needs. *Fuel Processing Technology* **71(1–3)**: 157-166.

de Beer, M., Kunene, A., Nabaho, D., Claeys, M., van Steen, E. 2014. Technical and economic aspects of promotion of cobalt-based Fischer-Tropsch catalysts by noble metals- a review. *Journal of the South African Institute of Mining and Metallurgy* **114**: 157-165.

den Breejen, J.P., Radstake, P.B., Bezemer, G.L., Bitter, J.H., FrøÃ¸seth, V., Holmen, A. & de Jong, K.P. 2009. On the origin of the cobalt particle size effects in Fischer-Tropsch catalysis. *Journal of the American Chemical Society* **131(20)**: 7197-7203.

Dlamini, H., Motjope, T., Joort, G., ter Stege, G., Mdleleni, M. 2001. Change in physico-chemical properties of iron-based Fischer-Tropsch catalyst induced by SiO_2 additions. *Catalysis Letters* ***78****: 201-207*.

Dry, M.E. 1996. Practical and theoretical aspects of the catalytic Fischer-Tropsch process. *Applied Catalysis A: General* ***138***: 319-344.

Dry, M.E. 2002. High quality diesel via the Fischer-Tropsch process - a review. *Journal of Chemical Technology and Biotechnology* **77**: 43-50.

Duvenhage, D.J and Coville, N.J. 1997. Fe:Co/TiO_2 bimetallic catalysts for the Fischer-Tropsch reaction: Part 1. Characterization and reactor studies. *Applied Catalysis A: General* **153(1-2)**: 43-67.

Ernst, F. 1995. *Metal-oxide interfaces*. *Materials Science and Engineering: Reports* **14(3)**: 97-156.

Fischer, N., Van Steen, E., Claeys, M. 2013. Structure sensitivity of the Fischer-Tropsch activity and selectivity on alumina supported cobalt catalyst. *Journal of Catalysis* **299**: 67-80

Förtsch, D., Pabst, K. & Groß-Hardt, E. 2015. The product distribution in the Fischer-Tropsch synthesis: An extension of the ASF model to describe common deviations. *Chemical Engineering Science* **138**: 333-346.

Fouad, O.A., Makhlouf, S.A., Ali, G.A.M. & El-Sayed, A.Y. 2011. Cobalt/silica nanocomposite via thermal calcination-reduction of gel precursors*. Materials Chemistry and Physics* **128(1-2)**: 70-76

Fu, Q. & Wagner, T. 2007. Interaction of nanostructured metal overlayers with oxide surfaces. *Surface Science Reports* **62(11)**: 431-498

Fu, T., Jiang, Y., Lv, J. & Li, Z. 2013. Effect of carbon support on Fischer–Tropsch synthesis activity and product distribution over Co-based catalysts. *Fuel Processing Technology* **110**: 141-149

Fu, T. & Li, Z. 2015. Review of recent development in Co-based catalysts supported on carbon materials for Fischer–Tropsch synthesis. *Chemical Engineering Science* **135**: 3-2

Garces, L.J., Hincapie, B., Zerger, R., Suib, S.L. 2015. The effect of temperature and support on the reduction of cobalt oxide: An in situ X-ray diffraction study. *The Journal of Physical Chemistry* **119**: 5484-5490

Gracia, J.M., Prinsloo, F.F. & Niemantsverdriet, J.W. 2009. Mars-van Krevelen-like Mechanism of CO Hydrogenation on an iron carbide surface. *Catalysis Letters* **133(3)**: 257-261.

Gulbransen, E.A. & Andrew, K.F. 1951. The kinetics of oxidation of cobalt. *Journal of the Electrochemical Society* **98(6)**: 241-251.

Hauman, M.M., Saib, A., Moodley, D.J., du Plessis, E., Claeys, M., van Steen, E. 2012. Re-dispersion of cobalt on a model Fischer-Tropsch catalyst during reduction-oxidation-reduction cycles. *ChemCatChem* **4**: 1411-1419

Honda, H., Suzaki, K., Sughara. 2001. Control of hydrolysis and condensation reactions of titanium *tert*-butoxide by chemical modification with catechol. *journal of Sol-Gel Science and Technology* **22**: 133-138

Huang, X. & Chen, Z. 2004. Preparation of CoFe2O4/SiO2 nanocomposites by sol–gel method. *Journal of Crystal Growth* **271(1-2)**: 287-293

Iglesia, E. 1997. Design, synthesis, and use of cobalt-based Fischer-Tropsch synthesis catalysts. *Applied Catalysis A: General* **161(1–2)**: 59-78.

Jacobs, G., Das, T.K., Zhang, Y., Li, J., Racoillet, G. & Davis, B.H. 2002. Fischer–Tropsch synthesis: support, loading, and promoter effects on the reducibility of cobalt catalysts. *Applied Catalysis A: General* **233(1–2)**: 263-281.

Jahangiri, H.; Bennett, J., Mahjoubi, P., Wilson, W., Gu, S. 2014. A review of advanced catalyst development for Fischer-Tropsch synthesis of hydrocarbons from biomass derived syn-gas. *Catalysis, Science and Technology* **4**: 2210-2229

Jiang, Z., Zhao, Y., Huang, C., Song, Y., Li, D., Liu, Z. & Liu, Z. 2018. Metal-support interactions regulated via carbon coating – A case study of Co/SiO2 for Fischer-Tropsch synthesis. *Fuel* **226**: 213-220

Johnson, G.R., Werner, S. & Bell, A.T. 2015. An investigation into the effects of Mn promotion on the activity and selectivity of Co/SiO2 for Fischer−Tropsch Synthesis: evidence for enhanced CO Adsorption and Dissociation. *American Chemical Society Catalysts* **5**: 5888-5903.

Jong, S. & Cheng, S. 1995. Reduction behavior and catalytic properties of cobalt containing ZSM-5 zeolites. *Applied Catalysis A: General* **126(1)**: 51-66.

Jun, Y., Choi, J., & Cheon, J. 2006. Shape control of semiconductor and metal oxide nanocrystals through nonhydrolytic colloidal routes. *Angewandte Chemie* **45**: 3414-3439.

Kababji, A.H., Joseph, B. & Wolan, J.T. 2009. Silica-supported cobalt catalysts for Fischer-Tropsch synthesis: effects of calcination temperature and support surface area on cobalt silicate formation. *Catalysis Letters* **130(1)**: 72-78.

Keyser, M.J., Everson, R.C., Espinoza, R.L. 1998. Fischer-Tropsch studies with cobalt-manganese oxide: Synthesis performance in a fixed bed reactor. *Applied Catalyst A: General* **171**: 99-107.

Khodakov, A.Y., Chu, W. & Fongarland, P. 2007. Advances in the development of novel cobalt Fischer-Tropsch catalysts for synthesis of long-chain hydrocarbons and clean fuels. *Chemical Reviews* **107(5)**: 1692-1744.

Kruit, K.D., Vervloet, D., Kapteijn, F., van Ommen, J.R. 2013. Selectivity of the Fischer-Tropsch process: deviations from single alpha product distribution explained by gradients in process conditions. *Catalysis Science & Technology* **3**: 2210-2213.

Li, L., Hu, C., Liu, W., Fei, P., Cui, X., Li, Y., Xu, J. 2017. The origin of Mo promotion during H_2 pretreatment on an Fe catayst for Fischer-Tropsch synthesis. *The Royal Society of Chemistry Advances* **7**:44474-44481

Li, Y., Fan, Y., Yang, H., Xu, B., Feng, L., Yang, M. & Chen, Y. 2003. Strong metal-support interactions and catalytic properties of anatase and rutile supported palladium catalyst Pd/TiO_2. *Chemical Physics Letters* **372**: 160-165.

Ling, C.K., Zabidi, N.A.M., Mohan, C. 2011. Synthesis and characterization of silica-supported cobalt nanocatalysts using strong electrostatic adsorption. *Journal of Applied Sciences* **11(8)**: 1436-1440

Liu, J.X., Wang, P., Xu, W. & Hensen, E.J.M. 2017. Particle size and crystal phase effects in Fischer-Tropsch catalysts. *Engineering **3***: 467-476.

Mabaso, E.I. 2005. Nanosized Iron Crystallites for Fischer-Tropsch Synthesis. PhD thesis. University of Cape Town.

Macheli, L. 2014. Silica modified Co_3O_4 nanocubes as a model system for metal-support interaction in Co/SiO_2 catalyst for Fischer-Tropsch synthesis. MSc dissertation. University of Cape Town

Macheli, L., Roy, A., Carleschi, E., Doyle, B.P. & van Steen, E. 2018. Surface modification of Co3O4 nanocubes with TEOS for an improved performance in the Fischer-Tropsch synthesis. Catalysis Today https://doi.org/10.1016/j.cattod.2018.10.018.

Mogorosi, R.P. 2012. Metal-support interaction in Fe-based Fischer-Tropsch Catalysts. PhD thesis. University of Cape Town

Mogorosi, R.P., Fischer, N., Claeys, M., van Steen, E. 2012. Strong-metal-support interactions by molecular design: Fe-silicate interactions in Fischer-TRopsch catalysis. Journal of Catalysis **289**: 140-150

Mondragón, M.A., Castaño, V.M., J. Garcia, M. & C.A. Téllez, S. 1995. Vibrational analysis of $Si(OC_2H_5)_4$ and spectroscopic studies on the formation of glasses via silica gels. *Vibrational Spectroscopy* **9(3)**: 293-304

Morales, F. & Weckhuysen, B.M. 2006. Promotion effects in Co-based Fischer-Tropsch catalysis. *Catalysis* **19**: 1-40.

Morales, F., de Groot, F.M.F., Gijzeman, O.L.J., Mens, A., Stephan, O. & Weckhuysen, B.M. 2005. *Mn promotion effects in Co/TiO2 Fischer–Tropsch catalysts as investigated by XPS and STEM-EELS.* Available: http://www.sciencedirect.com/science/article/pii/S0021951704005706 .

Mourdikoudis, S. & Liz-Marzan, L.M. 2013. Oleylamine in nanoparticle synthesis. *Chemistry of materials* **25**: 1465-1476.

Munirathinam, R., Minh, D.P., Nzihou, A. 2018.Effect of support and its surface modifications on cobalt-based Fischer-Tropsch synthesis. *Industrial & Engineering Chemistry Research* **57**: 16137-16161

Olthof, B., Khodakov, A.Y., Bell, A.T. & Iglesia, E. 2000. Effects of support composition and pretreatment conditions on the structure of vanadia dispersed on SiO_2, Al_2O_3, TiO_2, ZrO_2, and HfO_2. *The Journal of Physical Chemistry B* **104(7)**: 1516-1528.

Pan, C., Tsai, M., Su, W., Rick, J., Akalework, N. G., Agegnehu, A. K., Cheng, S., Hwang, B. 2017. Tuning/exploiting strong metal-support interactions (SMSI) in heterogeneous catalysis. *Journal of the Taiwan Institute of Chemical Engineers* **74**: 154-186.

Petersen, A.P., Forbes, R.P., Govender, S., Kooyman, P.J. & van Steen, E. 2018. Effect of alumina modification on the reducibility of Co3O4 crystallites studied on inverse-model catalysts. *Catalysis Letters* **148(4)**: 1215-1227.

Petitto, S.C., Marsh, E.M., Carson, G.A. & Langell, M.A. 2008. Cobalt oxide surface chemistry: The interaction of CoO(100), Co3O4(110) and Co3O4(111) with oxygen and water. Journal of Molecular Catalysis A: Chemical ***281(1-2)****: 49-58*

Pinna, N. & Niederberger, M. 2008. Surfactant-free nonaqueous synthesis of metal oxide nanostructures. *Angewandte Chemie **47***: 5292-5304.

Puskas, I., Fleisch, T.H., Full, P.R., Kaduk, J.A., Marshall, C.L., and Meyers, B.L. 2006. Novel aspects of physical chemisty of Co/SiO_2 Fischer-Tropsch catalyst preparation: The chemistry of cobalt silicate formation during catalyst preparation or hydrogenation. *Applied Catalysis A: General* **311**: 146-154

Puskas, I., Fleisch, T.H., Kaduk, J.A., Marshall, C.L., Meyers, B.L., Castagnola, M.J. and Indacochea, J.E. 2007. Novel aspects of physical chemistry of Co/SiO_2 Fischer-Tropsch catalyst preparation: Cobalt oxide-induced silica migration during calcination of cobalt nitrate-impregnation high surface area silica. *Applied Catalysis A: General* **316**: 197-206.

Rabiu, A.M., van Steen, E. & Claeys, M. 2012. Further Investigation into the formation of alcohol during Fischer-Tropsch Synthesis on Fe-based catalysts. *APCBEE Procedia.* **3**:110-115.

Riva, R., Miessner, H., Vitali, R. & Del Piero, G. 2000. Metal–support interaction in Co/SiO2 and Co/TiO2. *Applied Catalysis A: General* **196(1)**: 111-123.

Sabat, K.C., Paramguru, R.K., Pradhun, S., Mishra, B.K. 2014. Reduction of cobalt oxide (Co_3O_4) by low temperature hydrogen plasma. *Plasma chemistry and plasma processing* **35**: 387-399

Schulz. H., Gokcebay, H. 1984. *Catalysis of Organic Reactions* (J.R. Kosak, ed) 153-169

Schulz, H., van Steen, E. & Claeys, M. 1994. Selectivity and mechanism of Fischer-Tropsch synthesis with iron and cobalt catalysts*. Studies in Surface Science and Catalysis* **81**: 455-460

Schulz, H. 1999a. Short history and present trends of Fischer–Tropsch synthesis. *Applied Catalysis A: General* **186(1–2)**: 3-12.

Schulz, H. & Claeys, M. 1999b. Kinetic modelling of Fischer–Tropsch product distributions. *Applied Catalysis A: General* **186(1–2)**: 91-107.

Schulz, H. & Claeys, M. 1999c. Reactions of α-olefins of different chain length added during Fischer-Tropsch synthesis on a cobalt catalyst in a slurry reactor. *Applied Catalysis A: General* **186(1-2)**: 71-90.

Schulz, H. 2003. Major and minor reactions in Fischer-Trospch synthesis on cobalt catalysts. *Topics in Catalysis* **26**: 73-85.

Shukla, P., Sun, H., Wang, S., Ang, H.M. & Tadé, M.O. 2011. Nanosized Co3O4/SiO2 for heterogeneous oxidation of phenolic contaminants in waste water. *Separation and Purification Technology* **77(2)**: 230-236 .

Staniuk, M., Hirsch, O., Kränzlin, N., Böhlen, R., van Beek, W., Abdala, P.M. & Koziej, D. 2014. Puzzling mechanism behind a simple synthesis of cobalt and cobalt oxide nanoparticles: in situ synchrotron X-ray absorption and diffraction studies. *Chemistry of Materials* **26(6)**: 2086-2094.

Steynberg, A.P. & Dry, M.E. (Eds). 2004. *Fischer-Tropsch Technology*. *Studies in Surface Science and Catalysis* **152.** Elsevier.Amsterdam,

Storsæter, S., Borg, Ø., Blekkan, E.A. & Holmen, A. 2005. Study of the effect of water on Fischer–Tropsch synthesis over supported cobalt catalysts. *Journal of Catalysis* **230(2)**: 504-419

Stracey, R. 2013. Metal-Support-Interactions in Co/TiO_2 Fischer-Tropsch Catalysts. MSc-dissertation. University of Cape Town.

Tang, C., Wang, C., Chien, S. 2008. Characterisation of cobalt oxides studies by FTIR, TPR and TG-MS. *Thermochimica Acta* **473**: 68-73.

Tauster, S.J. & Fung, S.C. 1978. Strong metal-support interactions occurrences among the binary oxides of Groups IIA-VB. *Journal of Catalysis* **55**: 29-35.

Tavakoli, A., Sohrabi, M., Kargari, A. 2008. Application of Anderson-Schulz-Flory (ASF) equation in the product distribution of slurry phase Fischer-Tropsch synthesis with nanosized iron catalysts. *Chemical Engineering Journal* **136(2-3)**: 358-363.

Tejedor-Tejedor, M., Paredes, L. & Anderson, M.A. 1998. Evaluation of ATR-FTIR spectroscopy as an in situ tool for following the hydrolysis and condensation of alkoxysilanes under rich H_2O conditions. *Chemistry of Materials* **10(11)**: 3410-3421.

Thanh, N.T.K., Maclean, N. & Mahiddine, S. 2014. Mechanisms of nucleation and growth of nanoparticles in solution. *Chemical Reviews* **114(15)**: 7610-7630.

Todic, B., Nowicki, L., Nikacevic, N. & Bukur, D.B. 2016. Fischer-Tropsch synthesis product selectivity over industrial iron-based catalyst: Effect of process conditions. *Catalysis Today* **261**: 28-39.

Tsakoumis, N.E., Ronning, M., Borg, O., Rytter, E., Holmen, A. 2010. Deactivation of cobalt based Fischer-Tropsch catalysts: A review. *Catalysis Today* **154**: 162-182.

van der Laan, G.P. & Beenackers, A.A. 1999. Kinetics and selectivity of the Fischer-Tropsch Synthesis: a literature Review. *Catalysis Reviews Science and Engineering* **41(3-4)**:255-318.

van Heerden, T. & van Steen, E. 2017. Metal-support interaction on cobalt based Fischer-Tropsch catalysts: a DFT study of model inverse catalysts. *Faraday Discussions.* **197**: 87-99.

van Santen, R.A., Ciobîcă, I.M., van Steen, E. & Ghouri, M.M. 2011. Chapter 3 - Mechanistic issues in Fischer–Tropsch catalysis. *Advances in Catalysis* **54**: 87-99.

van Steen, E., Sewell, G.S., Makhote, R.A., Micklethwaite, C., Manstein, H., de Lange., O'Connor, C.T. 1996. TPR study on the preparation of impregnated CO/SiO_2 catalysts. *Journal of Catalysis.* 162(2):220-229.

van Steen, E. & Claeys, M. 2008. Fischer-Tropsch Catalysts for the Biomass-to-Liquid (BTL)-process. *Chemical Engineering & Technology* **31(5)**: 655-666.

Verelst, M., Ely, T.O., Amiens, C., Snoeck, E., Lecante, P., Mosset, A., Respaud, M., Broto, J.M., Chaudret, B. 1999. Synthesis and characterization of CoO, Co_3O_4 and mixed Co/CoO nanoparticles. *Chemistry of material* **11(10)**: 2702-2708

Wang, T., Ding, Y., Xiong, J., Zhu, H., Lu, Y., Lin, L. 2006. Effect of vanadium promotion on activated carbon-supported cobalt catalyst in Fischer-Tropsch synthesis. *Catalysis letters* **107(1-2)**: 47-52

Weststrate, C.J., Hauman, M.M., Moodley, D.J., Saib, A.M., van Steen, E., Niemantsverdriet, J.W. 2011. Cobalt Fischer-Tropsch catalyst regeneration: the crucial role of the Kirkendall effect for cobalt re-dispersion. *Topics in Catalysis* **54**: 811-816

Xiaoping, D., Changchun, Y., Ranjia, L., Haibo, S., Shikong, S. 2006. Role of CeO_2 catalyst for Fischer-Tropsch synthesis. *Chinese Journal of Catalysis* **27(10)**: 904-910

Yin, X.J., Peng, K., Hu, A.P., Zhou, L.P., Chen, J.H. & Du, Y.W. 2009. Preparation and characterization of core–shell structured Co/SiO2 nanosphere. *Journal of Alloys and Compounds* **479(1-2)**: 372-375

Chapter 8 Appendix

A1: Chromatograph (GC) HP6890

The concentration of TEOS in the aliquot withdrawn from the samples during catalyst modification was analysed using gas chromatograph HP 6890 equipped with a flame ionization detector (FID). The GC was calibrated by using standard n-hexane TEOS mixture that was prepared prior to the analysis of the aliquot. The analysis was conducted at constant temperature using hydrogen as the carrier gas. The aliquot was injected manually into the column this however had minimal effect on the sharpness of the peaks. The operating conditions and properties of the column used are given in

Table 8-1: Properties of column in HP6890 equipped with FID

	Column 1
Compound analysed	n-Hexane, TEOS
Column temperature (K)	393
Carrier gas	H2
Inlet Pressure (kPa)	3.12
Injection time (ms)	2
Injection temperature (K)	473
Sampling time (s)	0.5
Column type	Non-polar HP-5
Column dimensions	30m x 0.320mm Stationary phase: 0.25µm

A2: Tetraethoxysilane (TEOS) uptake calculations for oxidised cobalt nanoparticles

Table 8-2: TEOS uptake calculations for oxidised cobalt nanoparticles

Sample name			**Initial concentration – 0.9 mmol/l**			
			<001>	<002>	<003>	Average
Initial concentration	Area	n-Hexane	1068689963	1047608437	1013304236	1043200879
		TEOS	640218	657254	644000	647157
	ratio	TEOS/n-hexane	0.0005987 1	0.0006269	0.00063514 1	0.000620
			<004>	<005>	<006>	Average
30 min	Area	n-Hexane	1140205013	931411790	986097286	1019238030
		TEOS	675172	559213	595445	609943
	Ratio	TEOS/n-hexane	0.0005921 5	0.0006003 9	0.00060384	0.000599
			<007>	<008>	<009>	Average
1 hr.	Area	n-Hexane	934760740	1023393274	988205260	982119758
		TEOS	473226	607000	587524	555917
	Ratio	TEOS/n-hexane	0.0005062 5	0.0005931 2	0.00059453 6	0.000594
			<010>	<011>	<012>	Average
4 hr. 30 min	Area	n-Hexane	983758699	1040904588	978726808	1001130032
		TEOS	564898	617176	611476	597850
	Ratio	TEOS/n-hexane	0.0005742 2	0.0005929 2	0.00062476 7	0.000597
			<013>	<014>	<015>	Average
5 hr.	Area	n-Hexane	988011615	979568585	1029311174	998963791
		TEOS	591124	587484	617529	598712
	Ratio	TEOS/n-hexane	0.0005979 4	0.0005993 8	0.00059958 4	0.00059896 7
			<016>	<017>	<018>	Average
6 hr.	Area	n-Hexane	960465162	1015594494	963950387	980003348
		TEOS	555470	598857	605731	586686
	Ratio	TEOS/n-hexane	0.000578	0.0005893 1	0.00062798 9	0.00059843 4
			<025>	<026>	<021>	Average
7 hr.	Area	n-Hexane	972588454	1026586963	944143243	981106220
		TEOS	580827	623713	551665	585402
	Ratio	TEOS/n-hexane	0.0005968 4	0.0006071 9	0.00058396 1	0.00059599 8
			<028>	<029>	<030>	Average
8 hr.	Area	n-Hexane	998936099	991921336	912056828	967638088
		TEOS	591529	594648	546345	577507

	Ratio	TEOS/n-hexane	0.00059181	0.00059913	0.000598667	0.000596536
			<033>	<034>	<035>	Average
24 hr.	Area	n-Hexane	816028962	817055010	801921326	811668433
		TEOS	481604	489099	486135	485613
	Ratio	TEOS/n-hexane	0.000589833	0.000598225	0.000605846	0.000597977

A2: TCD calibration

The thermal conductivity detector is a detector that makes use of the differences in thermal conductivity of the gases compared to a reference gas to analyse what elutes from the GC column. The calibration of the GC is conducted with a known composition of gas mix to be able to quantify elutes. The internal standard that is used is N_2 or Ar. In this calibration N_2 was used as the internal standard.

The composition of the analysis gas that was used for the calibration is shown in table. The analysis on the gas is repeated several times.

Table 8-3: TCD analysis gas composition

Species	**Composition (%)**
N_2	5.2
Ar	9.8
CO_2	9.7
CH_4	14.6
CO	20.3
H_2	40.4

The average area for each component together with the compositions are used to calculate the response factors for each component. The retention factors were calculated using equation.

$$f_{Af(N_2)} = \frac{f_A}{f_{N_2}} = \frac{[N_2]A_A}{A_{N_2}[A]}$$

Where

f_x is the response factor of species X

$[A]$ is the concentration or flowrate of species X

A_x is the area of species X in the TCD spectrum

The calibration produced the retention factor shown in Table… The retention factors were used in the calculation of the conversion of the reactor.

Table 8-4: Retention factor for species in TCD

Species	**Retention factor**
H2	6.2
N2	1
CO2	1.3
CH4	3.9
CO	0.88

A3: TPR calibration calculations

The TPR calibration was conducted by reducing 34 mg Ag_2O in a Quartz reactor. When silver oxide is reduced under a hydrogen environment it produces metallic silver and water as depicted in Equation. From this balance equation it is observed that every mole of H_2 that reacts, one mole of silver oxide is reduced to metallic silver.

$$Ag_2O + H_2 \rightarrow Ag + H_2O$$

The reduction profile of the silver oxide is shown in Figure 8-1. The area under the curve is determined using Simpson's Rule to be 0.31 unit Area. Complete reduction of the silver oxide was assumed therefore it was calculated that 0.147 mmol of H_2 gas was consumed. Therefore it was calculated that 0.478 mmol of H_2 gas are consumed per unit area in the reduction profile.

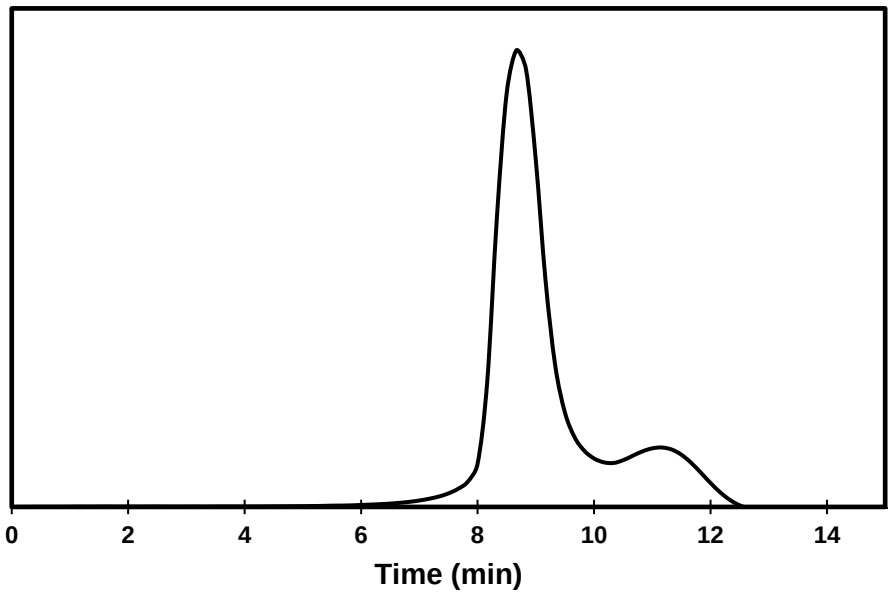

Figure 8-1: Reduction profile for Ag2O using a heating ramp of 10 °C/min

A4: TPD analysis

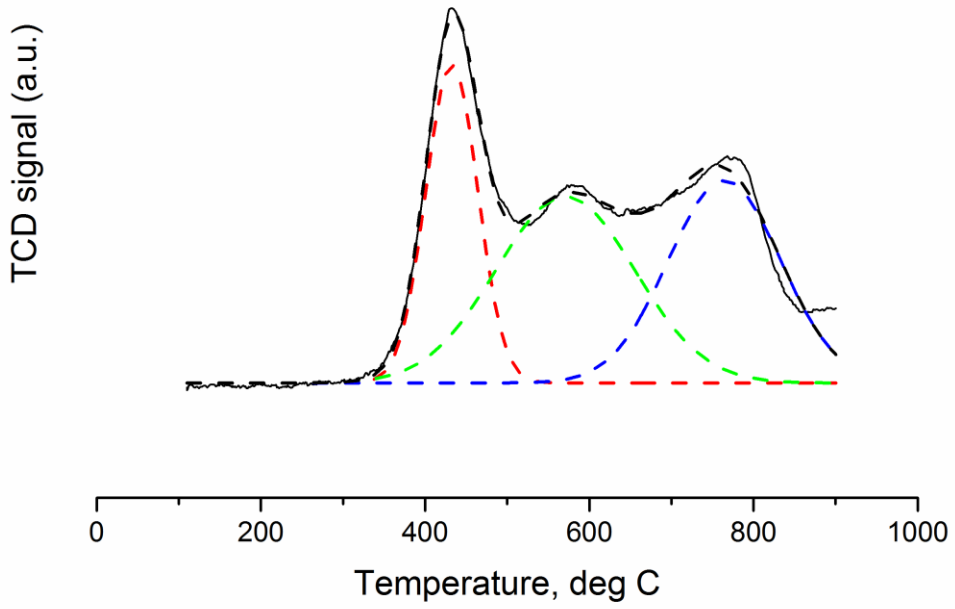

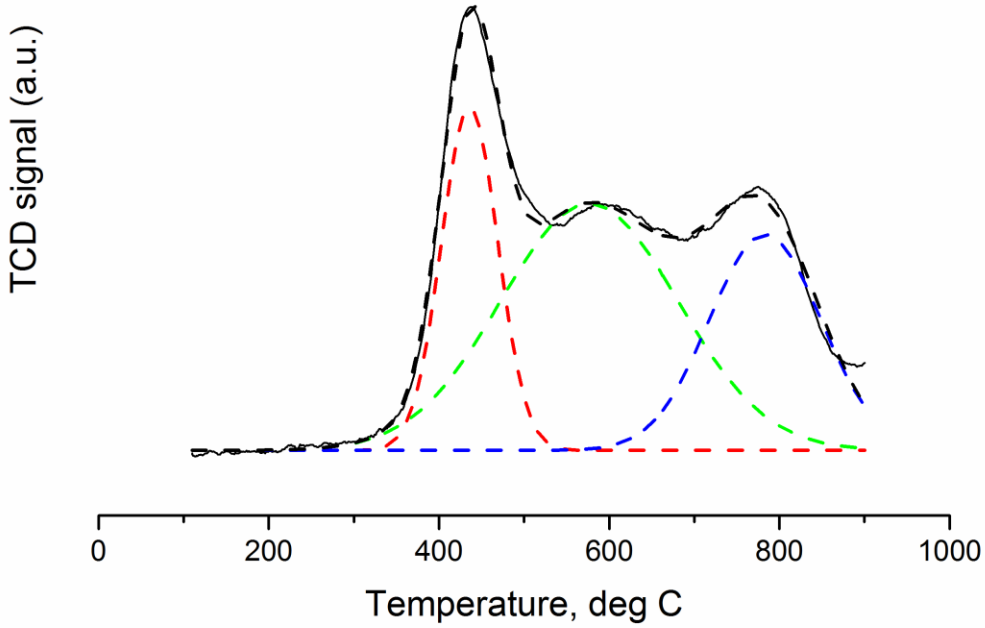
TCD signal (a.u.)
0
200
400
600
800
1000
Temperature, deg C

A5: Calibration curves for mass flow controllers

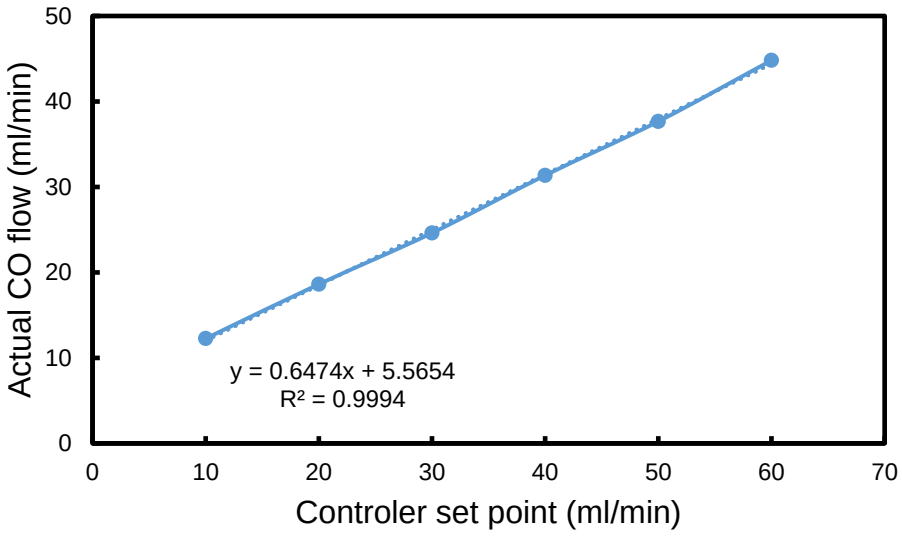

Figure 8-2: Calibration curve for CO mass flow controller

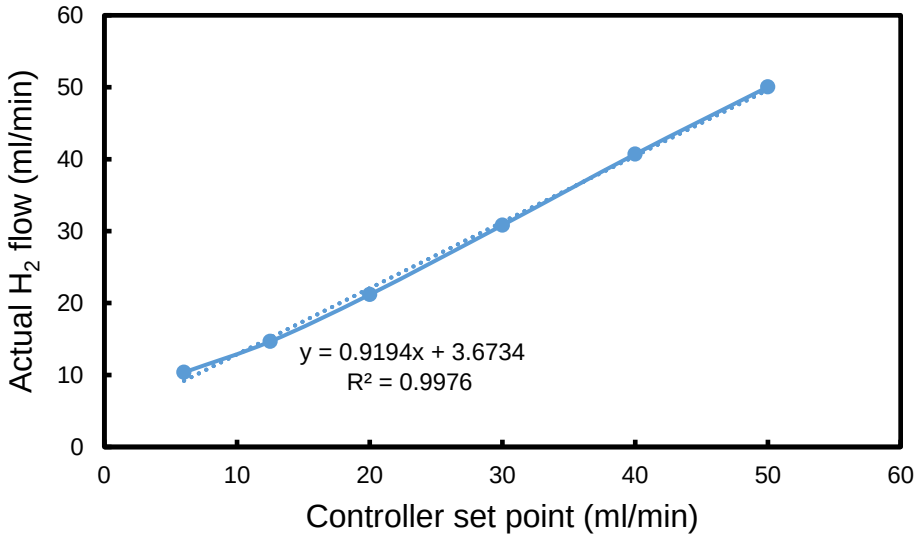

Figure 8-3: Calibration curve for CO mass flow controller

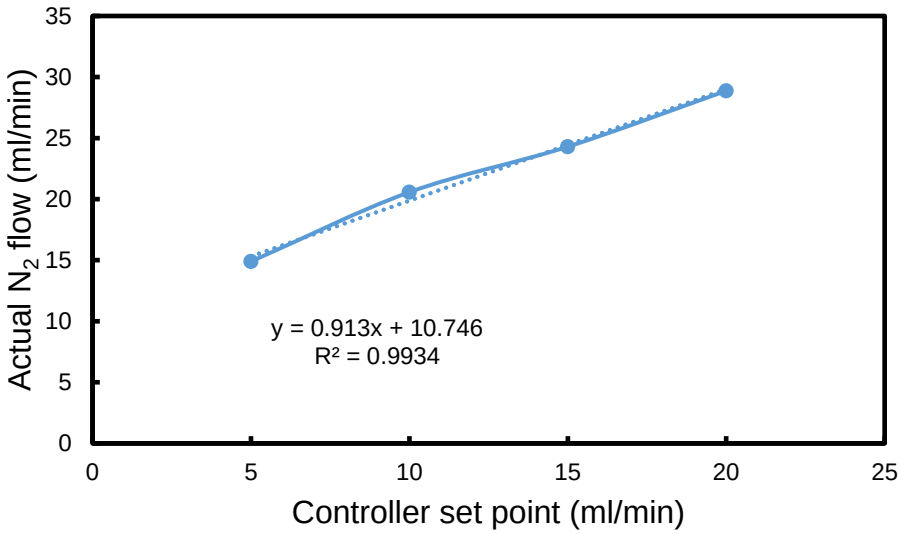

Figure 8-4: Calibration curve for N_2 mass flow controller

A6: Derivation of Johnson-Mehl-Avami_kolmogrov equation

In a system mentained isothermally the rate of growth of a particle can be expressed as shown in

$$r(t) = r^* + vt$$

Where

r(t): length of particle at time (t)

r^*: initial length of particle

v: radial velocity (length/unit time)

t: time

The number of isolated nuclei available in the systhem can be monitored with time using equation

$$n(t) = n[1 - x(t)]$$

Where

n(t): number of nuclei per unit volume at time t

n: number of nuclei per unit volume originally

x(t): volume fraction to be transfromed

The increase in the volume fraction of the growing nuclei as a function of time is expressed as

$$dx(t) = n(t) \cdot 4\pi \cdot r^2 dr = n \cdot [1 - x(t)] \cdot 4\pi \cdot (vt)^2 d(vt) = n \cdot [1 - x(t)] \cdot 4\pi \cdot v^3 \cdot t^2 dt$$

Separating the variables and integrating, the volume fraction becomes

$$x(t) = 1 - \exp[-\left(\frac{t}{\tau}\right)^3]$$

Where,

$\tau = [\frac{3}{4\pi n}]^{1/3} \frac{1}{v}$, τ- time costanct of the process